

NPS ARCHIVE
1960
HANGARTNER, L.

Lamont
U. S. Naval Postgraduate School
Monterey, California

INTERFEROMETRIC ANALYSIS OF THE TIME UNSTEADY
FLOW THROUGH A RADIAL TURBINE

L. G. HANGARTNER
//
D. H. McVAY, Jr.

UNIVERSITY OF MICHIGAN
ANN ARBOR, MICHIGAN

AUGUST 1960

NPS ARCHIVE

1960

HANGARTNER, L.

~~Thesis~~

~~4/19/60~~

List of Tables and Figures

Tables

I	Conversion of Isopycnic Fringes to Velocity
II	Sample Conversion of Rough Data to Corrected Data
III	Velocity versus Peripheral Distance for Picture Sequence UM - 435 to UM - 458
IV	Conversion of Reference Distances to Reference Time
V	Velocity and Potential versus Time for Selected Peripheral Distances
VI	Determination of Corrected Velocity by First Iteration
VII	Velocity and Potential versus Time for Selected Peripheral Distances by Second Iteration
VIII	Determination of Corrected Velocity by Second Iteration
IX	Verification of Nose Stagnation Point

Figures

1 - 24	University of Michigan Interferograms 435 - 458
25, 26	Velocity versus Blade Peripheral Distance, Actual and Theoretical
27	University of Michigan Interferogram Fringe Displacement Type Photo- graph
28 - 43	Velocity versus Blade Peripheral Distance, for Suction Side of Blades, UM 438 - 453
44 - 53	Velocity and Potential versus Time for First Iteration
54 - 61	Velocity versus Blade Peripheral Distance for Second Iteration
62 - 71	Velocity and Potential versus Time for Second Iteration
72 - 74	Velocity versus Time for the Two Iterations

TABLE OF SYMBOLS

P_0	- Reference total pressure of air in undisturbed flow field.
p_∞	- Reference static pressure of air in undisturbed flow field.
p_1	- Static pressure for any particular location on the nozzle blade.
ρ_∞	- Reference density of air in undisturbed flow field.
ρ_1	- Local density of air.
T_∞	- Reference static temperature in undisturbed flow field.
V_∞	- Reference velocity in undisturbed flow field.
V_1	- Local velocity for any particular location on the nozzle blade.
q_∞	- Reference dynamic pressure of air in undisturbed flow field.
g	- Gravitational constant.
γ	- Ratio of specific heats (c_p / c_v).
t	- Reference time.
S_s	- Peripheral distance around nozzle blade, measured from the trailing edge of the blade.
ϕ	- Velocity potential.

FOREWORD

For the past five years the Aircraft Propulsion Laboratory, Department of Aeronautical Engineering, University of Michigan, has made extensive experiments in interferometric techniques using a Mach-Zehnder Interferometer to study the flow of air through a single stage, radial turbine. These experiments were sponsored by the Large Steam Turbine Division of the General Electric Company, Schenectady, New York.

The above experiments resulted in several series of interferometric photographs for various running conditions of the turbine. Particularly interesting was the repeated shedding of small vortices from the trailing edges of the nozzle blades, at generally regular intervals. It was decided to analyze a series of these pictures, in an attempt to determine the nature of these vortices, and the accompanying flow patterns. This analysis, and the resulting conclusions, are the work of this report.

INTRODUCTION

The analysis of the flow in a single stage radial turbine by interferometric methods was undertaken in an attempt to determine the frequency and strength of small vortices, shed off the trailing edge of the nozzle blade. The flow was considered isentropic and the analysis made use of a sequence of 24 flash pictures taken for consecutive turbine blade positions. Thus it was assumed that the flow repeats itself for each revolution of the turbine wheel, if the total pressure and flow rate are constant. The pictures used, Figs. 1 to 24, were part of a series included in Ref. 2, which was generally a feasibility study for the interferometric technique with regard to a moving turbine.

The analysis was carried out during the academic year 1959 - 1960 at the Propulsion Laboratory, North Campus, University of Michigan, Ann Arbor. The work was sponsored jointly by the General Electric Company of Schenectady, New York and the United States Naval Postgraduate School, Monterey, California. Lt. L. G. Hangartner and Lt. D. H. McVay were the analysts although Mr. H. Kraft of General Electric Company and R. E. Cullen, of the University of Michigan, were close advisors in the project.

ANALYSIS

I GENERAL

In obtaining the interferometric photographs used for the analysis in this report, an 8-inch Mach-Zehnder Interferometer was employed. The turbine was a radial flow, single-stage impulse turbine designed and fabricated by the General Electric Company. This turbine has four cut-out positions, every 90^0 , located in the end plates. Thus, the air flow through these four bucket channels, is visible and may be photographed. Ref. 1, presents the description of this interferometer, turbine and accompanying apparatus. Figures from Ref. 1, and a brief discussion of the principles of interferometry may be found in Appendix I to this report.

Appendix I, also points out the difference between fringe displacement and infinite fringe type pictures. Although both were used in this report, the infinite fringe type picture was used much more extensively. Fig. 1 and 27, are examples of the infinite and fringe - displacement pictures, respectively.

These pictures were taken using an achromatic focusing lens and a 4 in. X 5 in. camera back, together with an air cooled mercury arc lamp flash apparatus. It was also possible to take pictures of the turbine in continuous operation, using a Fastax type of 16 mm. motion picture camera.

Figs. 1 to 24, corresponding to UM 435 to 458, respectively, are the interferometric photographs used in the analysis of this report. Assuming that the flow in the turbine repeats itself every revolution, it was possible to use these 24 flash pictures, taken over a period of minutes, but under the same turbine operating conditions,

and establish a true time study of a turbine blade passage. The flash apparatus was electronically synchronized, as discussed in Ref. 1, to "stop" the turbine, as the cut-out position progressed across the test section area. Using turbine RPM, held constant, in this case at 900 RPM, it was then possible to convert a reference distance to true time.

As mentioned previously the flow was considered isentropic. The air flowing through the turbine is assumed to be a perfect fluid. This assumption of a perfect fluid eliminates the property of viscosity found in actual fluids, due to internal friction, and the perfect fluid, therefore, can exert no shearing stress. The assumption of a perfect fluid also implies irrotational motion in the fluid. In addition, the flow was considered to be incompressible throughout the nozzle passage.

Due to the assumptions above, the standard equation of state and Bernoulli equation may be used to compute the velocities around the blade from the density measurements of the interferogram. As a result of the irrotational property of the flow, a velocity potential may be found, and using this potential in conjunction with Kelvins' equation, makes it possible to determine the final velocity profile about the nozzle blade.

II DETERMINATION OF VELOCITIES ON THE NOZZLE BLADE

In analyzing the pictures, Figs. 1 to 24, the following data taken from Ref. 2, was used:

Gap setting	.133 inches
RPM	900 RPM
P_0	29.02 (in. H_g abs.)
T_∞	70.1° F.
g_∞	1.41 (in. H_2O)

Converting the above to pressures in psia, and from the equation of state, determining the free stream density, the following values were obtained.

$$g_\infty = P_0 - p_\infty = \frac{1.41 \times 14.696}{13.546 \times 29.9213} = .0511 \text{ psia}$$

$$P_0 = 29.02 \times 14.696 / 29.9213 = 14.2533 \text{ psia}$$

$$p_\infty = P_0 - g_\infty = 14.2533 - .0511 = 14.2022 \text{ psia}$$

$$\rho_\infty = \frac{p_\infty \times 144}{T_\infty \times R} = \frac{14.2022 \times 144}{529.788 \times 53.34} = .072371 \text{ lb/cu.ft}$$

Using these free-stream state functions, it was then possible to determine the free-stream velocity, using the assumption of incompressible flow:

$$g_\infty = \frac{1}{2} \rho_\infty V_\infty^2 / g$$

$$V_\infty = \left(2 g_\infty g / \rho_\infty \right)^{1/2} = \left(2 \times .0511 \times 144 \times 32.174 / .072371 \right)^{1/2}$$

$$V_\infty = 80.88 \text{ ft/sec.}$$

In order to find velocities along the nozzle blade, corresponding to each interferometric fringe it was necessary to establish the change in density for each fringe shift. From Ref. 2, and as explained in Appendix I, this change in density for one fringe-shift was given as:

$$\Delta \rho / \rho_\infty = .01027.$$

For a half fringe shift from free stream conditions, then:

$$\Delta f / f_{\infty} = 1 - .01027 / 2 = 1.0 - .00513 = .99487$$

Using Bernoulli's equation, it was possible to solve for the velocity corresponding to each half fringe-shift.

$$\begin{aligned} \rho_1 + \rho_1 &= \rho_0 \\ \frac{V_1^2}{2} + \frac{\rho_1 g}{\rho_1} &= \frac{\rho_0 g}{\rho_1} \end{aligned}$$

In order to find p_1 , it was necessary to use the isentropic relation:

$$\begin{aligned} \frac{p_1}{\rho_1^{\gamma}} &= \frac{p_{\infty}}{\rho_{\infty}^{\gamma}} = \text{CONSTANT} \\ p_1 &= p_{\infty} \left(\frac{\rho_1}{\rho_{\infty}} \right)^{\gamma} \end{aligned}$$

Then the velocity was computed from:

$$V_1 = \sqrt{\frac{2 \times g \times 144}{f_1 / f_{\infty} \quad f_{\infty}} (p_0 - p_1)}$$

Table I, gives the velocities found in this manner for each 1/2 fringe-shift up to seven complete fringe-shifts.

It was now possible to determine the actual velocities around the nozzle blade. Referring again to Figs. 1 to 24, the blade on the right hand side was chosen as the one to be analyzed. Measurements around the blade were made from the trailing edge in a counterclockwise direction. The white area in the upper part of the Figure is the free-stream air flow. Beginning at the leading edge, the first black fringe indicates a half fringe-shift. Each consecutive black fringe indicates a full fringe-shift. Velocities corresponding to these fringe-shifts, as found in Table I, are then assigned to positions on the blade at the mid-point of the black fringe. The figures were enlarged about 1.75 times and actual positions on the blade were found using the known distance around the blade of 4.98 inches. Table II is a sample of this procedure. Table III

contains the final velocities and their true positions on the blades.

Table III also includes reference time, t , for each picture. This reference time was found using the reference distance from a permanent vertical wire down the center of the test section, to the mid-chord point on the suction face of the turbine bucket. This distance was converted to actual distance, and then converted to true time, using turbine RPM and the radius to the center of the turbine bucket.

RPM - 900

Rad. of turbine wheel-20.875"

Chord of turbine blade-.908"

Rad. to center of blade-20.421"

$$\begin{aligned} \text{Velocity of center of Blade} &= \frac{900 \text{ RPM} \times 2\pi^{\text{RAD}} / \text{REV} \times 20.421 \text{ IN}}{60 \text{ SEC} / \text{MIN}} \\ &= 1925 \text{ IN} / \text{SEC.} \end{aligned}$$

$$\text{then } t = \frac{\text{REF. DIST. IN INCHES}}{1925 \text{ IN} / \text{MS.}}$$

Table IV lists the values of the reference time, t , for each of the photographs, (where Fig. 1 was arbitrarily chosen as $t=0$), and the computations involved.

It should be noted in Table III that the leading edge stagnation point is listed at the same blade position for each photograph. Before assuming this point, three studies were made. Plots of V vs. s were made, of the results in Table III, omitting the stagnation point, and allowing the curve to pass through zero velocity. Examples of these curves, together with theoretical curves established by the equations found in Ref. 3, are shown in Figs. 25, and 26. The values of s , where V passed through zero, were found to extend from $s = 2.635''$ to $s = 2.78''$. The average of the 24 pictures

however was found to be $s = 2.715''$.

Secondly, the fringe displacement type interferograms, using the same turbine conditions and gap setting, were studied. Fig. 27, is an example of these interferograms and the series used included UM 413 to 434. Fig. 27 is photo number UM 413. A fringe in this case, which bends away from the vertical, indicates a finite velocity. Determining either the vertical fringe, or the point between two very slightly displaced fringes, indicated the location of the stagnation point. Table IX lists the position of the stagnation point as found in both of the above methods. The average of the fringe displacement pictures was $s = 2.741''$. The average of the two methods was $2.728''$ taken as $2.73''$. It was this value which was used in Table II.

The third method was somewhat a check of the other two. In reviewing Figs. 1 - 24, it was noted that in several cases, a faint fringe may be seen on the leading edge of the nozzle blade. By taking the geometrical center of this fringe, a fairly accurate position of the stagnation point may be located. Figs. 8, 9, 15 and 16 are examples of this, and in the pictures checked, a good corroboration to the value $s = 2.73''$ was obtained.

III Non-Steady Analysis

When the flow field around the nozzle blade was originally analyzed, the Bernoulli Equation,

$$\frac{V^2}{2} + \frac{P}{\rho} = P_0/\rho = \text{CONSTANT}$$

was used to determine the velocity at any point on the blade. However, in non-steady flow of the type encountered in the turbine, it is necessary to use Kelvin's Equation as found in Ref. 4:

$$\frac{\partial \phi}{\partial t} + \frac{V^2}{2} + \frac{P}{\rho} = F(t)$$

where $\frac{\partial \phi}{\partial t}$ is the non steady potential term. To explain this term a little of the theory of fluid flow will be presented. The term field denotes a region throughout which a quantity is defined as a function of location within the region and time. If the quantity is independent of time, the field is steady or stationary.

The field of gravitational force is a conservative field, meaning by this that the work done by the weight in taking a body from point A to another point B is independent of the path taken and depends on the vertical height between A and B only. A conservative field of force gives rise to potential energy, which is measured by the work done in taking a body from one standard position to another, independent of the path.

The velocity in a field is assumed to be the result of just such a potential field. While this is not physically true, it is an exact mathematical analogy. We may write:

$$\vec{V} = \frac{\partial \phi}{\partial s}$$

where the function ϕ is called the velocity potential. The velocity potential is, in general, a function of (x,y,t), and may be determined from:

$$\phi = \int \vec{V} \cdot d\vec{s}$$

provided the velocity is known. Since the velocity potential is a function of time, it necessarily follows that the velocity is a function of time.

To determine the strength of the shed vortices, the exact velocities in the field must be known. To determine the actual velocity, it was then necessary to determine the magnitude of the $\partial\phi/\partial t$ term.

For this analysis, only part of the series of pictures was considered. Figs. 4 through 20, were chosen, since they covered two turbine blade passages, and showed a clear case of the vortex shedding phenomenon. Since there was some question as to the probability of determining the exact magnitude of the $\partial\phi/\partial t$ term, a feasibility study was made. For several reasons, in this study, only the suction side of the nozzle blade was used. One reason was lack of information on the pressure side due to the very few fringes distinguishable. Secondly, the time and effort involved, even for a very limited analysis, was considerable when all the calculation is done manually. And thirdly, the experimental curve closely approximated the theoretical curve along the suction side, leading the investigators to believe, that limiting the investigation would improve the results.

Figs. 28 to 43, are plots of velocity versus perimeter distance, for the suction side of the nozzle from $s = .25$ in. to $s = 2.73$ in., the assumed stagnation point, for the series of pictures to be analyzed. The area from $s = 0$ to $s = .25$ " was not considered due to the problems encountered not only because of the wake and shed vortices in this area, but also because of the build-up of the boundary layer in this region.

Assuming a potential exists (irrotational flow), the line integral of the velocity component in the direction of the path between any two points in an irrotational field

is equal to the difference in potential between these points. That is:

$$\int_A^B \nabla \cdot d\vec{s} = \phi_B - \phi_A$$

If point A is a position of zero potential, the line integral from A to any point in the field is the value of the potential at that point.

Beginning where $V = 0$, at the nose stagnation point, or at $s = 2.73$ in., these figures were graphically integrated to obtain the potential function ϕ . This integration was made every $s = .25$ in., and was additive along the periphery of the blade. Values of ϕ and V versus s are tabulated in Table V. These values of ϕ and V were plotted versus time, using the reference time for each of the pictures, for each of the even intervals along the periphery, i.e. .25 inches, .50 inches, etc. These plots are found in Figs. 44 to 53.

Taking the slope of the ϕ versus t curve at any particular time, gave the instantaneous value of $\partial\phi/\partial t$. Using this value of $\partial\phi/\partial t$ in the Kelvin Equation with an iteration process, it should be possible to determine the actual velocity distribution about the blade.

The iteration is based on the general formula:

$$\frac{\partial\phi}{\partial t} + \frac{p}{\rho} + \frac{V^2}{2} = \text{CONSTANT}$$

Where the $F(t)$ of the Kelvin Equation is assumed to be a constant, as suggested by Lamb in Ref. 4.

The zeroth iteration or initial determination of the velocity is based on the premise $\partial\phi/\partial t = 0$, which reduces the equation to the Bernoulli equation. Hence,

$$\begin{aligned} \frac{\partial\phi}{\partial t} = 0, \quad C_0 = p_0/\rho &= \frac{p}{\rho} + \frac{V_0^2}{2} \\ \frac{V_0^2}{2} = C_0 - p/\rho &= \frac{p_0}{\rho} - \frac{p}{\rho} \end{aligned}$$

$$V_o = \sqrt{2 \left(\frac{P_o}{f} - \frac{p}{f} \right)}$$

Where V_o is the velocity determined from the interferometric pictures and tabulated in Table III.

For the first iteration,

$$\frac{\partial \phi_1}{\partial t} + \frac{p}{f} + \frac{V_1^2}{2} = C_1$$

or,

$$\frac{V_1^2}{2} = C_1 - \frac{p}{f} - \frac{\partial \phi_1}{\partial t}$$

For this iteration C_1 is assumed to equal to C_o and throughout the analysis p/f is assumed to be constant. Therefore,

$$\frac{V_1^2}{2} = \left[\frac{V_o^2}{2} + \frac{p}{f} \right] - \frac{p}{f} - \frac{\partial \phi_1}{\partial t} = \frac{V_o^2}{2} - \frac{\partial \phi_1}{\partial t}$$

or,

$$V_1 = \sqrt{V_o^2 - 2 \frac{\partial \phi_1}{\partial t}}$$

Since trial calculations showed that the term $2 \frac{\partial \phi}{\partial t}$ was quite large and tended to make the values of V oscillate widely, hence making the iterative process extremely lengthy, it was decided to use one-half this value or just $\frac{\partial \phi}{\partial t}$ to speed convergence.

Therefore,

$$V_1 = \sqrt{V_o^2 - \frac{\partial \phi_1}{\partial t}}$$

For the second iteration,

$$\frac{\partial \phi_2}{\partial t} + \frac{p}{f} + \frac{V_2^2}{2} = C_2$$

It may be shown mathematically that the constants C_o , C_1 , C_2 , etc. are all equal, and henceforth, will be known simply as C . Therefore,

$$\frac{\partial \phi_2}{\partial t} + \frac{p}{f} + \frac{V_2^2}{2} = C = \frac{V_o^2}{2} + \frac{p}{f}$$

Cancelling $\dot{\phi}/\dot{s}$ and solving for V_2 ,

$$V_2 = \sqrt{V_0^2 - \frac{\partial \phi_2}{\partial t}}$$

likewise it can be shown:

$$V_3 = \sqrt{V_0^2 - \frac{\partial \phi_3}{\partial t}}$$

or in general terms:

$$V_n = \sqrt{V_0^2 - \frac{\partial \phi_n}{\partial t}}$$

This iteration process has been carried out several times, in an attempt to determine the rate of convergence and the approximate magnitude of the final velocity.

The original velocities, as stated before, are tabulated in Table III and the ϕ and V versus time plots are Figs. 44 - 53. For the first iteration, the original velocities, the value of $\partial\phi/\partial t$ determined from the ϕ plots, and the corrected velocities are tabulated in Table VI.

From these corrected velocities new plots of velocity versus perimeter distance were made and are included in the report as Figs. 54 to 61. These figures were again graphically integrated and the values of ϕ and V versus s tabulated in Table VII. From this data, plots were made of the new ϕ and V versus time and are included in the report as Figs. 62 to 71. From these plots the new values of $\partial\phi/\partial t$ were found and the corrected velocity again computed. The tabulated values of $\partial\phi/\partial t$ and the corrected velocities are included as Table VIII.

At this point three iterations had been completed and the three time histories of velocity for a specified peripheral distance (s) are plotted in Figs. 72 to 74.

During the iterative process the question of sign for the $\partial\phi/\partial t$ term arose, and for all the calculations the term was taken as plus. That is, negative slopes on the ϕ

versus t plot were $-\partial\phi/\partial t$.

This has by no means been a complete analysis of the non-steady flow in the turbine, for many reasons, foremost of which is the limited time available. But the work is considered very useful and the foundation for more advanced and continued work has been laid. The problems encountered, decisions made, conclusions drawn, and recommendations made will all be covered in detail in the discussion and conclusions sections of this report.

DISCUSSION

The preceding analysis outlines the general method used to reduce the interferometric data obtained from a picture series, for a given inlet nozzle blade in the turbine. It was hoped that the analysis would provide a clear quantitative indication of the strength and frequency of the vortex, which is periodically shed from the trailing edge of the blade. This vortex may be seen in Fig. 1, just below and to the left of the trailing edge, of the right-hand blade.

It was the general intent of the complete analysis to obtain a plot of circulation around the blade versus time. By analyzing the changes in circulation, which were believed to be affected by the vortex shedding, it was thought that a good indication of the strength of the shed vortex could be found. Also it was believed that the circulation versus time plot would be sinusoidal in nature, and give a good indication of the frequency and actual times of shedding.

From the above data a general idea of the power loss associated with the vortex shedding phenomenon could be gained, and compared with any experimental data available on this subject.

The results, however, from this limited analysis have not explained, nor substantiated, the pictures of the vortex shedding. Some of the reasons for this deficiency, and recommendations for future investigations are the main subjects of this discussion.

Some idea of the frequency of the vortex shedding was gained from studying movies of the flow, using a high speed motion picture camera. It appears that a vortex is shed from the trailing edge of the nozzle, every time the turbine bucket leading

edge passes the nozzle tip. This helped to fix the frequency of the vortex shedding, although it was of little help in determining the strength.

In analyzing this particular sequence, the blade on the far right of the test section was chosen. The main reason for this choice, was the fact that, this blade was mounted most nearly parallel to the flow. It should be noted, the nozzle blades are mounted in a slight arc so as to conform to the radial shape of the turbine, thus maintaining a constant gap setting, between stationary and moving blade rows. The test section is just to one side of the center-line of this arc. The flow entering the nozzles is laminar, and parallel to the reference wire, mounted in the center of the test section. Hence, the right hand blade was chosen, in order to eliminate any corrections necessary, when the blade is mounted at an angle to the flow.

It is conceded that there may be advantages to analyzing the flow around other blades, particularly the center-most blade, i.e. the second from the right. For the series considered, this blade clearly showed the shedding of the vortex, plus giving a more detailed picture of the complete flow field, due to its location in the center of the test section. The error, resulting from the blade being slightly misaligned from the direction of flow, is assumed to be negligible compared with measurement errors.

In reality, it would be desirable to have a complete analysis of all the blades in the test section for the series. This is a prohibitive amount of work when the whole analysis is made using manual methods, but it may be possible to refine the technique and use machine calculation to greatly simplify the work.

The shedding of vortices from blades adjacent to the blade under consideration, is believed to have an effect, of unknown magnitude, on the entire flow field, and

particularly on the blade considered. This would all tend to indicate the desired analysis is of the whole flow field, the center blade in particular, with cross-plots of circulation to determine the effects of other vortex shedding on the circulation around this blade.

In observing pictures of the sequence chosen, it will be seen that a considerable boundary layer exists along the last half inch of the nozzle blade. Also on some of the pictures a fairly large wake off the trailing edge of the nozzle may be observed. Both of these factors make it difficult to determine the exact edge of the blade itself. Although this edge was used as the zero point for measuring peripheral distance, a much better starting point would be one with a specific reference to a stationary object in the test section, notably, one of the vertical reference wires, or the crack in the glass of the test section, which runs horizontally between the blades. (As was mentioned in Ref. 1, this crack does not affect the flow pattern, as can be seen by noting the continuation of the fringes, on both sides of it.)

The centers of the fringes were established as accurately as possible, since these center points correspond most closely with the actual density, hence velocity on the blade. The boundary layer in the vicinity of the trailing edge presented some problems, but use was made of the assumption that the pressure is constant through the boundary layer, in a direction normal to the surface, to establish location of the fringes. This assumption is one conclusion of the order of magnitude analysis of the Navier-Stokes equation.

The following assumptions were made in reducing the data obtained from the photo sequence, and are reviewed here:

- 1.) $f = f_{\infty} = \text{constant}$. Actually the highest velocity on the blade was 432 ft./sec., which corresponds to the 6 1/2 fringe shifts. This is obtained from a value of $f/f_{\infty} = .933245$, which indicates the degree of validity of this assumption.
- 2.) The flow is isentropic and the presence of the boundary layer is neglected.
- 3.) All functions including V , ϕ , and $\frac{\partial \phi}{\partial t}$ are continuous functions.
- 4.) In Bernoulli's Equation, the term ρ/ρ for a given point is considered a constant at any one instant in time. This makes it possible to find the velocity, using an iterative process.
- 5.) The stagnation point on the leading edge of the blade is constant at a peripheral distance from the trailing edge of 2.73 inches.

This last assumption was the object of an extensive analysis. Theoretically, the basis for finding the potential function lies in the fact that one starts at a constant potential, preferably at an infinite distance upstream. However, due to the impracticality of this, the stagnation point on the leading edge was chosen. Since the location of this stagnation point was quite critical a lengthy analysis was made, the results of which are tabulated in Table IX, and discussed in detail in the analysis section of this report. Since the location of this point varied very little, it seemed logical to assume that the location was constant. This, in turn, besides simplifying the analysis, seemed to reduce the fairly large variations in the graphical integrations which followed. On the other hand, in future analyses this assumption and the actual location of the stagnation point should be checked very thoroughly. Errors may actually be introduced by such an assumption.

In addition to the above, an attempt was made to determine the location of the

trailing edge stagnation point, which is a great aid in determining the actual velocity profile around the blade. From examination of the photographs little could be learned, except that the stagnation point is nearly constant, and located very near the trailing edge of the blade. The best indication is that the point is approximately .02 inches from the trailing edge on the pressure side of the blade.

At this point in the analysis it was possible to check all the previous assumptions, calculations, and results by comparing the velocity profile determined from analyzing the pictures with theoretical results.

In Ref. 3, Bueckner and Schnackel, outline a method whereby the theoretical velocity profile around a turbine blade can be found with the aid of high speed computers. The General Electric Company, used this method to find the theoretical velocity profile for the blades under consideration, with unity velocity upstream. The results of this program are plotted in Fig. 26 for an upstream velocity of 80.88 ft./sec., the same value determined for the picture series analyzed. Fig. 25 is a plot of V vs. S for one of the pictures, analyzed to show the type of results obtained in the analysis. Also plotted in Fig. 26 are several of the velocity profiles determined from other of the pictures analyzed. It is very interesting to note the excellent agreement in shape of the profile and in the actual velocities determined. If the theoretical curve is to be the guide, the initial assumptions and analysis are valid and yield excellent results.

For reasons mentioned in the analysis section, only the suction side of the blade was considered in the integration involved to find $\frac{\partial \phi}{\partial z}$. The method of graphical integration used in the analysis was strictly a manual one. Since the velocity curve was continuous with no radical changes in slope, the mean ordinate for relatively

small values of s was multiplied by ds , beginning at $S = 2.73$ in. and progressing at even intervals to $S = .25$ in. It is also possible to use a planimeter or integrator for this type of work. Since the problem becomes one of iteration the best method, by far, would be to utilize a high speed computer.

In the iteration process, values of $\partial\phi/\partial t$ obtained as slopes from Figs. 44 - 53 and Figs. 62 - 71, were taken considering ϕ to be a positive value. Ref. 5 indicates this to be a valid conclusion.

In the interest of simplification, and to reduce calculations, only eight values of V and $\partial\phi/\partial t$ were selected from the curves in the first iteration. These corresponded to reference times, .16, .22, .28, .34, .40, .46, .52, .58 milliseconds. In the second iteration the intermediate times were used to give finite values of $\partial\phi/\partial t$ many of which would have been zero if the same times as for the first iteration had been used. Hence, the times, .19ms., .25ms., and .31ms. etc. were used. It was believed that this choice of different times for the second iteration may have induced errors in the calculations by shifting the velocity curve. To check this hypothesis, the second iteration was recalculated using the same times as for the first iteration, i.e., .16ms., .22ms., .28ms., etc. It was encouraging to note that these additional values did not change the curve, but more exactly defined the shape of the curve. This accounts for the fact that velocities were calculated for fifteen values of time in the second iteration.

Figs. 72 to 74, are plots of V versus t for three values of S , after two iterations. The velocity for the zeroth iteration can be seen to vary for $S = 1.00$ inches, approximately 10 ft./sec. which corresponds to a $1/4$ fringe-shift. For $S = 2.50$

inches, the velocity variation approaches 1/10 fringe shift. This accuracy is considered to be quite adequate for an interferometric type analysis. However, as can also be seen in these figures, the variation for the first and second iteration appears to increase in amplitude. This divergence, and the factor of time, caused the analysts to discontinue the iteration at this point. However, the third or fourth iteration might have begun a converging trend. It is believed that more points for the same time span are necessary, to more accurately portray the true unsteady behavior of the flow. If possible, it is also felt a more constant time interval between each photo is necessary. However, this particular study was more of a feasibility experiment, and thus, the time variation between points is understandable. A possible way to meet both of these requirements is with a very high-speed Fastax-type motion picture camera which would give up to 12 or 16 frames per bucket passing sequence. The advantage of such a camera is that a true time study is made of the flow, where the assumption that the flow exactly repeats itself need not be made.

At this point the photos were checked to note any correlation with the velocity plots in Figs. 72 to 74. The curves would indicate that a change in the flow field should be observed between $t = .34$ ms. and $t = .37$ ms. These times correspond to Figs. 10 and 11 respectively. Unfortunately no appreciable change could be noted, and no indication of any vortex shedding was evident. However, it is thought that the total blade must be considered, and more convergent velocities determined, before any comparison should be made with the interferometric pictures.

When the analysts could not explain the apparent divergence in the velocities, and the poor correlation with interferometric photos, a conference was held with Mr.

Hans Kraft and Mr. R. Fowler of General Electric Company, in July 1960. At this conference, possible sources of errors were discussed.

In the analysis, for reasons previously stated, the nose stagnation point was considered fixed in location on the blade periphery. It was noted this may result in small errors in the potential term, if a small area is neglected in the integration to determine the potential. However, it was assumed that this small error would be negligible when compared with the overall magnitude of the potential. But since ϕ is plotted versus time for a fixed peripheral distance, small plus or minus errors in the integration, due to shift of the stagnation point, could cause substantial changes in the ϕ versus t curve. This change in shape varies the slope of the curves and changes the magnitude of the $\partial\phi/\partial t$ term. This slope is quite critical, since small changes in slope, for the small time intervals considered, may result in large variation in the magnitude of $\partial\phi/\partial t$.

Due to the time element, the magnitude of this error could not be investigated further, but the data already obtained was give a cursory examination. The area involved is quite small, as the shift of the stagnation point was at the most, .05 inches on either side of the assumed stagnation point, $S \pm 2.73$ inches. The resulting error, however, may be compounded in the iterative process, and account for some of the large divergence in velocity from successive iterations.

In order to determine the exact magnitude of any error induced it would be necessary to determine the exact location of the leading edge and trailing edge stagnation points at all times. The approximate location may be obtained from the interferograms if a fringe is located on the leading edge, but this would necessitate a

refinement in interferometric technique and a whole new series of pictures. This, plus the fact, that the techniques used in the analysis can not give the kind of accuracy needed to pinpoint the location exactly, indicate some of the problems involved.

General Electric Company has recently determined the theoretical location of the stagnation point, for various flow conditions. Should a future analysis be made, the location of the stagnation point should certainly be considered, and experimental results compared with the theoretical data of the General Electric Company.

If the iteration process would have converged to a final velocity, the analysis would have required the following steps. First it would be necessary to repeat the process for the entire blade, both suction and pressure sides. Having the final velocities for the blade, the integral of $\hat{V} \cdot d\vec{s}$ around the entire blade, will give the circulation around the blade. By noting the change in circulation with time, and the amount of that change, it may be possible to correlate the shedding of the vortices with changes in circulation, and to determine the strength of the vortices shed.

CONCLUSIONS

Several changes should be made in interferometric technique and in the analysis of the data before concrete results can be obtained.

With regard to technique the following recommendations are made:

- (1) More pictures per bucket passing sequence, should be obtained.
- (2) Equal time spacing, for each of the pictures in the bucket passing sequence, should be obtained.

With regard to analysis of the data, the following recommendations are made:

- (1) The blade to be analyzed should be the center blade in the picture.
- (2) Methods of measuring the distance around the nozzle blade need to be simplified, and at the same time remain accurate. A template to the exact scale of the blade would save considerable time.
- (3) A complete analysis of the location of the leading edge and trailing edge stagnation points, and the variation with flow conditions and time, should be made.
- (4) Since the number of iterations required, and the type of analysis involved indicate a computer solution, the use of a computer to speed the analysis, and to more easily investigate the effect of variations in the parameters involved, is recommended.

In general, three other recommendations are also made,

- (1) For a more complete analysis, the flow fields around the other blades, and their effect on the blade being analyzed should be investigated.

- (2) An investigation into the assumption that the flow repeats itself, should be conducted before future analyses are made with regard to vortex shedding.
- (3) An order of error analysis should be made to determine the magnitude of the error induced by neglecting the shift of the stagnation point. Such analyses should also be made for errors induced in analyzing the interferometric picture, plotting the data and determining $\partial\phi/\partial t$.

Although as stated in the discussion, it was impossible to correlate the results of this report, with the interferometric pictures, this type of analysis appears to be feasible. Good correlation was obtained between the experimental and theoretical velocity distributions around the blade. The assumptions made appear to be valid, except for that of a constant leading edge stagnation point. Therefore, using the above recommendations, it should be possible to ultimately determine the actual flow around a nozzle blade, and to also quantitatively establish the strength of the shed vortex.

REFERENCES

1. Cullen, R. E. and Poe, H. R., "Preliminary Studies of the Nonsteady Flow of Air through a Radial, Single Stage Turbine Using the Mach-Zehnder Interferometer", University of Michigan Research Institute, Report No. 2388 - 13 - P, Ann Arbor, Michigan, August 1958.
2. Cullen, R. E., "The Recent Experiments in the Interferometric Turbine Study at the University of Michigan", Preliminary Status Report, Ann Arbor, Michigan, 1958.
3. Bueckner, H. F., and Schnackel, H. C., "The Calculation of Incompressible Flow through Turbine Cascades", Paper Presented at the 1959 Annual Meeting of the American Society of Mechanical Engineers, November 30 - December 4, 1959, Atlantic City, New Jersey.
4. Lamb, H., "Hydrodynamics", Sixth Edition, Cambridge University Press, London, 1932.
5. Kuethe, A. M. and Schetzer, J. D., "Foundations of Aerodynamics", John Wiley and Sons, Inc., New York, 1950.

GENERAL REFERENCES

1. Milne - Thomson, L. M., "Theoretical Aerodynamics, 3rd Edition, MacMillan and Company, Ltd., London, 1958.
2. Rauscher, M., "Introduction to Aeronautical Dynamics", John Wiley and Sons, New York, 1953.

TABLE I

CONVERSION OF ISOPYCNIC FRINGES TO VELOCITY

1	2	3	4	5	6	7	8	9	10
Fringe	ρ/ρ_0	$\log \rho/\rho_0$	$4 \log \rho/\rho_0$	$(\rho/\rho_0)^4$	$14.2022(\rho/\rho_0)^4$	$\rho_0/\rho/\rho_0$	(7)-(6)	$A \times (8) = V^2$	V
0	1	-	-	1	14.2022	14.2533	.0511	6,542.65	80.88
1/2	.994865	9.99777-10	-1.99911	.99795	14.1731	14.3269	.1538	19,686.8	140.25
1	.989730	9.99552-10	-1.99821	.99588	14.1437	14.4012	.2575	32,969	181.5
1 1/2	.984595	9.99326-10	-1.997304	.99381	14.1143	14.4763	.3620	46,349	215.3
2	.979460	9.99098-10	-1.996392	.99173	14.0847	14.5522	.4675	59,857	244.6
2 1/2	.974325	9.98870-10	-1.99548	.98965	14.0552	14.6289	.5737	73,454	271.0
3	.969190	9.98641-10	-1.994564	.98756	14.0255	14.7064	.6809	87,180	295.2
3 1/2	.964055	9.98410-10	-1.99364	.98546	13.9957	14.7847	.7890	101,021	317.9
4	.958920	9.98178-10	-1.99271	.98335	13.9657	14.8639	.8982	115,002	339.1
4 1/2	.953785	9.97945-10	-1.99178	.98125	13.9359	14.9439	1.0080	129,061	359.3
5	.948650	9.97711-10	-1.99084	.97912	13.9057	15.0248	1.1191	143,285	378.5
5 1/2	.943515	9.97475-10	-1.98990	.97702	13.8758	15.1066	1.2308	157,587	396.8
6	.938380	9.97238-10	-1.98895	.97488	13.8454	15.1893	1.3439	172,068	414.7
6 1/2	.933245	9.96999-10	-1.98800	.97275	13.8152	15.2728	1.4576	186,626	432.0
7	.928110	9.96760-10	-1.98704	.97060	13.7847	15.3573	1.5726	201,350	448.7

A = 128036.26

SAMPLE CALCULATION (FOR 1/2 FRINGE SHIFT)

$$V = \sqrt{\frac{2 \times 4 \times 144 (\rho_0 - \rho)}{\rho/\rho_0 \times \rho_0}} = \sqrt{\frac{2 \times 4 \times 144}{.072371} \left(\frac{\rho_0}{\rho/\rho_0} - \rho_0 \left(\frac{\rho}{\rho_0} \right)^{8-1} \right)}$$

FOR $\gamma = 1.4$:

$$V = \sqrt{128,036.26 \left(\frac{14.2533}{\rho/\rho_0} - 14.2022 \left(\frac{\rho}{\rho_0} \right)^4 \right)}$$

FOR 1/2 FRINGE:

$$V = \sqrt{128,036.26 \left(\frac{14.2533}{.994865} - 14.2022 (.99795) \right)} = \sqrt{19686.8} = 140.25 \frac{FT}{SEC}$$



TABLE II
SAMPLE CONVERSION OF ROUGH DATA TO
CORRECTED DATA

UM Photo Number 435				
Ref. Length .41 Inches				
Right Hand Blade Analyzed				
dS' Between Points Uncorrected	$\Sigma dS'$ From Tip Uncorrected	ΣdS Corrected $\Sigma dS' \times \frac{496}{7.68}$	V Feet/Second	Non Dimensional V V/80.88
.06	.06	.04	359.3	3.82
.35	.41	.27	396.8	4.21
.57	.98	.64	414.7	4.41
.57	1.55	1.005	396.8	4.21
.21	1.76	1.14	359.3	3.82
.20	1.96	1.27	317.9	3.38
.30	2.26	1.47	271.0	2.95
.50	2.76	1.79	215.3	2.32
.78	3.54	2.30	140.25	1.56
1.14	4.68	3.04	-140.25	-1.56
.40	5.08	3.30	-159.0	-1.735
.58	5.66	3.68	-140.25	-1.56
1.20	6.86	4.45	-181.5	-1.98
.29	7.15	4.64	-215.3	-2.32
.29	7.44	4.82	-271.0	-2.95
.13	7.57	4.91	-317.9	-3.38
.11	7.68	4.98	-359.3	-3.82

TABLE III
VELOCITY VERSUS PERIPHERAL DISTANCE FOR
PICTURE SEQUENCE UM 435 TO UM 458

UM 435		UM 436		UM 437	
S	V	S	V	S	V
.04	359.3	.06	378.5	.04	378.5
.27	396.8	.232	396.8	.27	396.8
.64	414.7	.513	414.7	.70	414.7
1.005	396.8	.807	396.8	1.03	396.8
1.14	359.3	.911	359.3	1.19	359.3
1.27	317.9	1.30	317.9	1.31	317.9
1.47	271.0	1.488	271.0	1.51	271.0
1.79	215.3	1.850	215.3	1.89	215.3
2.30	140.25	2.36	140.25	2.42	140.25
2.73	0	2.73	0	2.73	0
3.04	-140.25	3.00	-140.25	2.94	-140.25
3.30	-159.0	3.32	-181.50	3.34	-181.5
3.68	-140.25	3.81	-140.25	3.71	-140.25
4.45	-181.5	4.02	-159.0	4.28	-181.5
4.64	-215.3	4.39	-181.5	4.65	-215.3
4.82	-271.0	4.65	-215.3	4.85	-271.0
4.91	-317.9	4.84	-271.0	4.93	-317.9
4.98	-359.3	4.93	-317.9	4.98	-359.3
		4.98	-359.3		

t = 0 ms

t = .0707ms

t = .0774ms

S - inches

V - ft/sec

t - Relative Time, Milliseconds

Table III (Continued)

UM 438		UM 439		UM 440	
S	V	S	V	S	V
.15	378.5	.10	378.5	.10	378.5
.34	396.8	.26	396.8	.27	396.8
.69	414.7	.67	414.7	.68	406.1
1.02	396.8	1.03	396.8	.995	396.6
1.16	359.3	1.16	359.3	1.13	359.3
1.29	317.9	1.29	317.9	1.26	317.9
1.52	271.0	1.50	271.0	1.47	271.0
1.86	215.3	1.87	215.3	1.84	215.3
2.40	140.25	2.34	140.25	2.35	140.25
2.73	0	2.73	0	2.73	0
2.94	-140.25	2.93	-140.25	3.02	-140.25
3.27	-181.50	3.23	-159.0	3.28	-159.0
3.88	-140.25	3.62	-140.25	3.61	-140.25
4.43	-181.50	3.86	-159.0	3.89	-159.0
4.64	-215.3	4.40	-181.50	4.47	-181.50
4.84	-271.0	4.64	-215.3	4.71	-215.3
4.93	-317.9	4.83	-271.0	4.86	-271.0
4.98	-359.3	4.92	-317.9	4.94	-317.9
		4.98	-359.3	4.98	-359.3
t = .1148ms		t = .1585ms		t = .1753ms	

Table II (Continued)

UM 441		UM 442		UM 443	
S	V	S	V	S	V
.078	378.5	.14	378.5	.13	378.5
.239	396.8	.36	396.8	.34	396.8
.64	409.0	.68	414.7	.69	414.7
1.02	396.8	.99	396.8	1.01	396.8
1.15	359.3	1.13	359.3	1.16	359.3
1.27	317.9	1.26	317.9	1.30	317.9
1.46	271.0	1.42	271.0	1.47	271.0
1.81	215.3	1.71	215.3	1.77	215.3
2.30	140.25	2.23	140.25	2.29	140.25
2.73	0	2.73	0	2.73	0
3.08	-140.25	3.02	- 80.7	3.02	- 80.7
3.33	-159.0	3.62	- 80.7	3.59	- 80.7
3.78	-140.25	4.00	-108.0	4.00	- 80.7
4.07	-140.25	4.30	-140.25	4.27	-140.25
4.55	-181.50	4.70	-215.3	4.69	-215.3
4.70	-215.3	4.85	-271.0	4.86	-271.0
4.86	-271.0	4.94	-317.9	4.94	-317.9
4.93	-317.9	4.98	-359.3	4.98	-359.3
4.98	-359.3				
t = .2159ms		t = .2832ms		t = .3102ms	

Table III (Continued)

UM 444		UM 445		UM 446	
S	V	S	V	S	V
.13	378.5	.13	378.5	.14	378.5
.32	396.8	.30	396.8	.33	396.8
.67	414.7	.66	414.7	.69	414.7
1.05	396.8	1.02	396.8	1.04	396.8
1.17	359.3	1.15	359.3	1.18	359.3
1.30	317.9	1.28	317.9	1.30	317.9
1.48	271.0	1.46	271.0	1.46	271.0
1.82	215.3	1.83	215.3	1.80	215.3
2.28	140.25	2.32	140.25	2.27	140.25
2.73	0	2.73	0	2.73	0
3.16	-140.25	3.11	-140.25	3.17	-127.0
3.63	-110.00	3.32	-140.25	3.70	-108.0
3.90	-140.25	3.59	-127.00	4.34	-140.25
4.16	-140.25	4.17	-140.25	4.70	-215.3
4.54	-181.5	4.55	-181.50	4.85	-271.0
4.69	-215.3	4.70	-215.30	4.93	-317.9
4.87	-271.0	4.88	-271.0	4.98	-359.3
4.95	-317.9	4.94	-317.9		
4.98	-359.3	4.98	-359.3		
t = .3408 ms		t = .3679ms		t = .3980ms	



Table III (Continued)

UM 447		UM 448		UM 449	
S	V	S	V	S	V
.153	378.5	.079	378.5	.08	396.8
.312	396.8	.19	396.8	.301	414.7
.681	414.7	.734	420.2	.671	426.7
1.05	396.8	1.07	396.8	1.05	396.8
1.18	359.3	1.13	359.3	1.17	359.3
1.31	317.9	1.31	317.9	1.30	317.9
1.49	271.0	1.52	271.0	1.51	271.0
1.81	215.3	1.83	215.3	1.87	215.3
2.22	140.25	2.26	140.25	2.35	140.25
2.73	0	2.73	0	2.73	0
3.15	-127.0	3.17	-132.0	3.14	-132.0
3.75	-110.0	3.77	-110.0	3.80	-110.0
4.44	-140.25	4.33	-140.25	4.32	-140.25
4.71	-215.3	4.68	-215.3	4.70	-215.3
4.85	-271.0	4.85	-271.0	4.84	-271.0
4.93	-317.9	4.91	-317.9	4.92	-317.9
4.98	-359.3	4.98	-359.3	4.98	-359.3
t = .4687ms		t = .4785ms		t = .5227ms	



Table III (Continued)

UM 450		UM 451		UM 452	
S	V	S	V	S	V
.10	396.8	.05	396.8	.065	396.8
.36	414.7	.32	414.7	.28	405.7
.74	420.2	.695	429.0	.72	414.7
1.05	396.8	1.06	396.8	1.00	396.8
1.17	359.3	1.17	359.3	1.14	359.3
1.30	317.9	1.29	317.9	1.26	317.9
1.46	271.0	1.47	271.0	1.42	271.0
1.81	215.3	1.82	215.3	1.75	215.3
2.30	140.25	2.35	140.25	2.25	140.25
2.73	0	2.73	0	2.73	0
3.14	-127.0	3.17	-132.0	3.15	-120.6
3.79	-108.0	3.75	-109.0	3.75	- 87.6
4.40	-140.25	4.25	-140.25	4.31	-140.25
4.71	-215.3	4.67	-215.3	4.67	-215.30
4.85	-271.0	4.84	-271.0	4.85	-271.0
4.93	-317.9	4.93	-317.9	4.93	-317.9
4.98	-359.3	4.98	-359.3	4.98	-359.3
t = .5393ms		t = .5799ms		t = .5934ms	

Table III (Continued)

UM 453	
S	V
.045	396.8
.28	414.7
.65	438.0
1.02	396.8
1.14	359.3
1.27	317.9
1.45	271.0
1.80	215.3
2.32	140.25
2.73	0
3.05	-140.25
3.26	-157.50
4.07	-140.25
4.47	-181.5
4.69	-215.3
4.85	-271.0
4.92	-317.9
4.98	-359.3

t = .6370ms

UM 454	
S	V
.065	396.8
.375	432.0
.634	448.7
.873	432.0
1.04	396.8
1.16	359.3
1.27	317.9
1.43	271.0
1.76	215.3
2.26	140.25
2.73	0
2.99	-140.25
3.34	-157.50
4.03	-140.25
4.47	-181.50
4.64	-215.3
4.83	-271.0
4.93	-317.9
4.98	-359.3

t = .6838ms

UM 455	
S	V
.052	378.5
.117	396.8
.38	432.0
.606	448.7
.80	432.0
1.03	396.8
1.17	359.3
1.28	317.9
1.45	271.0
1.76	215.3
2.22	140.25
2.73	0
3.22	-140.25
3.68	-110.00
4.09	-140.25
4.47	-181.50
4.77	-215.3
4.84	-271.0
4.92	-317.9
4.98	-359.3

t = .7357ms



Table III (Continued)

UM 456		UM 457		UM 458	
S	V	S	V	S	V
.11	396.8	.08	359.3	.08	359.3
.20	414.7	.15	378.5	.15	396.8
.38	432.0	.39	396.8	.33	414.7
.72	432.0	.76	414.7	.61	432.0
1.00	396.8	1.00	396.8	1.02	396.8
1.13	359.3	1.14	359.3	1.14	359.3
1.25	317.9	1.24	317.9	1.26	317.9
1.44	271.0	1.43	271.0	1.41	271.0
1.80	215.3	1.74	215.3	1.78	215.3
2.24	140.25	2.28	140.25	2.29	140.25
2.73	0	2.73	0	2.73	0
3.13	-132.0	3.12	-127.0	3.08	-140.25
3.71	-110.0	3.76	-127.0	3.71	-127.0
4.31	-140.25	4.24	-140.25	4.20	-140.25
4.68	-215.3	4.67	-215.3	4.53	-181.5
4.85	-271.0	4.85	-271.0	4.69	-215.3
4.93	-317.9	4.91	-317.9	4.85	-271.0
4.98	-359.3	4.98	-359.3	4.92	-317.9
				4.98	-359.3
t = .7669ms		t = .8163ms		t = .8344ms	

TABLE IV
CONVERSION OF REFERENCE DISTANCES
TO REFERENCE TIME

UM Number	Reference Distance (Uncorrected) Inches	Reference Distance (Corrected) Inches	Reference Distance From Zero Inches	Reference Time Milliseconds
435	.41	.266	0	0
436	.20	.130	.136	.070662
437	.18	.117	.149	.077417
438	.07	.045	.221	.114827
439	- .06	- .039	.305	.158471
440	- .11	- .0714	.3375	.175306
441	- .23	- .1495	.4155	.215885
442	- .43	- .279	.5450	.283171
443	- .51	- .331	.597	.310189
444	- .60	- .390	.656	.340844
445	- .68	- .442	.708	.367862
446	- .77	- .50	.766	.397998
447	- .98	- .636	.902	.468661
448	-1.01	- .655	.921	.478533
449	-1.14	- .740	1.006	.522697
450	-1.19	- .772	1.038	.539323
451	-1.31	- .850	1.116	.579851
452	-1.35	- .876	1.142	.593360
453	-1.48	- .96	1.226	.637004
454	-1.62	-1.05	1.316	.683767
455	-1.77	-1.15	1.416	.735725
456	-1.87	-1.21	1.476	.766899
457	-2.01	-1.305	1.571	.816259
458	-2.06	-1.34	1.606	.834445

TABLE V
VELOCITY AND POTENTIAL VERSUS TIME
FOR SELECTED PERIPHERAL DISTANCES

FIRST ITERATION

<u>UM</u> <u>Pictures</u>	<u>Ref. Time</u>	<u>S = 2.50</u> <u>V</u>	<u>S = 2.25</u> <u>V</u>	<u>S = 2.00</u> <u>V</u>
438	.1148	126	169	195
439	.1585	118	152	189
440	.1753	119	153	188
441	.2159	111	148	187
442	.2832	108	138	173
443	.3102	112	145	180
444	.3408	113	145	181
445	.3679	118	150	183
446	.3980	113	144	177
447	.4687	109	136	175
448	.4785	110	141	182
449	.5227	118	155	193
450	.5393	115	148	184
451	.5799	120	155	191
452	.5934	109	141	178
453	.6370	114	150	186
		<u>S = 1.75</u>	<u>S = 1.50</u>	<u>S = 1.25</u>
438	.1148	235	280	330
439	.1585	228	274	327
440	.1753	226	270	319
441	.2159	225	265	322
442	.2832	212	256	320
443	.3102	218	255	331
444	.3408	223	268	334
445	.3679	220	264	329
446	.3980	215	262	335
447	.4687	221	271	336
448	.4785	226	276	335
449	.5227	234	282	337
450	.5393	224	269	321
451	.5799	228	267	329
452	.5934	216	258	319
453	.6370	223	264	321

Table V (Continued)

UM Pictures	Ref. Time	S = 1.00 V	S = .75 V	S = .50 V
438	.1148	400	415	405
439	.1585	398	414	412
440	.1753	395	405	405
441	.2159	398	407	409
442	.2832	395	415	408
443	.3102	398	415	408
444	.3408	404	415	410
445	.3679	399	414	411
446	.3980	403	415	408
447	.4687	403	414	411
448	.4785	408	421	416
449	.5227	403	425	424
450	.5393	403	420	420
451	.5799	405	429	425
452	.5934	397	414	414
453	.6370	402	434	427
		S = .25		
438	.1148	388		
439	.1585	396		
440	.1753	395		
441	.2159	398		
442	.2832	388		
443	.3102	390		
444	.3408	392		
445	.3679	391		
446	.3980	390		
447	.4687	390		
448	.4785	403		
449	.5227	411		
450	.5393	408		
451	.5799	410		
452	.5934	405		
453	.6370	411		

TABLE V-a

VELOCITY AND POTENTIAL VERSUS TIME

FOR SELECTED PERIPHERAL DISTANCES

FIRST ITERATION

UM Pictures	Ref. Time	S = 2.50 <u>ϕ</u>	S = 2.25 <u>ϕ</u>	S = 2.00 <u>ϕ</u>
438	.1148	17.54	55.79	100.04
439	.1585	16.45	50.45	92.95
440	.1753	16.65	50.90	93.40
441	.2159	15.92	48.42	90.17
442	.2832	15.85	45.60	84.10
443	.3102	16.30	48.55	89.30
444	.3408	16.61	48.11	88.86
445	.3679	17.14	50.64	92.14
446	.3980	16.67	48.92	88.92
447	.4687	16.12	46.62	86.62
448	.4785	16.47	47.58	88.85
449	.5227	16.62	50.62	94.12
450	.5393	16.71	49.46	90.96
451	.5799	17.11	51.36	94.36
452	.5934	16.41	47.41	86.91
453	.6370	16.62	50.62	92.37
		S = 1.75 <u></u>	S = 1.50 <u></u>	S = 1.25 <u></u>
438	.1148	153.54	217.54	293.29
439	.1585	144.95	207.70	284.70
440	.1753	145.15	206.65	279.90
441	.2159	141.92	203.42	275.42
442	.2832	132.10	190.35	261.60
443	.3102	139.05	199.05	273.05
444	.3408	139.36	200.61	275.61
445	.3679	142.64	202.89	278.64
446	.3980	137.92	197.15	270.66
447	.4687	135.12	196.47	271.47
448	.4785	138.58	201.08	277.33
449	.5227	147.12	211.62	288.37
450	.5393	141.71	203.46	276.71
451	.5799	146.61	208.61	281.86
452	.5934	136.16	195.16	265.66
453	.6370	143.37	204.37	276.62

Table V-a (Continued)

UM Pictures	Ref. Time	S = 1.00 <u>ϕ</u>	S = .75 <u>ϕ</u>	S = .50 <u>ϕ</u>
438	.1148	385.79	488.54	591.54
439	.1585	377.25	479.25	582.75
440	.1753	370.40	471.15	572.65
441	.2159	367.17	468.17	570.42
442	.2832	351.35	454.10	557.35
443	.3102	364.80	467.30	570.55
444	.3408	369.61	472.61	575.86
445	.3679	370.14	472.64	575.89
446	.3980	365.67	468.67	571.92
447	.4687	366.12	468.87	572.62
448	.4785	372.33	477.08	582.08
449	.5227	382.62	486.62	593.12
450	.5393	370.46	474.95	579.21
451	.5799	376.11	480.61	586.86
452	.5934	357.16	459.16	563.16
453	.6370	368.87	474.12	582.12
		<u>S = .25</u>		
438	.1148	691.04		
439	.1585	684.50		
440	.1753	673.15		
441	.2159	672.67		
442	.2832	657.20		
443	.3102	670.80		
444	.3408	676.36		
445	.3679	676.64		
446	.3980	671.92		
447	.4687	673.12		
448	.4785	685.08		
449	.5227	698.12		
450	.5393	683.21		
451	.5799	691.61		
452	.5934	665.66		
453	.6370	688.62		

TABLE VI (1)

DETERMINATION OF CORRECTED
VELOCITY BY FIRST ITERATION

t = .16 ms					
S	V	V ²	$\partial\phi/\partial t$	$V^2 \partial\phi/\partial t$	Vcorr
2.73	0	0	0	0	0
2.50	118.0	13,924	- 1,540	15,464	124.3
2.25	152.7	23,340	- 5,660	29,000	170.3
2.00	189.3	35,830	- 9,820	45,650	213.7
1.75	229.0	52,441	-13,020	65,461	255.8
1.50	273.0	74,529	-14,450	98,979	314.7
1.25	323.2	104,329	-16,120	120,449	347.0
1.00	397.8	158,200	-24,850	183,050	427.9
.75	409.6	167,750	-22,222	189,972	435.7
.50	408.6	166,850	-22,222	189,072	434.8
.25	395.0	156,025	-18,050	174,075	417.2

t = .22					
S	V	V ²	$\partial\phi/\partial t$	$V^2 \partial\phi/\partial t$	Vcorr
2.73	0	0	0	0	0
2.50	111.3	12,400	- 625	13,025	114.1
2.25	145.0	21,025	- 3,560	24,585	156.7
2.00	181.5	32,900	- 7,360	40,260	200.5
1.75	219.6	47,250	-11,100	58,350	241.6
1.50	263.5	69,350	-11,400	80,750	284.1
1.25	320.5	102,700	-14,600	117,300	342.5
1.00	396.0	156,816	-14,600	171,416	414.0
.75	407.6	166,100	-14,850	180,950	425.4
.50	408.2	166,600	-16,800	183,400	428.3
.25	397.8	158,200	-23,300	181,500	426.0

TABLE VI (2)

t = .28					
S	V	V ²	$\partial\phi/\partial t$	$V^2 - \frac{\partial\phi}{\partial t}$	Vcorr
2.73	0	0	0	0	0
2.50	108.2	11,720	973	10,747	103.5
2.25	139.0	19,321	-1,500	20,821	144.2
2.00	176.0	30,976	0	30,976	176.0
1.75	212.2	45,000	-1,390	46,390	215.4
1.50	256.1	65,600	-1,805	67,405	260.6
1.25	325.5	106,000	0	106,000	325.5
1.00	395.5	156,600	-1,529	158,129	397.6
.75	414.2	171,400	0	171,400	414.2
.50	408.0	166,500	-7,000	173,500	416.6
.25	387.9	150,000	4,860	145,140	381.0

t = .34					
S	V	V ²	$\partial\phi/\partial t$	$V^2 - \frac{\partial\phi}{\partial t}$	Vcorr
2.73	0	0	0	0	0
2.50	113.5	12,880	1,250	11,630	108.0
2.25	146.5	21,450	5,410	16,040	126.6
2.00	182.7	33,400	7,980	25,420	159.5
1.75	222.8	49,700	10,410	39,290	198.1
1.50	267.6	71,600	8,680	62,920	250.9
1.25	331.8	110,000	9,450	100,550	317.0
1.00	403.5	162,800	6,530	156,270	395.3
.75	415.0	172,225	4,720	167,505	409.3
.50	410.0	168,100	6,600	161,500	401.8
.25	391.8	153,500	7,640	145,860	381.8

TABLE VI (3)

t = .40					
S	V	V ²	$\partial\phi/\partial t$	$V^2 - \partial\phi/\partial t$	Vcorr
2.73	0	0	0	0	0
2.50	114.5	13,100	- 1,320	14,420	120.0
2.25	145.0	21,025	- 5,000	26,025	161.1
2.00	176.5	31,150	-11,650	42,800	206.9
1.75	214.8	46,100	-21,700	67,800	260.4
1.50	261.8	68,500	-14,450	82,950	288.0
1.25	334.6	111,900	-15,300	127,200	356.8
1.00	401.6	161,250	- 7,500	168,750	410.7
.75	414.1	171,450	- 5,960	177,410	421.2
.50	409.5	167,600	- 5,280	172,880	415.7
.25	389.6	151,800	-20,900	172,700	415.6

t = .46					
S	V	V ²	$\partial\phi/\partial t$	$V^2 - \frac{\partial\phi}{\partial t}$	Vcorr
2.73	0	0	0	0	0
2.50	109.6	12,000	0	12,000	109.6
2.25	140.8	19,810	833	18,977	137.7
2.00	174.5	30,420	3,750	26,670	163.5
1.75	218.0	47,524	3,190	44,344	210.6
1.50	265.8	70,650	5,980	64,670	254.2
1.25	335.6	112,600	16,120	96,480	310.7
1.00	404.1	163,300	5,980	157,320	396.8
.75	415.4	172,500	8,330	164,170	405.2
.50	411.4	169,300	10,000	159,300	399.1
.25	389.5	151,700	15,280	136,420	369.4

TABLE VI (4)

t = .52					
S	V	V ²	$\partial\phi/\partial t$	$V^2 \partial\phi/\partial t$	Vcorr
2.73	0	0	0	0	0
2.50	114.6	13,150	556	12,594	112.1
2.25	149.6	22,400	4,100	18,300	135.2
2.00	188.6	35,600	2,910	32,690	183.5
1.75	233.8	54,600	3,850	50,750	229.5
1.50	282.0	79,524	1,667	77,857	279.0
1.25	335.2	112,350	7,500	104,850	323.8
1.00	403.6	162,900	4,580	158,320	397.8
.75	423.5	179,300	3,470	175,830	419.2
.50	420.8	-	0	-	420.8
.25	409.5	-	0	-	409.5

t = .58					
S	V	V ²	$\partial\phi/\partial t$	$V^2 \partial\phi/\partial t$	Vcorr
2.73	0	0	0	0	0
2.50	117.3	-	0	-	117.3
2.25	153.4	23,530	417	23,113	152.0
2.00	186.3	34,700	-5,140	39,840	199.5
1.75	223.3	49,825	-5,000	54,825	234.2
1.50	261.2	68,200	-8,890	77,090	277.7
1.25	326.4	106,500	-9,880	116,380	341.2
1.00	404.5	163,600	-11,670	175,270	418.7
.75	423.9	179,500	-9,310	188,810	434.7
.50	424.2	179,900	-7,230	187,130	432.6
.25	408.4	166,600	-7,920	174,520	417.7

TABLE VII
VELOCITY AND POTENTIAL VERSUS TIME
FOR SELECTED PERIPHERAL DISTANCES
SECOND ITERATION

τ MILLISEC. Ref. Time	S = 2.50		S = 2.25		S = 2.00	
	V	ϕ	V	ϕ	V	ϕ
.16	124.3	17.81	170.3	54.81	213.7	102.81
.22	114.1	16.78	156.7	50.53	200.5	95.03
.28	103.5	15.16	144.2	46.91	176.0	86.91
.34	108.0	16.54	126.6	45.04	159.5	80.29
.40	120.0	17.34	161.1	52.59	206.9	98.09
.46	109.6	16.42	137.7	46.92	163.5	85.67
.52	112.1	17.04	135.2	47.04	183.5	87.04
.58	117.3	17.24	152.0	50.24	199.5	93.74

Ref. Time	S = 1.75		S = 1.50		S = 1.25	
	V	ϕ	V	ϕ	V	ϕ
.16	255.8	161.81	314.7	232.56	347.0	316.06
.22	241.6	150.03	284.1	215.53	342.5	293.53
.28	215.4	135.41	260.6	194.41	325.5	270.41
.34	198.1	125.29	250.9	182.04	317.0	252.54
.40	260.4	155.09	288.0	223.84	356.8	305.59
.46	210.6	133.67	254.2	191.92	310.7	262.42
.52	229.5	138.19	279.0	202.29	323.8	277.79
.58	234.2	147.49	277.7	210.99	341.2	287.74

Ref. Time	S = 1.00		S = .75		S = .50	
	V	ϕ	V	ϕ	V	ϕ
.16	427.9	417.31	435.7	525.81	434.8	634.81
.22	414.0	389.78	425.4	495.03	428.3	601.78
.28	397.6	362.41	414.2	464.41	416.6	568.66
.34	395.3	342.92	409.3	444.42	401.8	546.42
.42	410.7	401.84	421.2	506.34	415.7	610.59
.46	396.8	352.67	405.2	453.42	399.1	554.67
.52	397.8	367.66	419.2	470.66	420.8	576.16
.58	418.7	385.24	434.7	492.24	432.6	599.74

TABLE VII (Continued)

<u>Ref. Time</u>	S = .25	
	<u>V</u>	<u>ϕ</u>
.16	417.2	741.56
.22	426.0	708.53
.28	381.0	670.41
.34	381.8	644.67
.40	415.6	714.34
.46	369.4	651.42
.52	409.5	680.16
.58	417.7	706.24

TABLE VIII (1)

DETERMINATION OF CORRECTED
VELOCITY BY SECOND ITERATION

t = .16					
S	Va	Va ²	$\partial\phi/\partial t$	$V^2 - \partial\phi/\partial t$	Vcorr
2.73	0	0	-	-	-
2.50	118.0	13,924	- 750	14,674	121.1
2.25	152.7	23,340	- 7,500	30,840	175.6
2.00	189.3	35,830	-11,100	46,930	216.7
1.75	229.0	52,441	-13,600	66,041	257.0
1.50	273.0	74,529	-18,200	92,729	304.5
1.25	323.2	104,329	-21,400	135,729	368.5
1.00	397.8	158,200	-29,900	188,100	433.7
.75	409.6	167,750	-39,200	206,950	454.8
.50	408.6	166,850	-51,400	218,250	467.2
.25	395.0	156,025	-35,400	191,425	437.5

t = .22					
S	Va	Va ²	$\partial\phi/\partial t$	$V^2 - \partial\phi/\partial t$	Vcorr
2.73	0	0	-	-	-
2.50	111.3	12,400	- 3,680	16,080	126.7
2.25	145.0	21,025	- 5,550	26,575	163.0
2.00	181.5	32,900	-11,100	44,000	209.8
1.75	219.6	47,250	-17,350	64,600	254.1
1.50	263.5	69,350	-29,700	99,050	314.7
1.25	320.5	102,700	-31,700	134,400	366.7
1.00	396.0	156,816	-41,700	198,516	445.5
.75	407.6	166,100	-45,000	211,100	459.5
.50	408.2	166,600	-46,100	212,700	461.2
.25	397.8	158,200	-52,500	210,700	459.0

TABLE VIII (2)

t = .28					
S	V	V ²	$\partial\phi/\partial t$	$V^2 - \partial\phi/\partial t$	Vcorr
2.73	0	0	-	-	-
2.50	108.2	11,720	- 570	12,290	110.9
2.25	139.0	19,321	- 3,610	22,931	151.3
2.00	176.0	30,976	-11,100	42,076	205.1
1.75	212.2	45,000	-23,100	68,100	260.9
1.50	256.1	65,600	-24,400	90,000	300.0
1.25	325.5	106,000	-28,500	134,500	366.8
1.00	395.5	156,600	-35,200	191,800	437.9
.75	414.2	171,400	-38,700	210,100	458.5
.50	408.0	166,500	-37,500	204,000	451.7
.25	387.9	150,000	-45,000	195,000	441.7

t = .34					
S	V	V ²	$\partial\phi/\partial t$	$V^2 - \partial\phi/\partial t$	Vcorr
2.73	0	0	0	-	-
2.50	113.5	12,880	2,080	10,800	103.9
2.25	146.5	21,450	- 505	21,955	148.2
2.00	182.7	33,400	- 6,250	39,650	194.0
1.75	222.8	49,700	3,190	52,890	230.0
1.50	267.6	71,600	0	71,600	267.6
1.25	331.8	110,000	0	110,000	331.8
1.00	403.5	162,800	0	162,800	403.5
.75	415.0	172,225	0	172,225	415.0
.50	410.0	168,100	0	168,100	410.0
.25	391.8	153,500	0	153,500	391.8

TABLE VIII (3)

t = .40					
S	V	V ²	$\partial\phi/\partial t$	$V^2 - \partial\phi/\partial t$	Vcorr
2.73	0	0	-	-	-
2.50	114.5	13,100	0	13,100	114.5
2.25	145.0	21,025	4,170	16,855	129.9
2.00	176.5	31,150	2,430	28,720	169.5
1.75	214.8	46,100	0	46,100	214.8
1.50	261.8	68,500	0	68,500	261.8
1.25	334.6	111,900	0	111,900	334.6
1.00	401.6	161,250	0	161,250	401.6
.75	414.1	171,450	0	171,450	414.1
.50	409.5	167,600	0	-	409.5
.25	389.6	151,800	0	-	389.6

t = .46					
S	V	V ²	$\partial\phi/\partial t$	$V^2 - \partial\phi/\partial t$	Vcorr
2.73	0	0	-	-	-
2.50	109.6	12,000	- 500	12,500	111.8
2.25	140.8	19,810	- 2,710	22,520	150.0
2.00	174.5	30,420	- 8,470	38,890	197.2
1.75	218.0	47,524	- 2,920	50,444	224.6
1.50	265.8	70,650	0	70,650	265.8
1.25	335.6	112,600	0	112,600	335.6
1.00	404.1	163,300	0	163,300	404.1
.75	415.4	172,500	0	172,500	415.4
.50	411.4	169,300	0	-	411.4
.25	389.5	151,700	0	-	389.5

TABLE VIII (4)

t = .52					
S	V	V ²	$\partial\phi/\partial t$	$V^2 - \frac{\partial\phi}{\partial t}$	Vcorr
2.73	0	0	-	-	-
2.50	114.6	13,150	625	12,525	112.0
2.25	149.6	22,400	2,640	19,760	140.7
2.00	188.6	35,600	7,640	27,960	167.4
1.75	233.8	54,600	12,200	42,400	205.9
1.50	282.0	79,524	17,100	62,424	249.9
1.25	335.2	112,350	22,500	89,850	299.8
1.00	403.6	162,900	23,300	139,600	373.7
.75	423.5	179,300	28,100	151,200	388.8
.50	420.8	177,000	32,500	144,500	380.1
.25	409.5	167,700	45,000	122,700	350.3

t = .58					
S	V	V ²	$\partial\phi/\partial t$	$V^2 - \frac{\partial\phi}{\partial t}$	Vcorr
2.73	0	0	-	-	-
2.50	117.3	13,760	139	13,521	116.2
2.25	153.4	23,530	6,390	17,140	131.0
2.00	186.3	34,700	11,100	23,600	153.7
1.75	223.3	49,825	10,830	38,995	197.5
1.50	261.2	68,200	4,580	63,620	252.3
1.25	326.4	106,500	4,450	102,050	319.5
1.00	404.5	163,600	25,300	138,300	371.9
.75	423.9	179,500	31,700	147,800	384.5
.50	424.2	179,900	32,500	147,400	384.0
.25	408.4	166,600	31,900	134,700	367.0

TABLE VIII (5)

t = .19 ms					
S	V	V ²	$\partial\phi/\partial t$	$V^2 - \partial\phi/\partial t$	Vcorr
2.73	0	0	0	0	0
2.50	114.0	12,996	- 1,250	14,246	119.3
2.25	148.0	21,904	- 5,980	27,884	167.0
2.00	185.4	34,340	-10,820	45,160	212.5
1.75	224.5	50,350	-16,400	66,750	258.4
1.50	268.0	71,824	-23,900	95,724	309.4
1.25	320.0	102,400	-31,900	134,300	366.6
1.00	396.8	157,400	-38,100	195,500	442.2
.75	405.6	164,500	-41,700	206,200	454.1
.50	406.5	165,200	-45,800	211,000	459.4
.25	397.5	158,000	-45,100	203,100	450.6

t = .25 ms					
S	V	V ²	$\partial\phi/\partial t$	$V^2 - \partial\phi/\partial t$	Vcorr
2.73	0	0	0	0	0
2.50	109.4	11,950	- 2,710	14,660	121.0
2.25	141.5	19,950	- 4,660	24,610	156.9
2.00	177.8	31,500	-10,820	42,320	205.8
1.75	214.9	46,150	-20,600	66,750	258.2
1.50	259.5	67,300	-29,200	96,500	310.7
1.25	319.6	102,100	-30,600	132,700	364.4
1.00	395.4	156,200	-38,900	195,100	441.7
.75	411.6	169,500	-41,700	211,200	459.6
.50	408.2	166,600	-43,800	210,400	458.8
.25	391.8	153,500	-51,400	204,900	452.6

TABLE VIII (6)

t = .31 ms					
S	V	V ²	$\partial\phi/\partial t$	$V^2 - \partial\phi/\partial t$	Vcorr
2.73	0	0	0	0	0
2.50	110.0	12,100	2,500	9,600	98.0
2.25	142.0	20,164	- 2,500	22,664	150.3
2.00	177.0	31,329	- 8,750	40,079	200.1
1.75	216.0	46,656	-17,100	63,756	252.4
1.50	254.9	65,000	-18,600	83,600	289.2
1.25	327.5	107,200	-26,400	133,600	365.5
1.00	398.2	158,500	-28,350	186,850	432.3
.75	415.0	172,225	-33,300	205,525	453.2
.50	408.5	166,800	-34,200	201,000	448.3
.25	390.1	152,150	-39,700	191,850	438.0

t = .37 ms					
S	V	V ²	$\partial\phi/\partial t$	$V^2 - \partial\phi/\partial t$	Vcorr
2.73	0	0	0	0	0
2.50	117.5	13,800	1,210	12,590	113.1
2.25	149.6	22,400	10,410	11,990	109.5
2.00	183.2	33,550	24,700	8,850	94.0
1.75	222.0	49,284	41,500	7,784	88.3
1.50	264.8	70,000	58,100	11,900	109.4
1.25	333.6	111,300	73,600	37,700	194.1
1.00	402.8	162,200	82,000	80,200	283.2
.75	414.5	171,800	86,000	85,800	292.9
.50	410.4	168,400	89,200	79,200	281.5
.25	391.0	152,881	96,800	56,081	236.8

TABLE VIII (7)

t = .43 ms					
S	V	V ²	$\partial\phi/\partial t$	$V^2 - \partial\phi/\partial t$	Vcorr
2.73	0	0	0	0	0
2.50	111.0	12,321	- 2,220	14,540	120.5
2.25	140.8	19,750	- 7,780	27,530	166.0
2.00	174.4	30,450	-17,100	47,550	218.0
1.75	213.8	45,700	-30,000	75,700	275.2
1.50	261.7	68,000	-44,000	112,000	334.6
1.25	335.3	112,400	-59,000	171,400	414.0
1.00	402.1	161,650	-67,800	229,450	479.0
.75	414.1	171,450	-72,300	243,750	493.0
.50	409.3	167,400	-73,600	241,000	491.0
.25	389.0	151,300	-88,900	240,200	490.0

t = .49 ms					
S	V	V ²	$\partial\phi/\partial t$	$V^2 - \partial\phi/\partial t$	Vcorr
2.73	0	0	0	0	0
2.50	111.0	12,321	820	11,501	107.5
2.25	140.4	19,700	0	19,700	140.4
2.00	183.5	33,600	2,220	31,380	177.1
1.75	229.8	52,800	13,900	38,900	197.3
1.50	280.2	78,500	14,600	63,900	252.8
1.25	335.9	112,800	19,900	92,900	304.8
1.00	405.0	164,000	22,200	141,800	376.6
.75	422.1	178,100	23,600	154,500	393.0
.50	417.0	173,900	32,600	151,300	389.0
.25	408.0	166,450	45,900	120,550	347.2

TABLE VIII (8)

t = .55 ms					
S	V	V ²	$\partial\phi/\partial t$	$V^2 - \partial\phi/\partial t$	Vcorr
2.73	0	0	0	0	0
2.50	117.0	13,700	347	13,353	115.6
2.25	154.6	23,850	4,300	19,550	139.9
2.00	188.6	35,500	9,450	26,050	161.2
1.75	231.0	53,360	12,630	40,730	201.8
1.50	271.8	73,800	12,500	61,300	247.6
1.25	332.8	110,700	15,280	95,420	309.0
1.00	403.3	162,600	23,900	138,700	372.5
.75	421.6	177,600	29,600	148,000	384.7
.50	423.0	178,900	30,900	148,000	384.7
.25	409.0	167,300	38,900	128,400	358.4



TABLE IX

VERIFICATION OF NOSE STAGNATION POINT

INFINITE FRINGE PICTURES			FRINGE DISPLACEMENT PICTURES		
Picture No.	Estimated Stagnation Pt.	Fringe on Nose Visible in Pictures	Picture No.	Stagnation Pt. Location Dist. from Tail Inches	Ref. Distance Corrected to Act. Inches
U. M.	Dist. from Tail Inches		U. M.		
435	2.67		413	2.74	.240
436	2.68		414	2.74	.136
437	2.68		415	2.73	.110
438	2.67		416	2.73	.052
439	2.635		417	2.70	-.006
440	2.685		418	2.75	-.123
441	2.69	YES	419	2.72	-.136
442	2.69	YES	420	2.75	-.240
443	2.78	YES	421	2.76	-.298
444	2.72	YES	422	2.74	-.396
445	2.715	YES	423	2.75	-.430
446	2.75	YES	424	2.73	-.460
447	2.74	YES	425	2.74	-.570
448	2.725	YES	426	2.74	-.577
449	2.75	YES	427	2.74	-.695
450	2.77	YES	428	2.72	-.734
451	2.76	YES	429	2.76	-.792
452	2.71	YES	430	2.75	-.838
453	2.685		431	2.755	-.960
454	2.74		432	2.745	-1.00
455	2.72	YES	433	2.75	-1.08
456	2.76	YES	434	2.755	-1.14
457	2.75	YES			
458	2.68	YES			

AVERAGE DISTANCE FOR UM 435 - 458 - 2.715

AVERAGE DISTANCE FOR UM 413 - 434 - 2.741

FINAL AVERAGE DISTANCE - 2.728





Figure 1





Figure 2





Figure 3





Figure 4





Figure 5





Figure 6





Figure 7





Figure 8





Figure 9





Figure 10





Figure 11





Figure 12





Figure 13





Figure 14





Figure 15





Figure 16





Figure 17





Figure 13





Figure 19





Figure 20





Figure 21



Figure 22



Figure 23





Figure 24

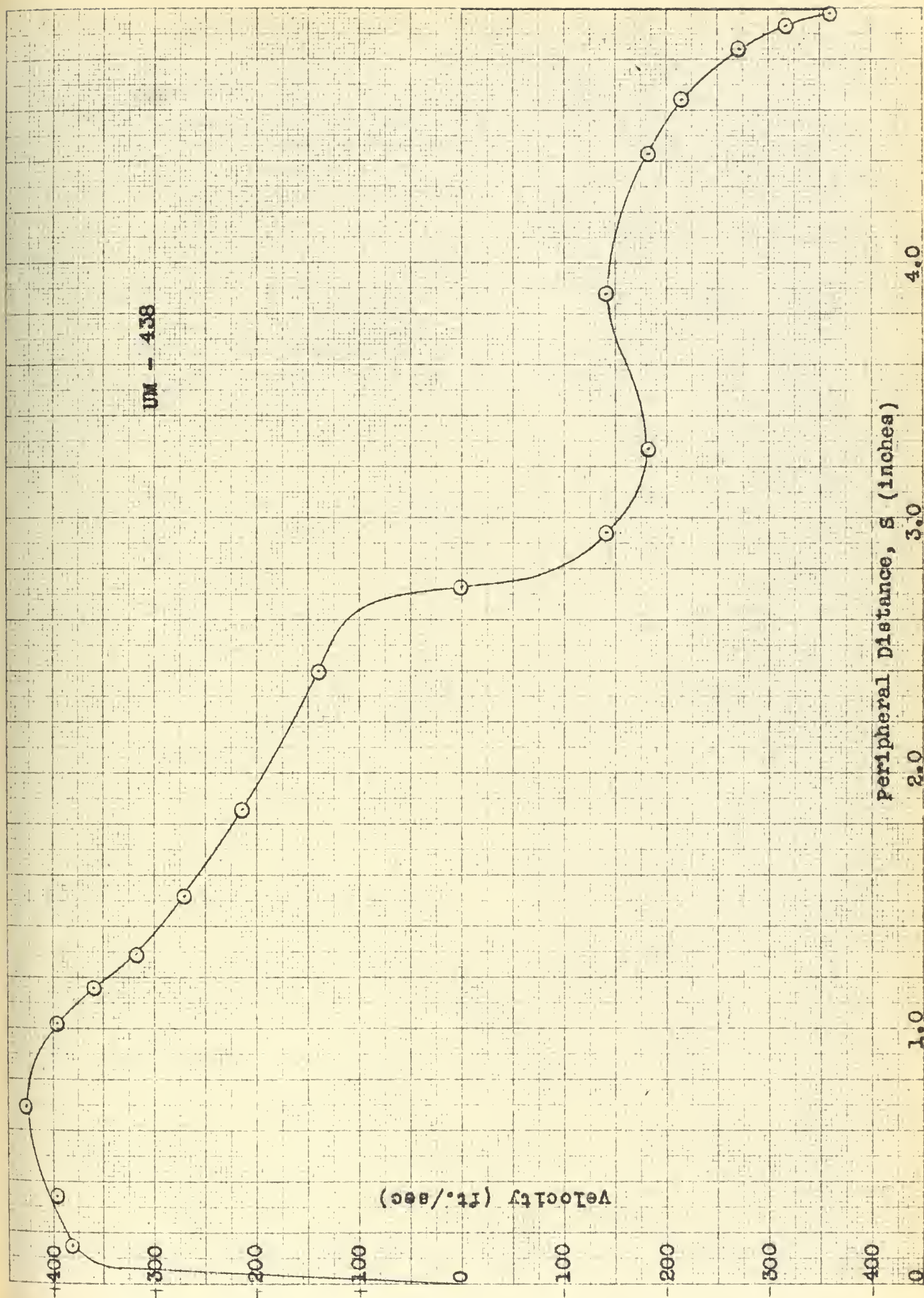


Fig. 25 sample plot of velocity versus peripheral distance UM- 438

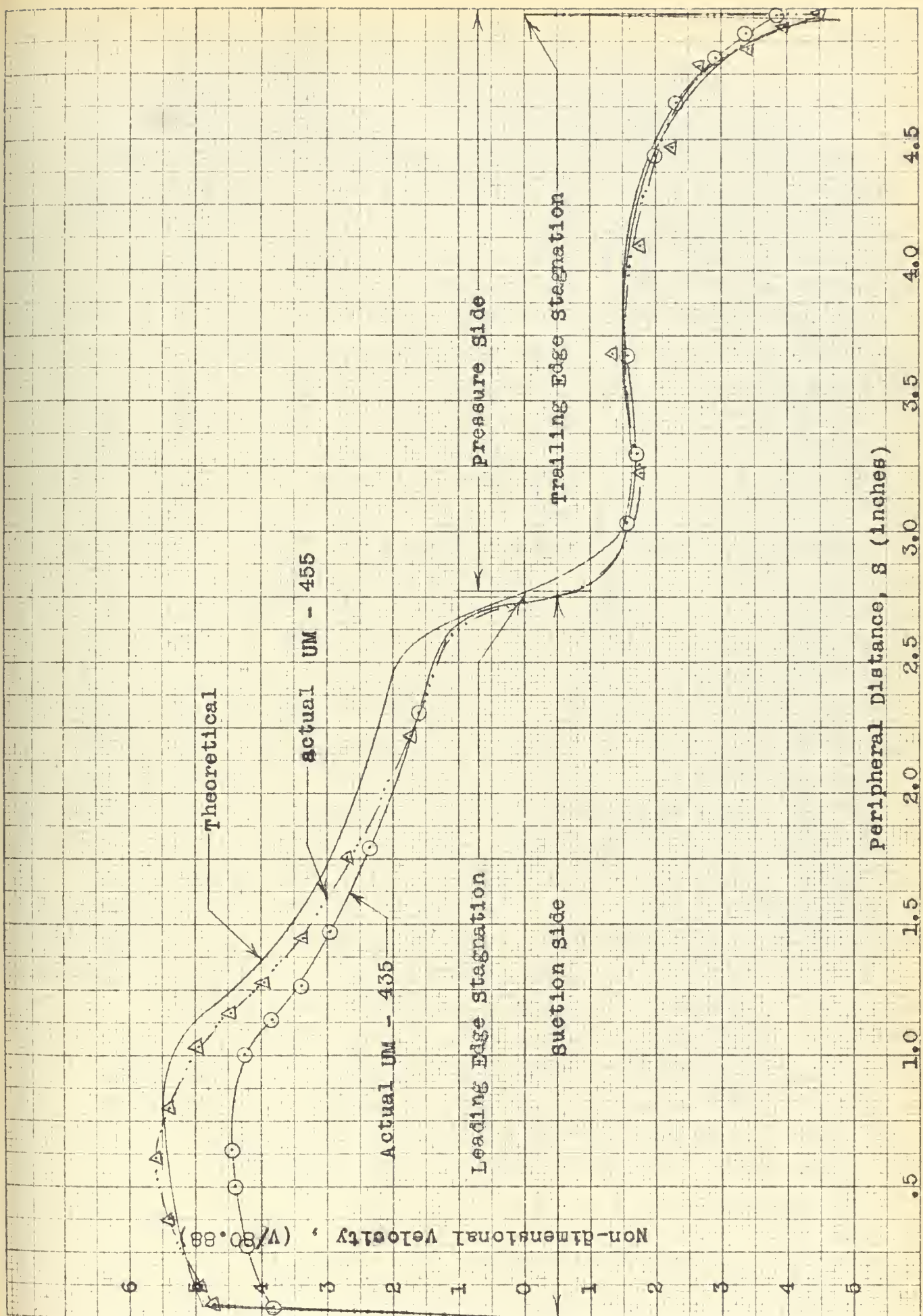


Fig. 26 Comparison of Actual And Theoretical velocity profiles





Figure 27

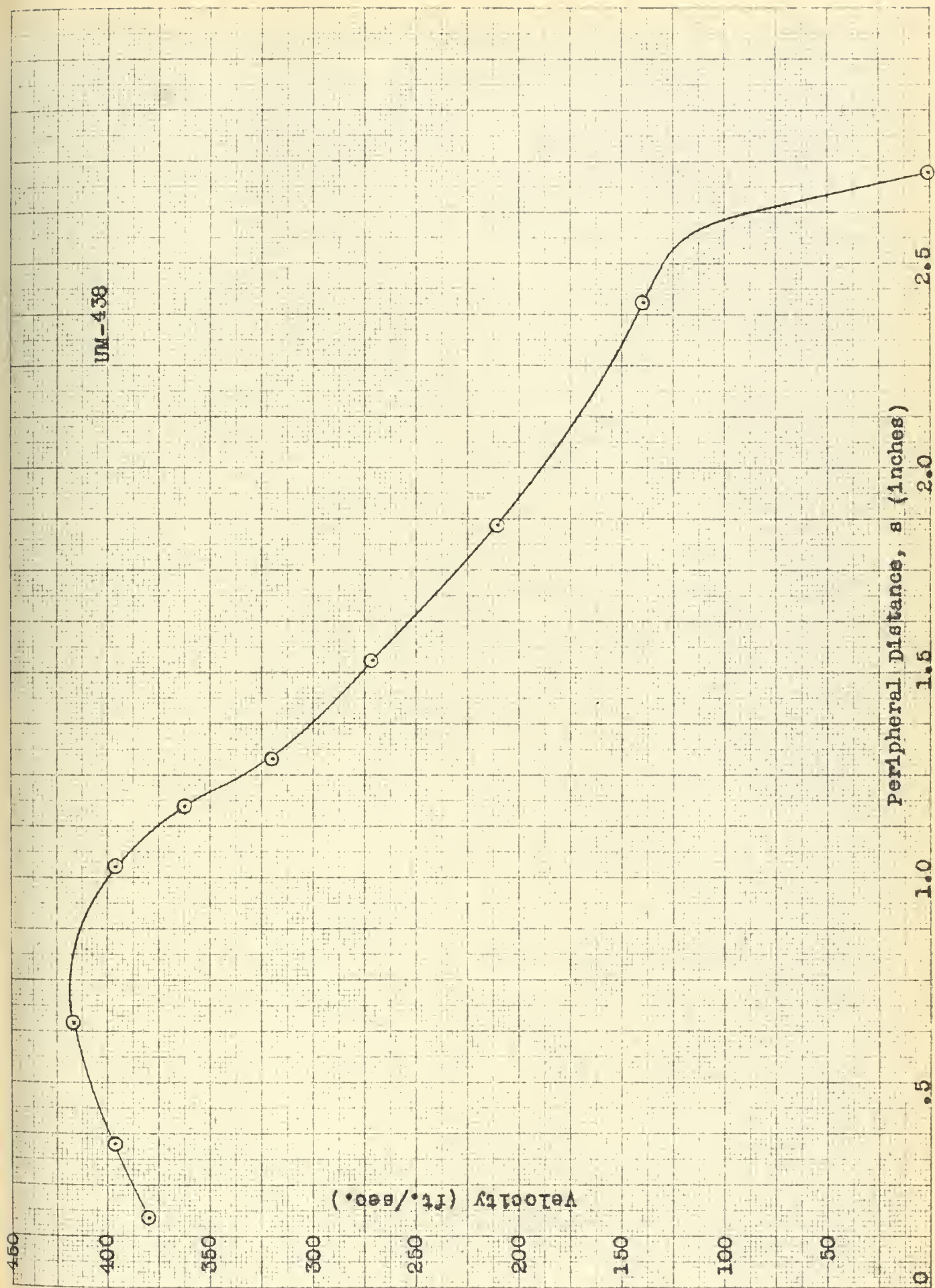


Fig. 28 Velocity versus peripheral distance UM - 438

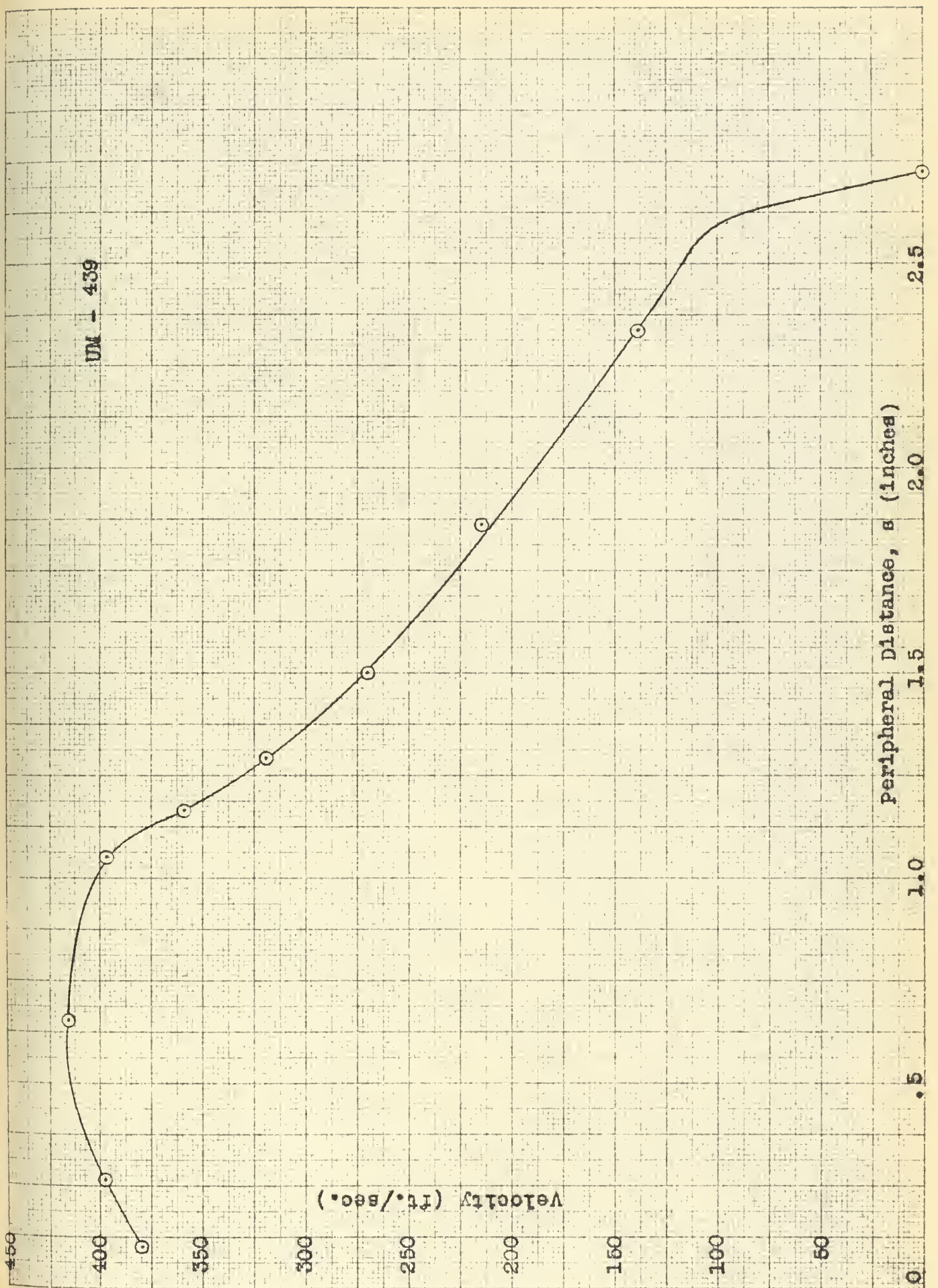


Fig. 29 Velocity Versus peripheral Distance UM - 439

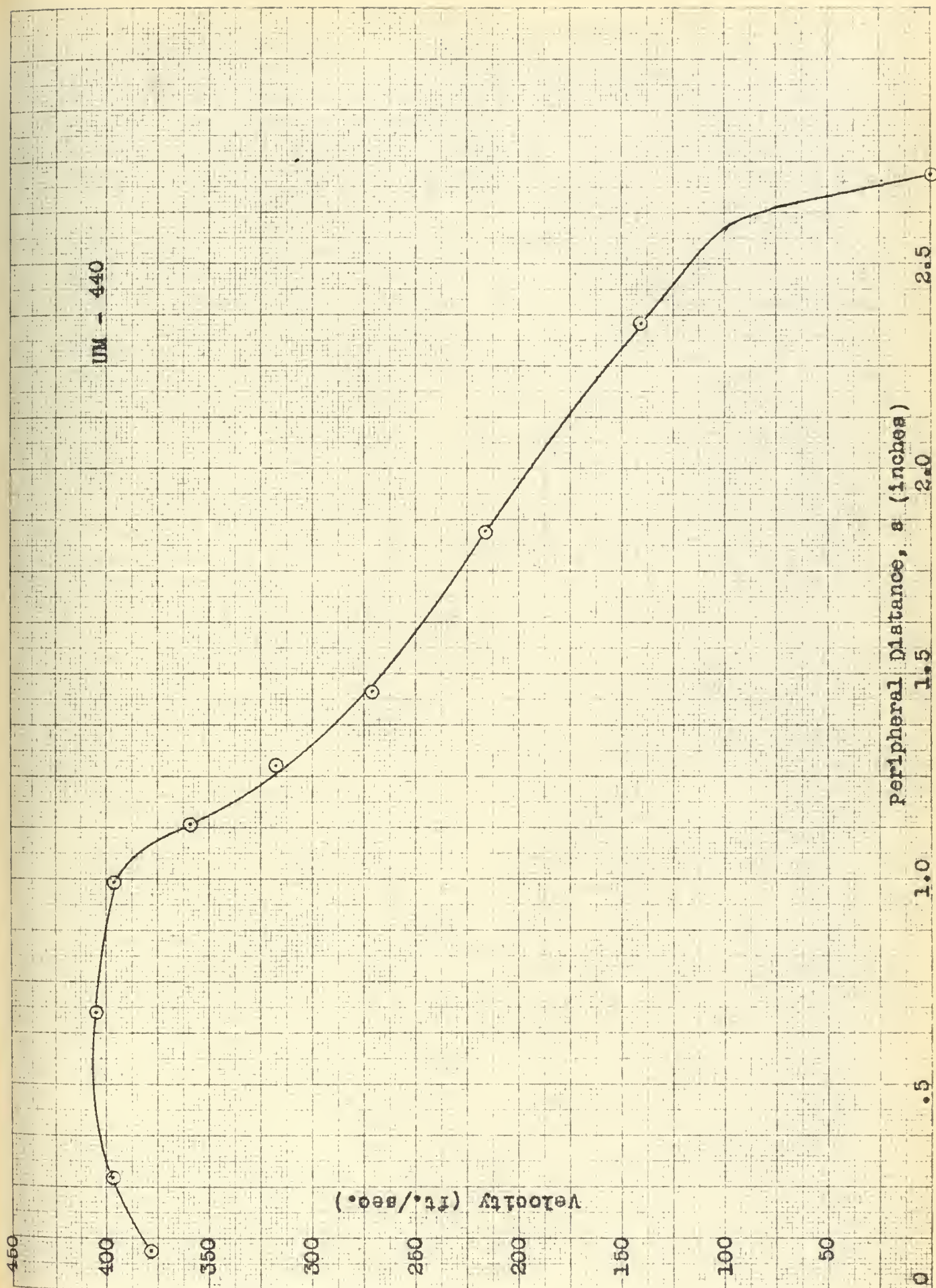


Fig. 30 Velocity versus Peripheral Distance UM - 440

UM - 441

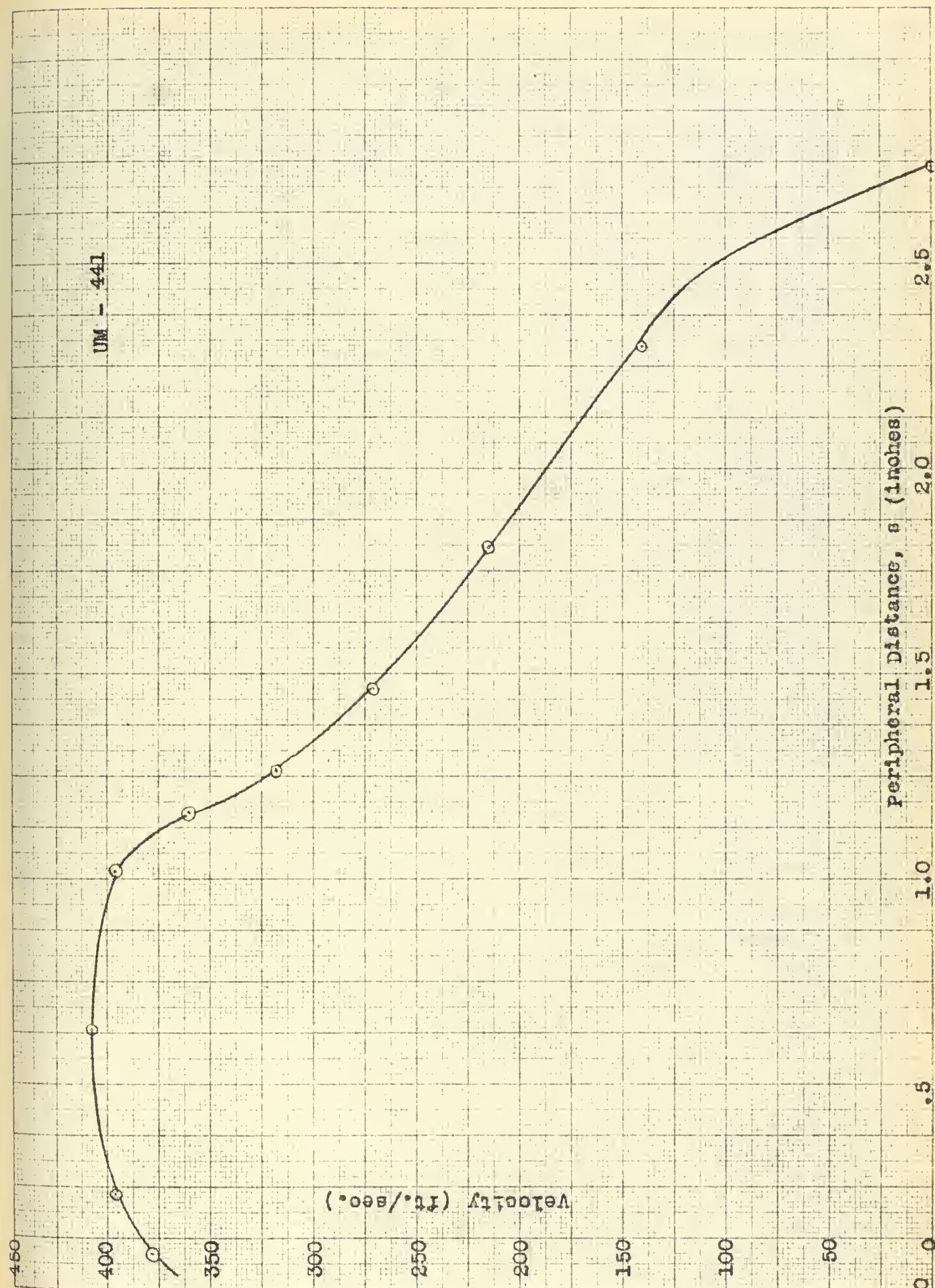


Fig. 31 Velocity versus peripheral distance UM - 441

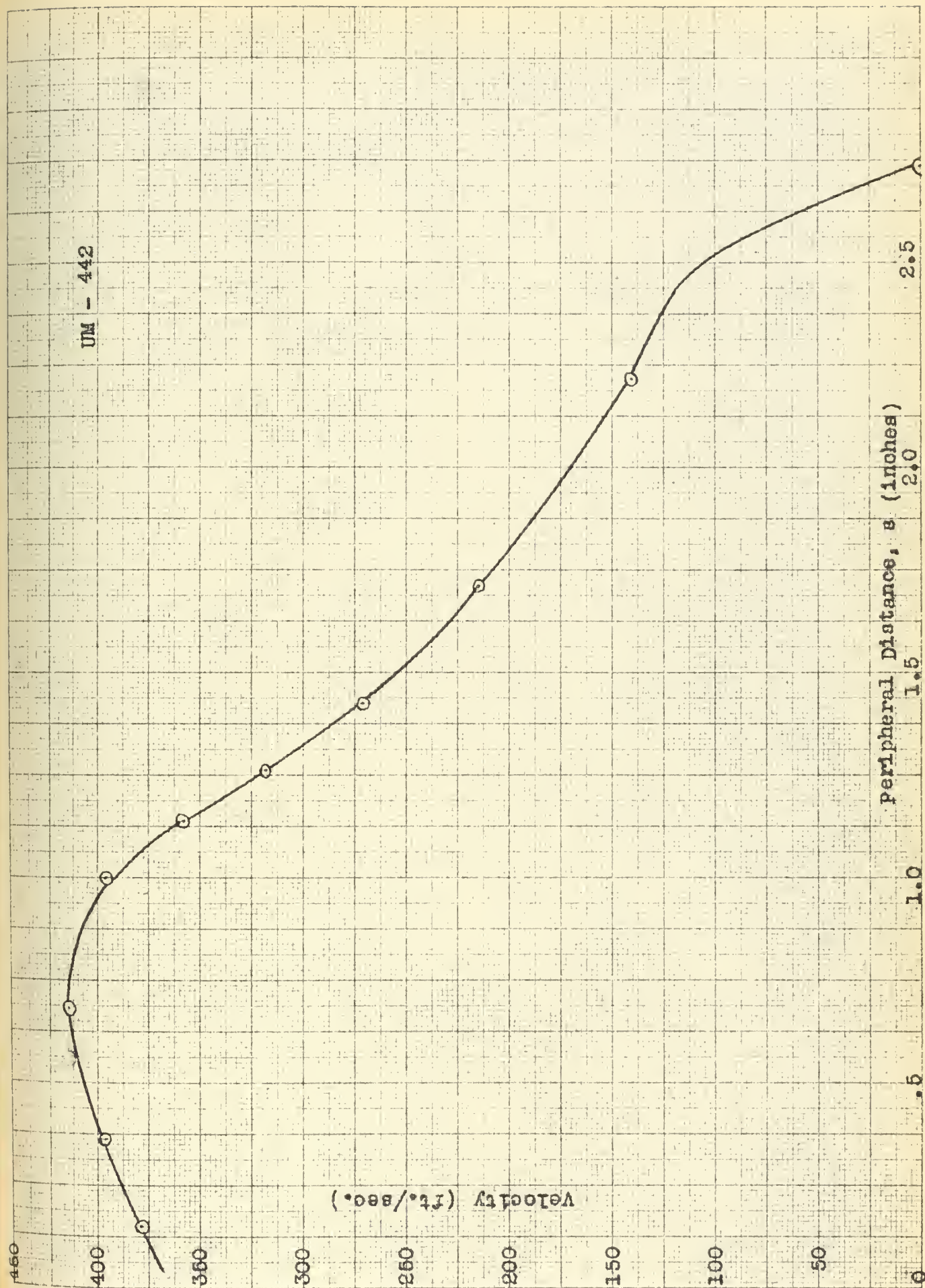


Fig. 32 velocity versus Peripheral Distance UM - 442

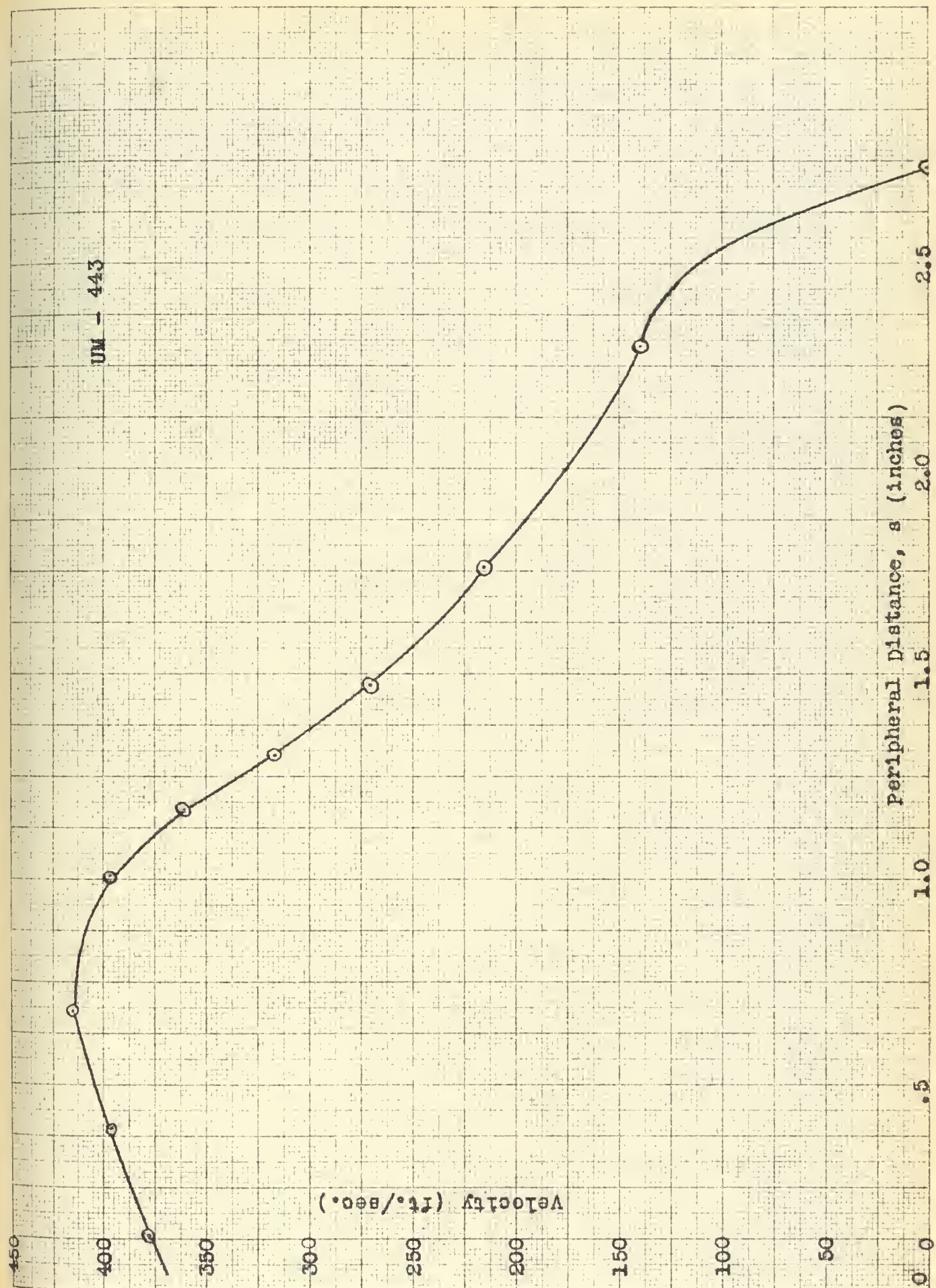


Fig. 33 velocity versus peripheral distance UM - 443

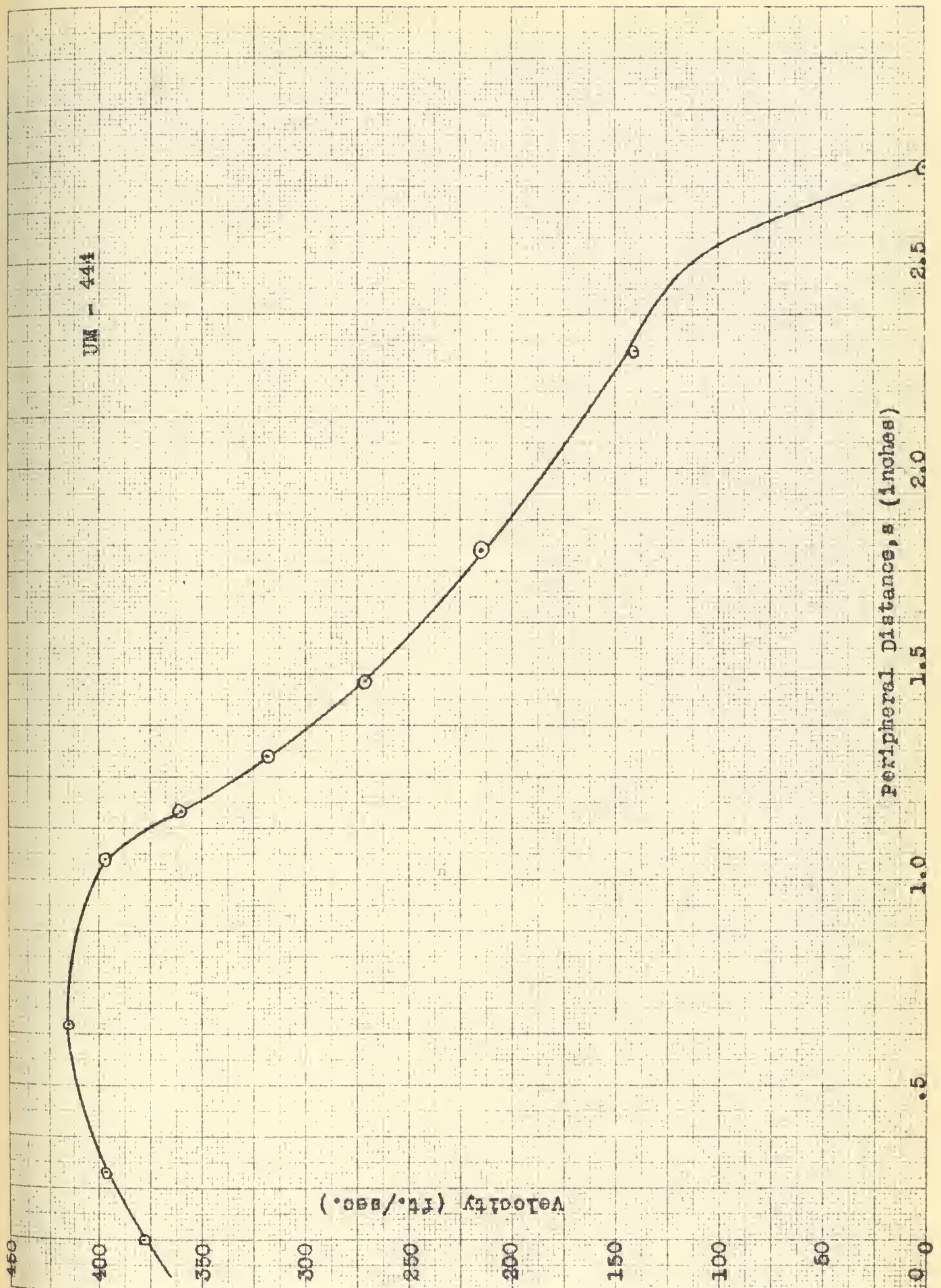


Fig. 34 Velocity versus Peripheral Distance UM - 444

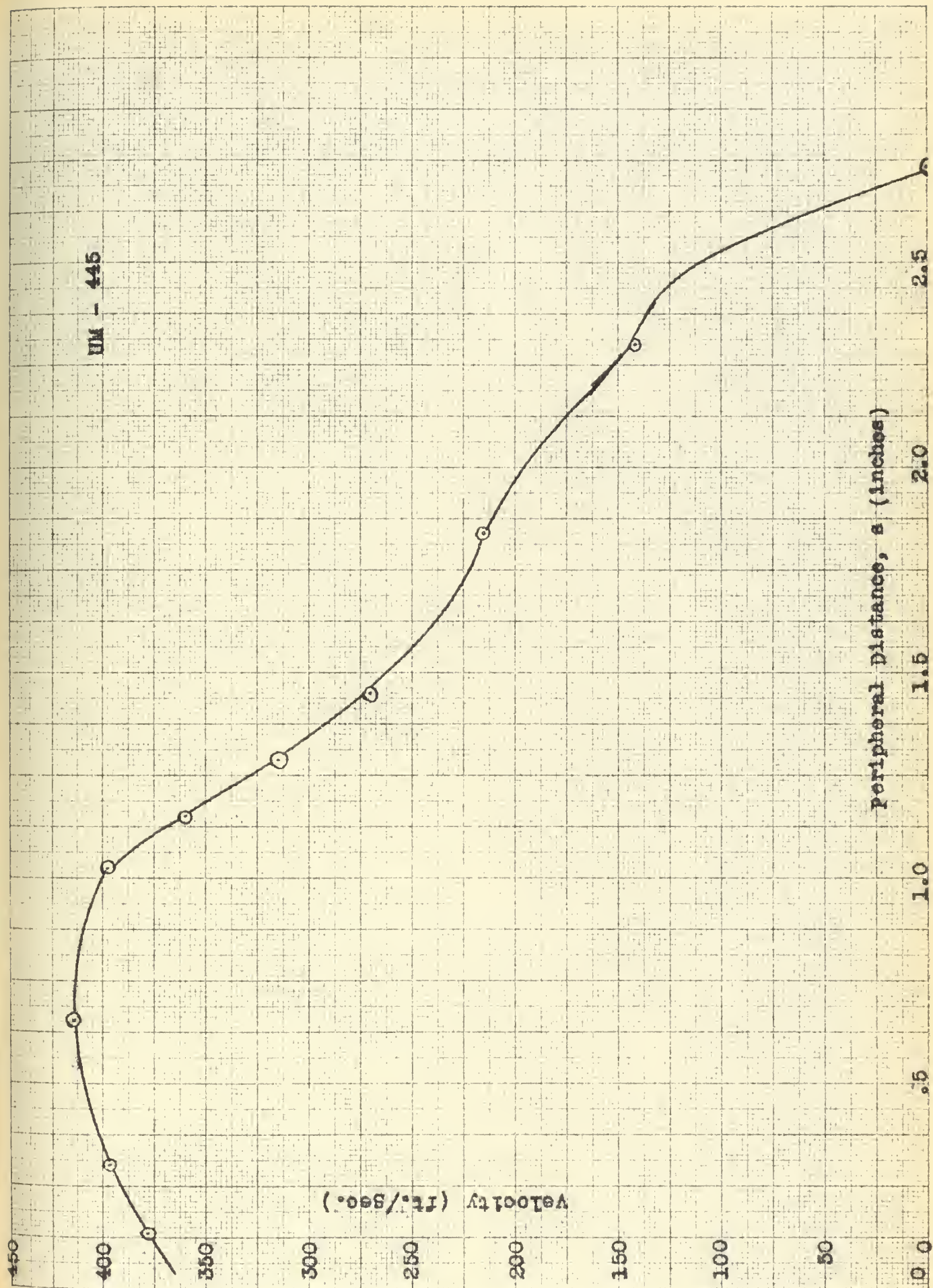


Fig. 35 velocity versus peripheral distance UM - 445

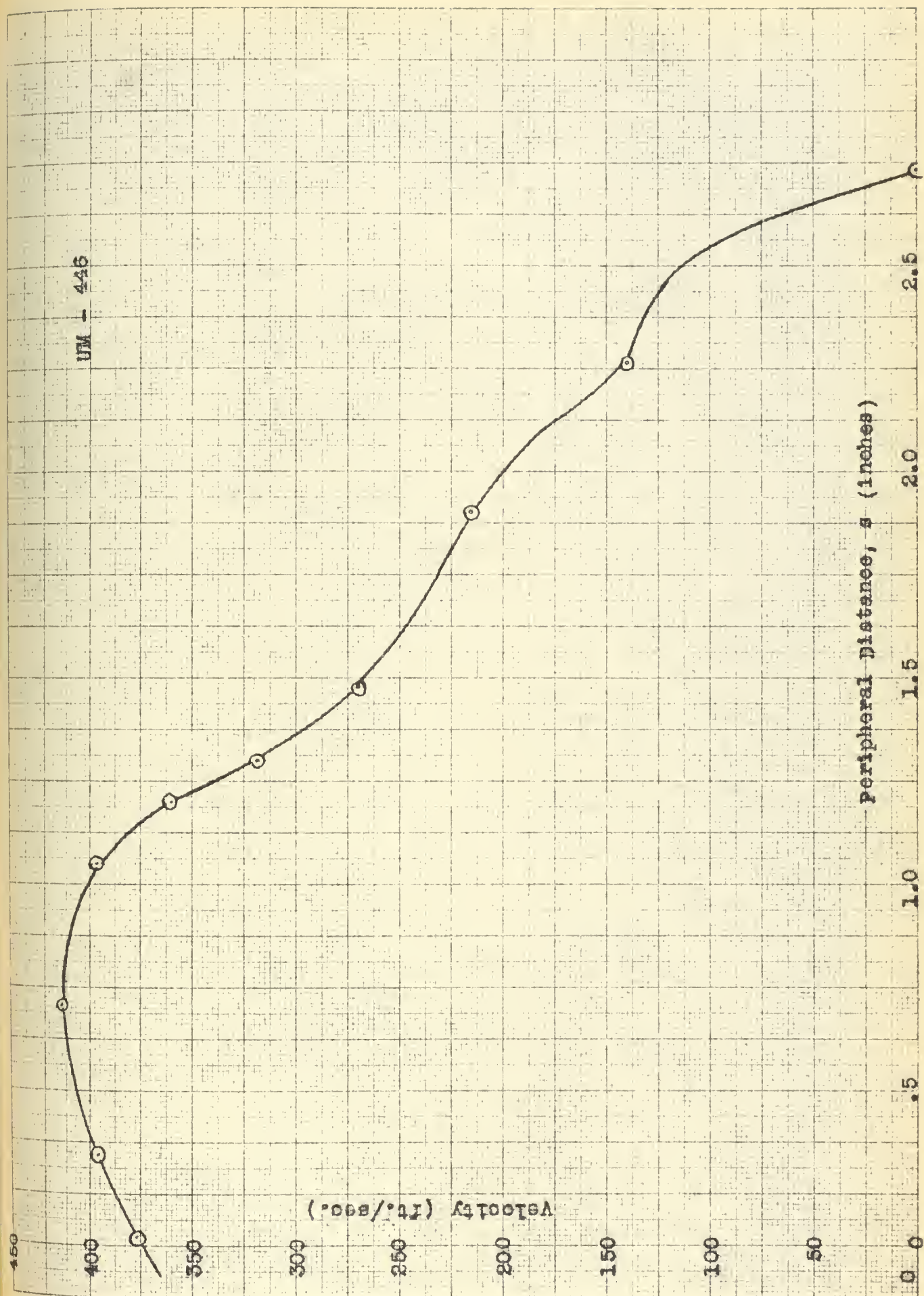


Fig. 36 velocity versus peripheral distance UM-446

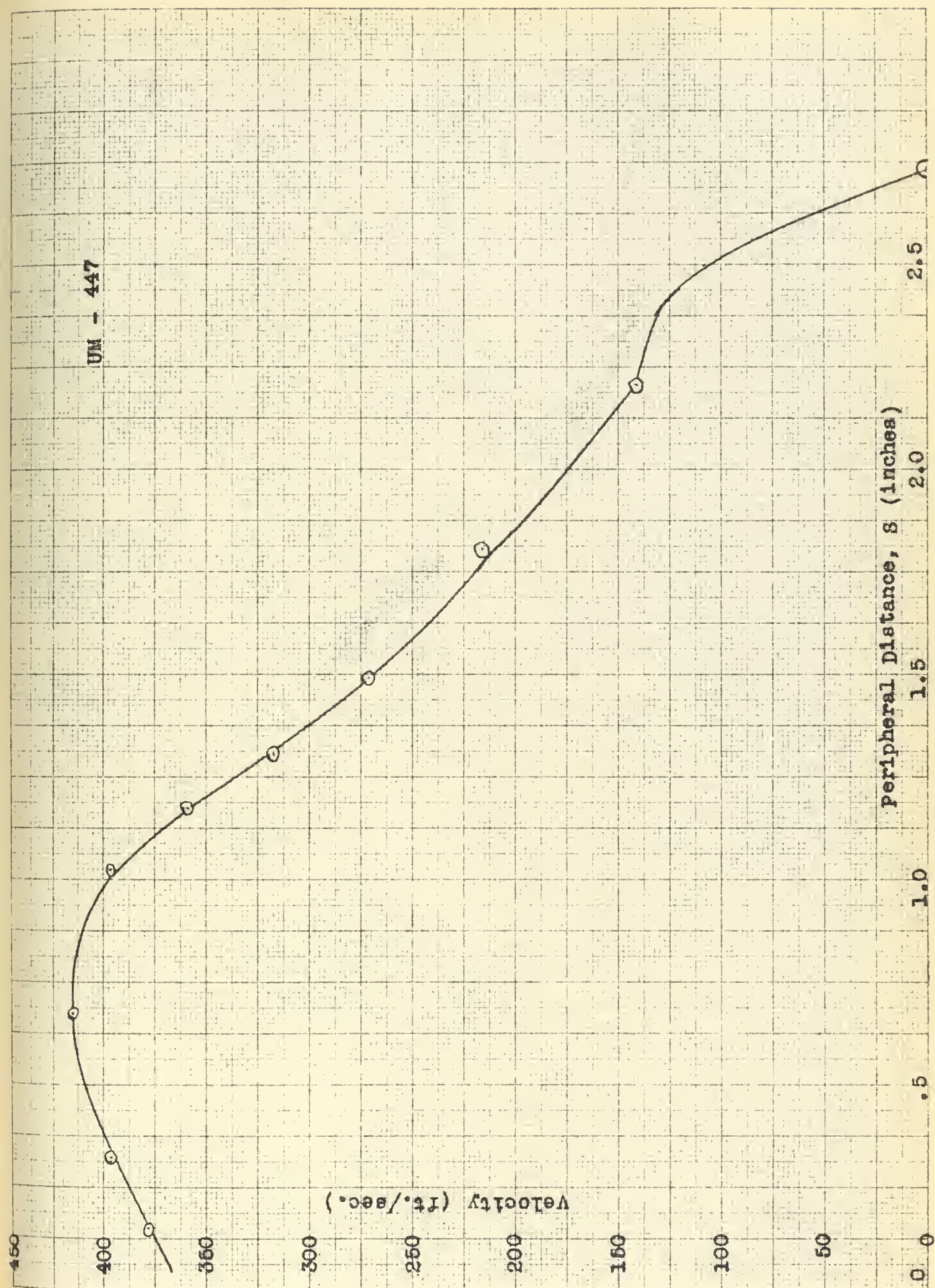


Fig. 37 velocity versus peripheral distance UM - 447

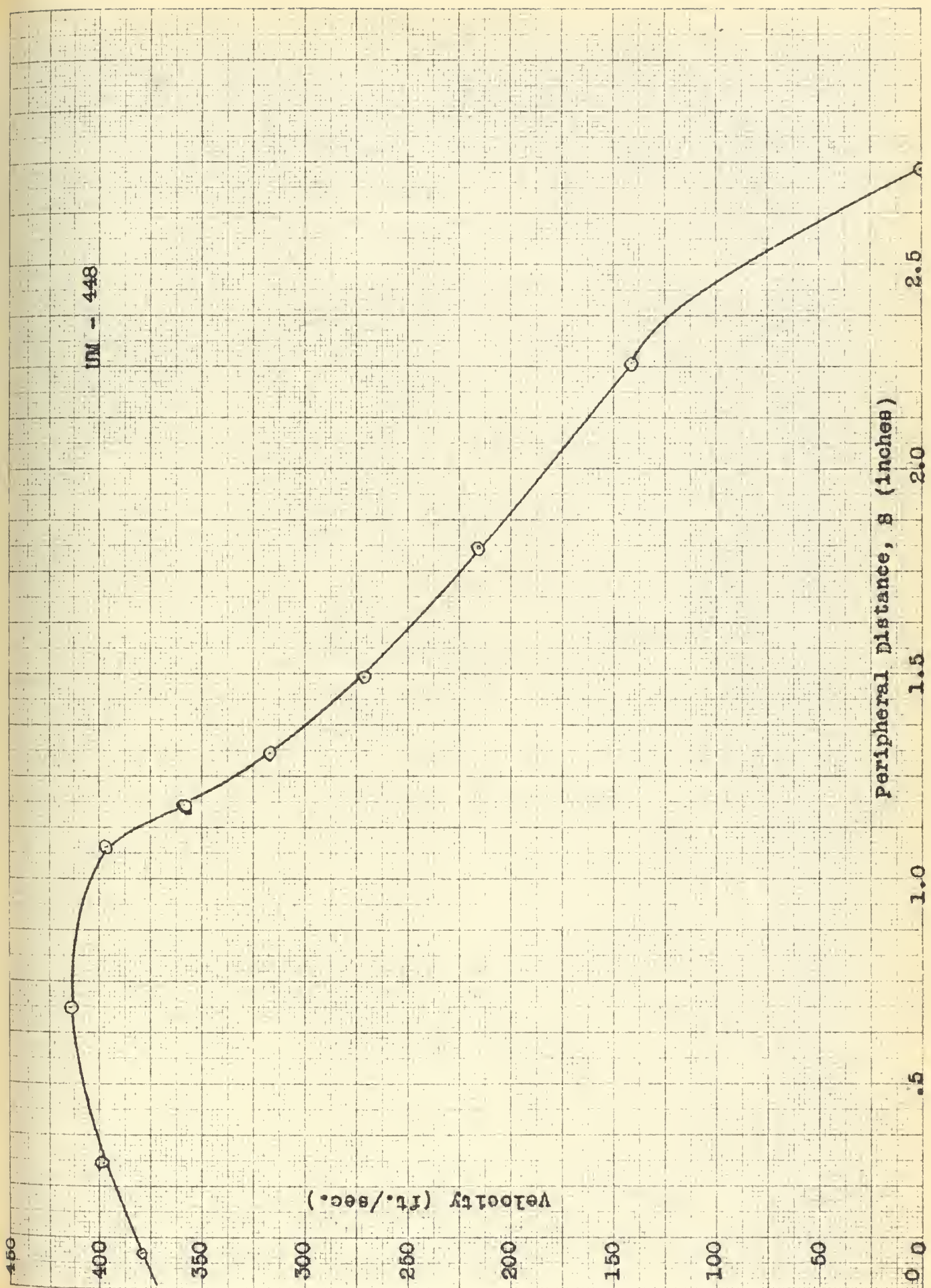


Fig. 38 velocity versus peripheral distance UM - 448

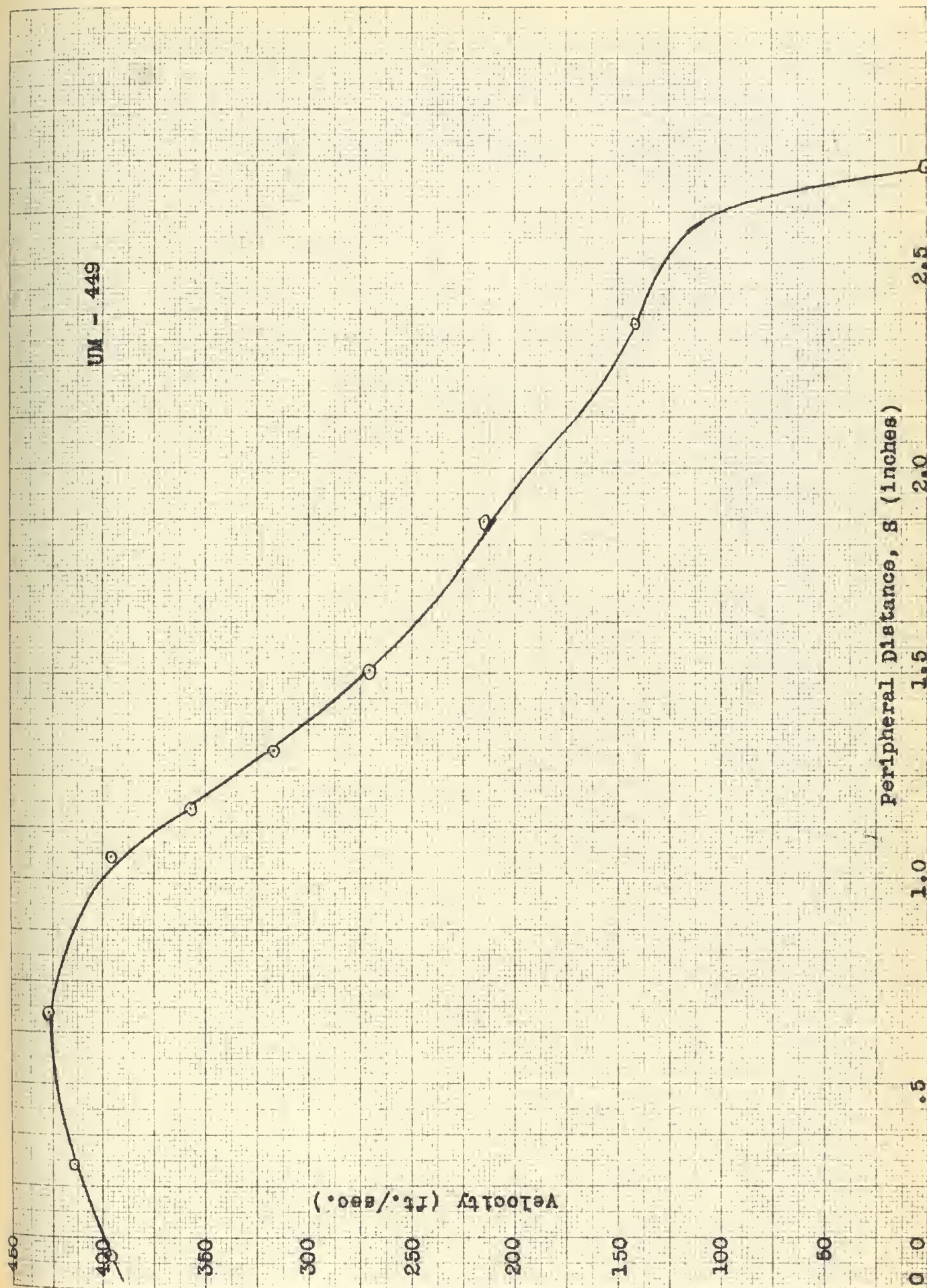


Fig. 39 velocity versus peripheral distance UM - 449

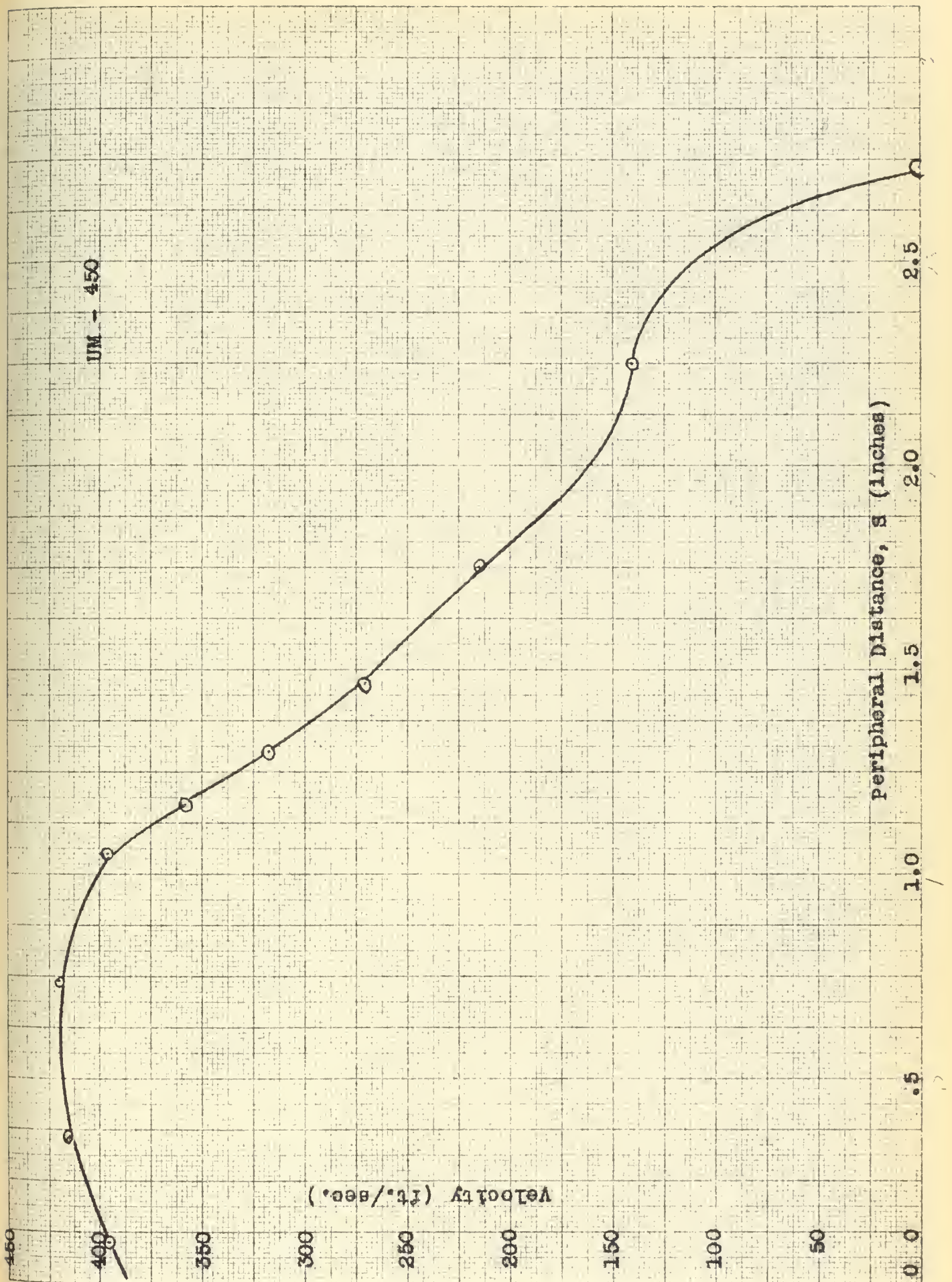


Fig. 40 velocity versus peripheral distance UM - 450

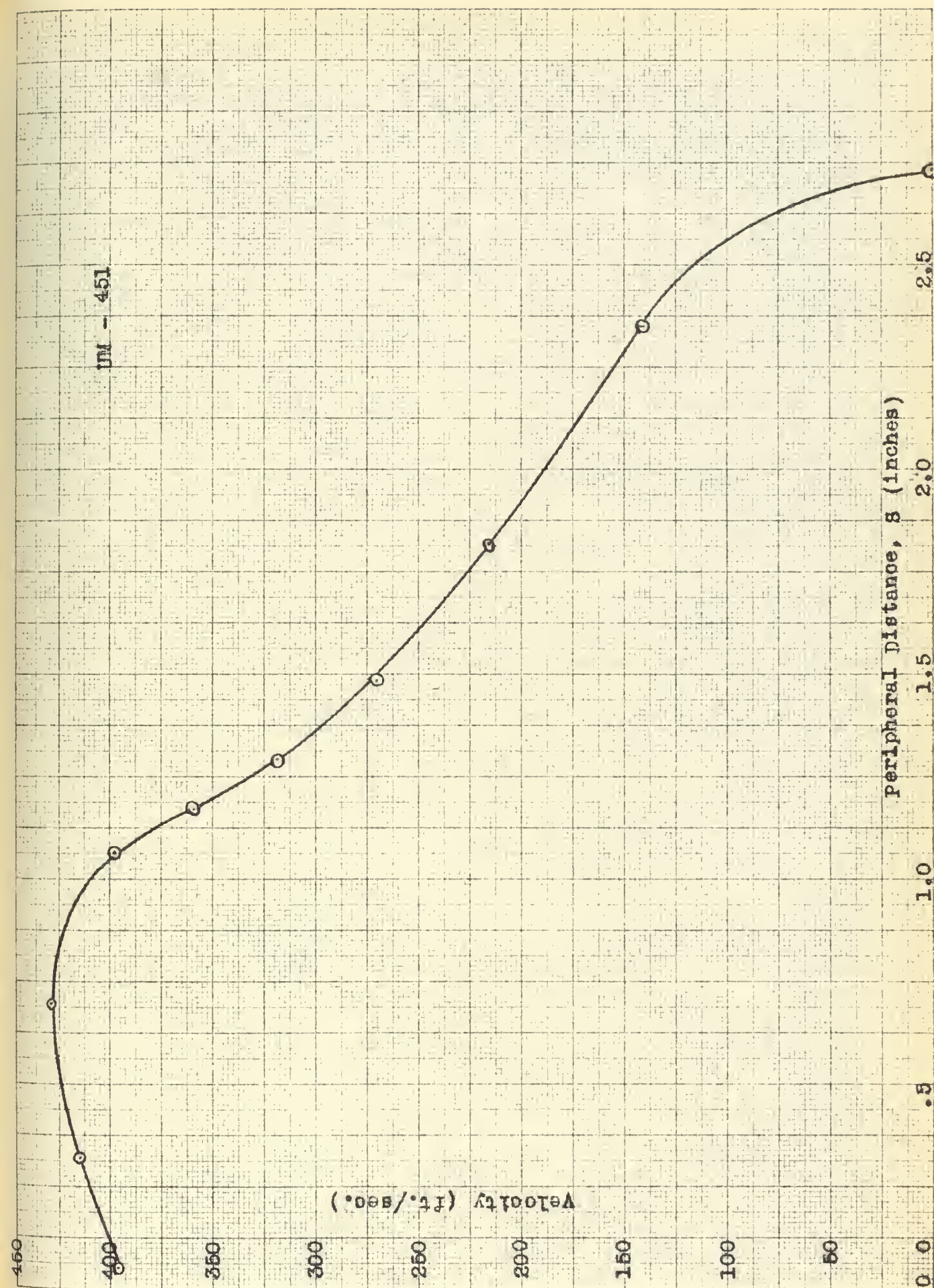


Fig. 41 velocity versus peripheral Distance UM - 451

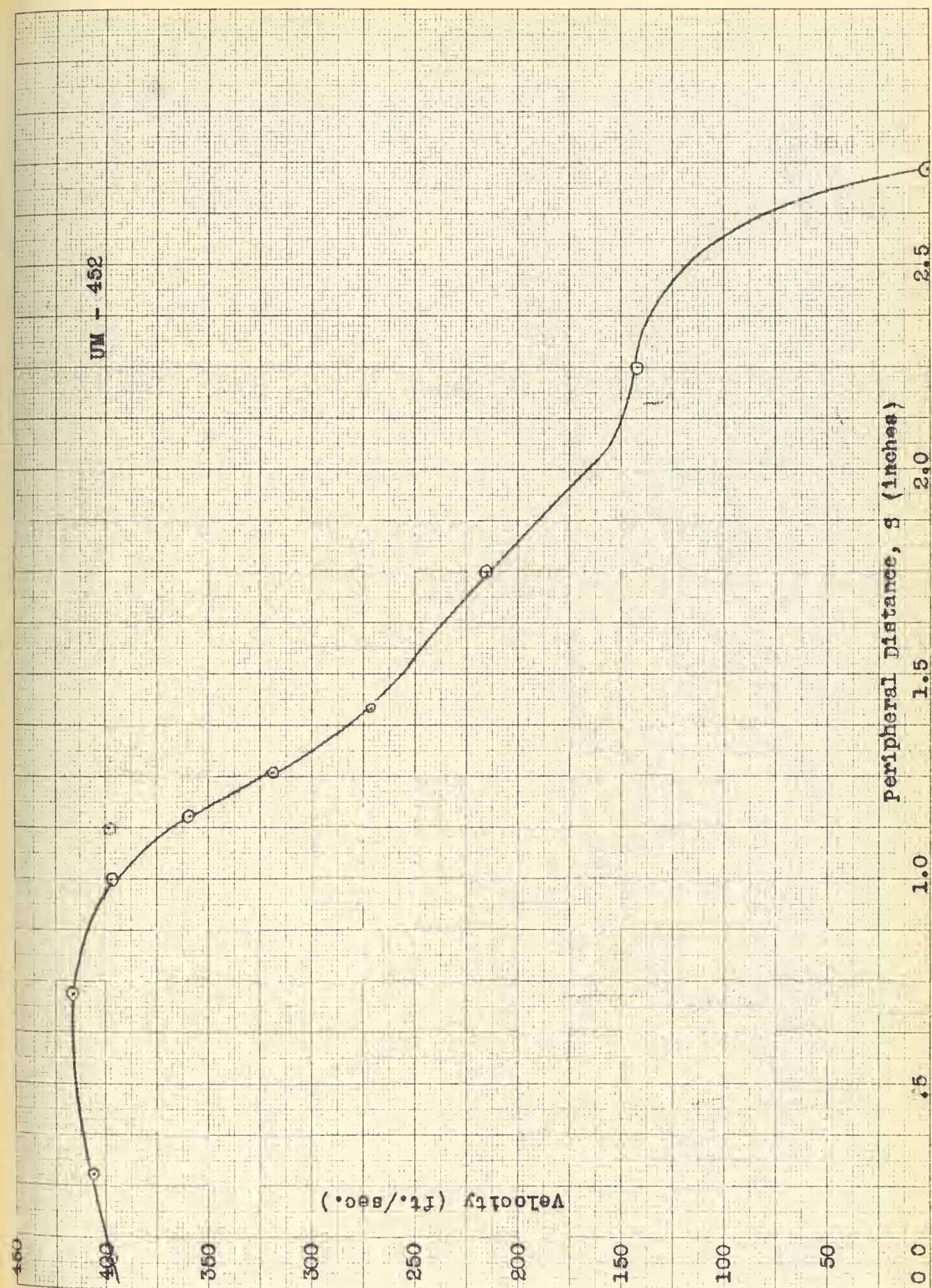


Fig. 42 velocity versus peripheral distance UM - 452

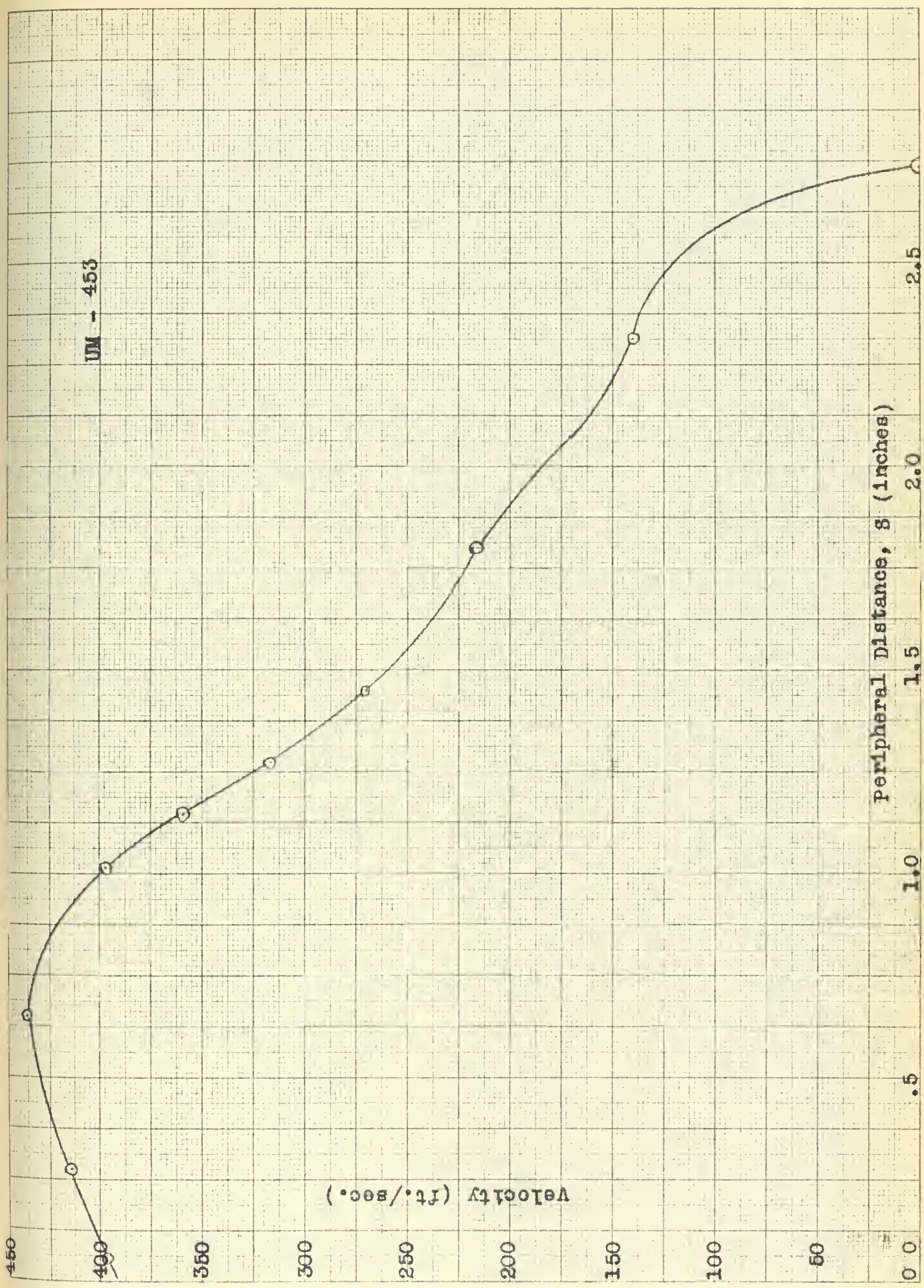


Fig. 43 velocity versus peripheral distance UM - 453

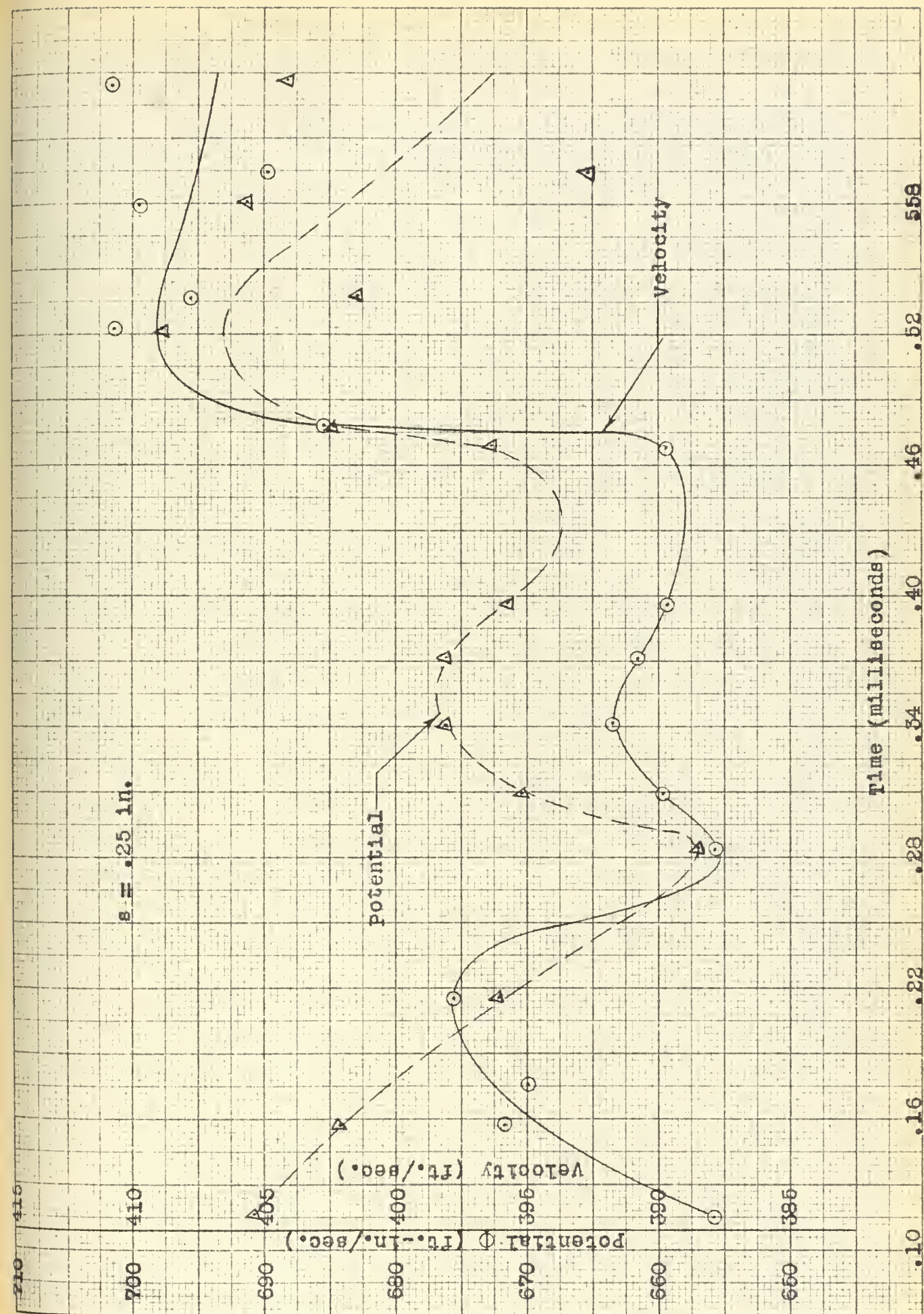


Fig. 44 potential and velocity versus time for $s = .25$ inches

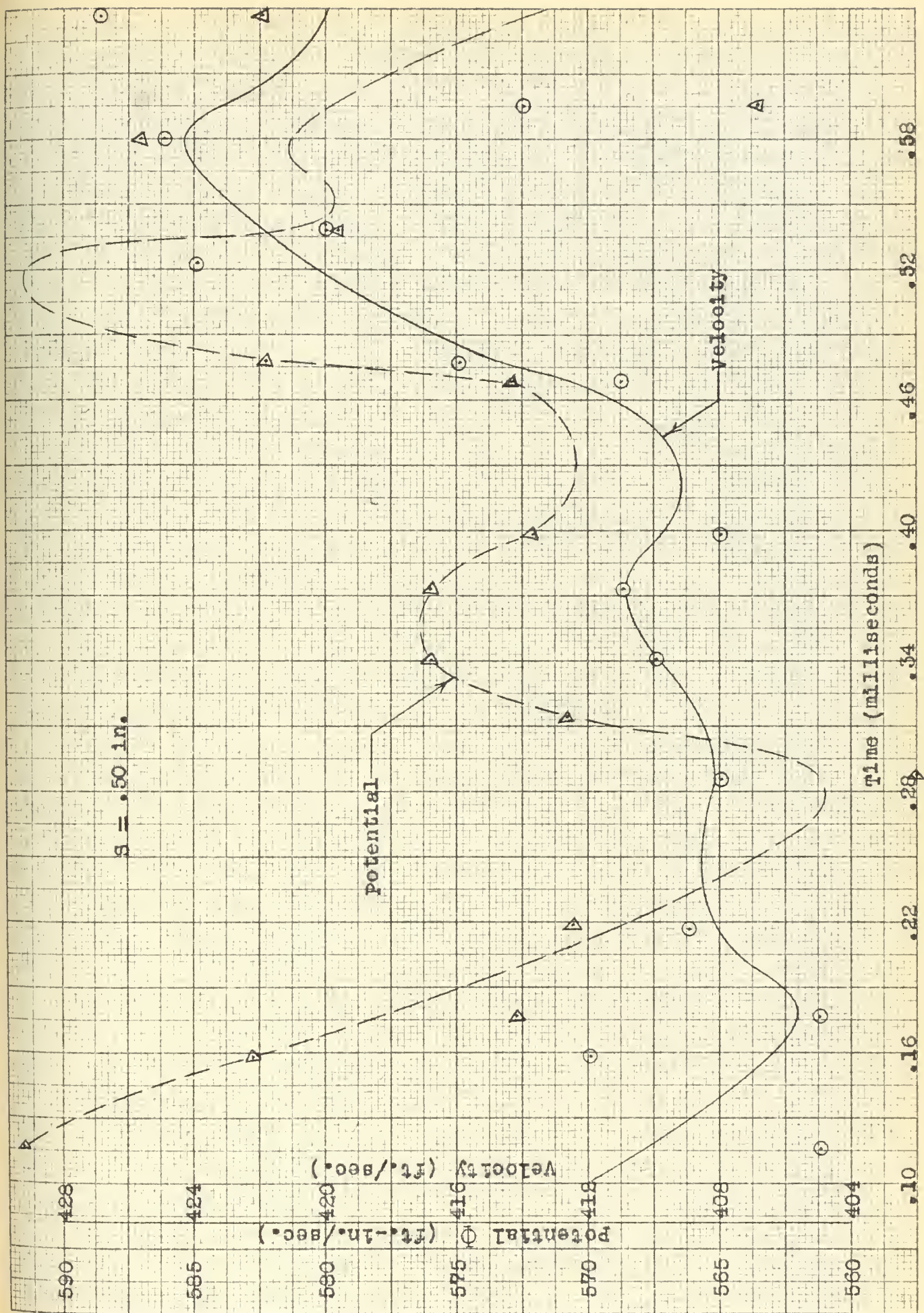


Fig. 45 potential and velocity versus Time for $s = .50$ inches

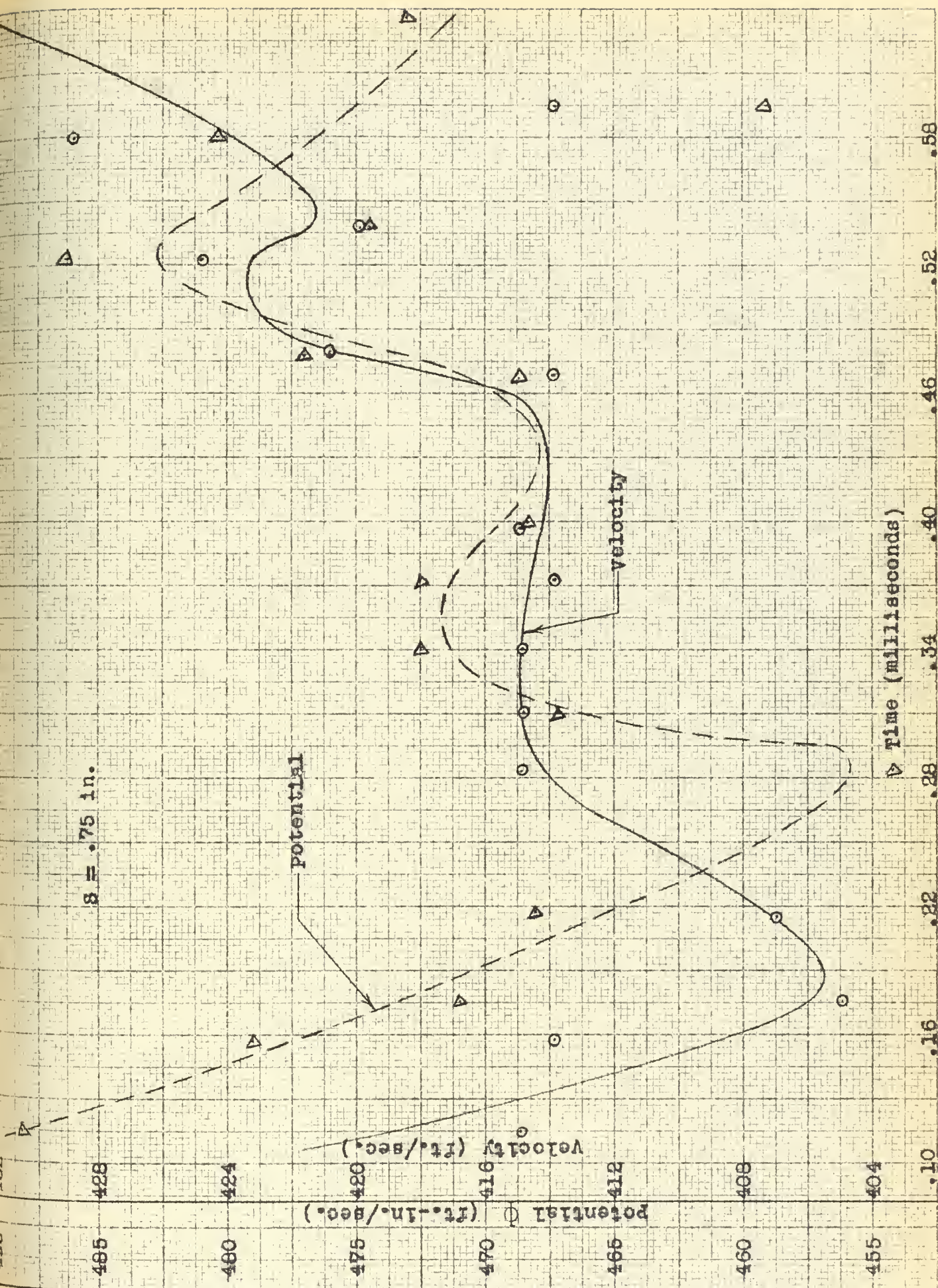


Fig. 46 potential and velocity versus time for $g = .75$ inches

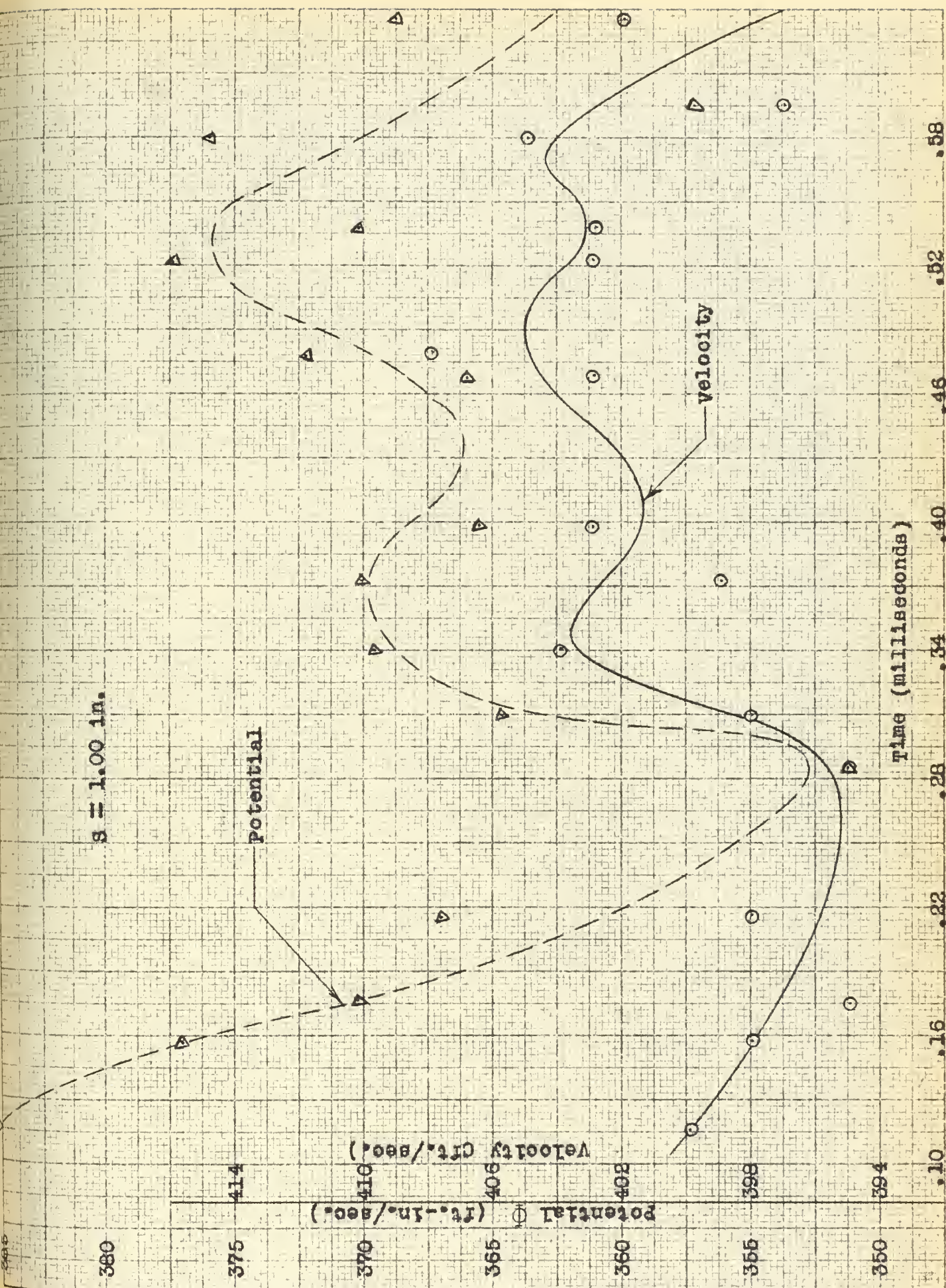


Fig. 47 potential and velocity versus time for $s = 1.00$ inches

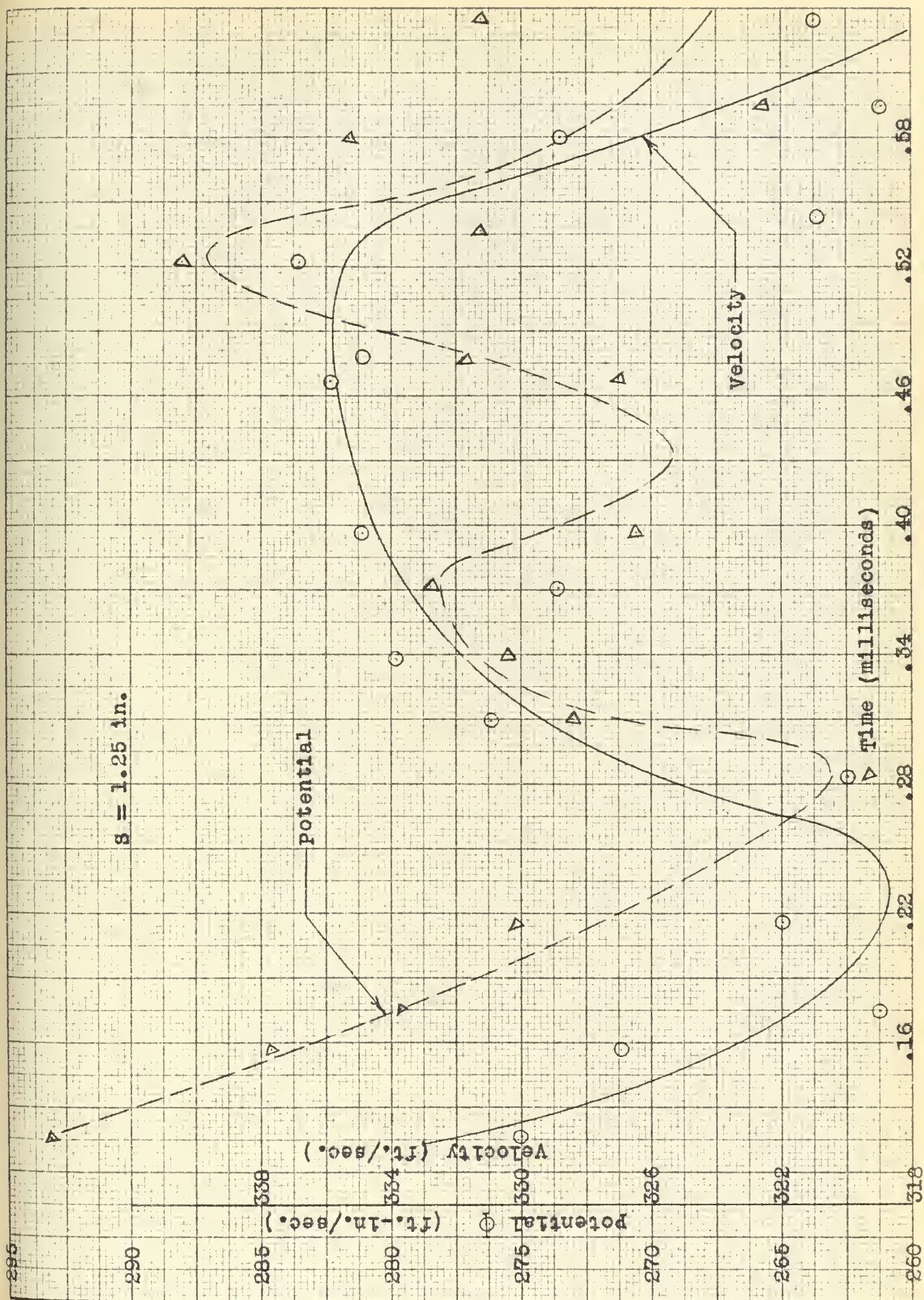


Fig. 48 potential and Velocity versus Time for $s = 1.25$ inches

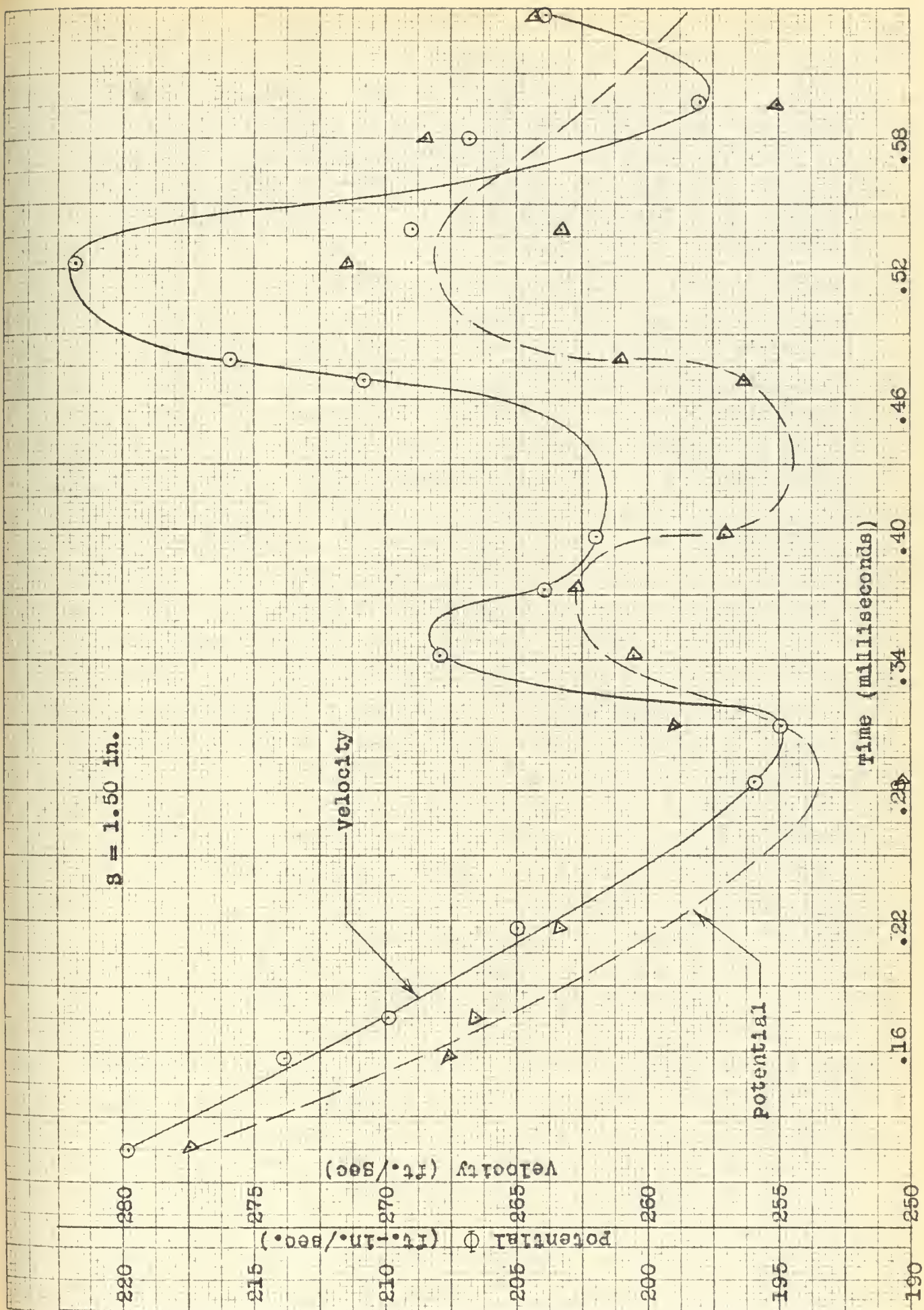


Fig. 49 potential and velocity versus Time for $g = 1.50$ inches

$g = 1.75 \text{ in.}$

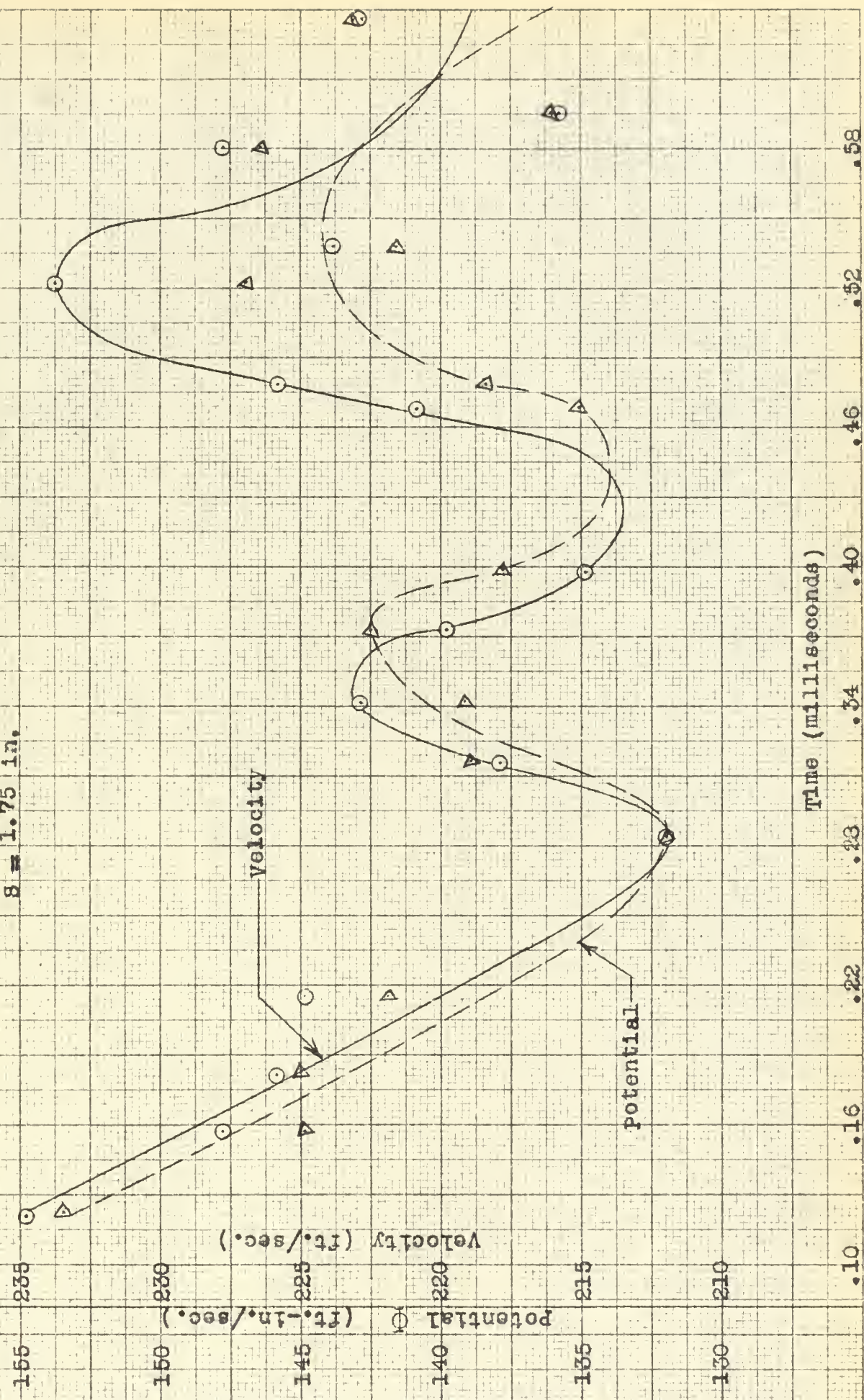


Fig. 50 potential and velocity versus time for $g = 1.75$ inches

$g = 2.00 \text{ in.}$

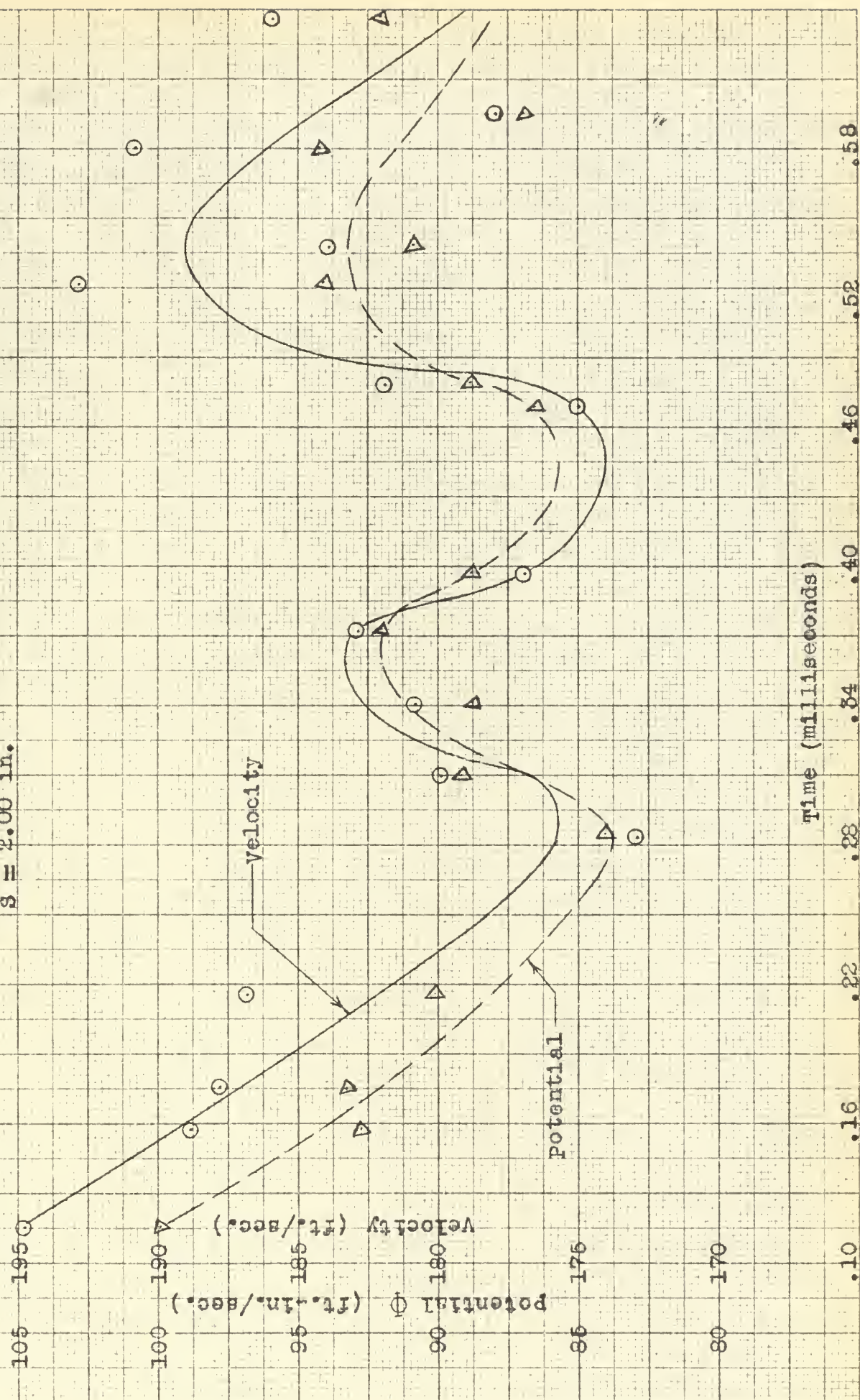


Fig. 51 potential and Velocity versus time for $g = 2.00$ inches

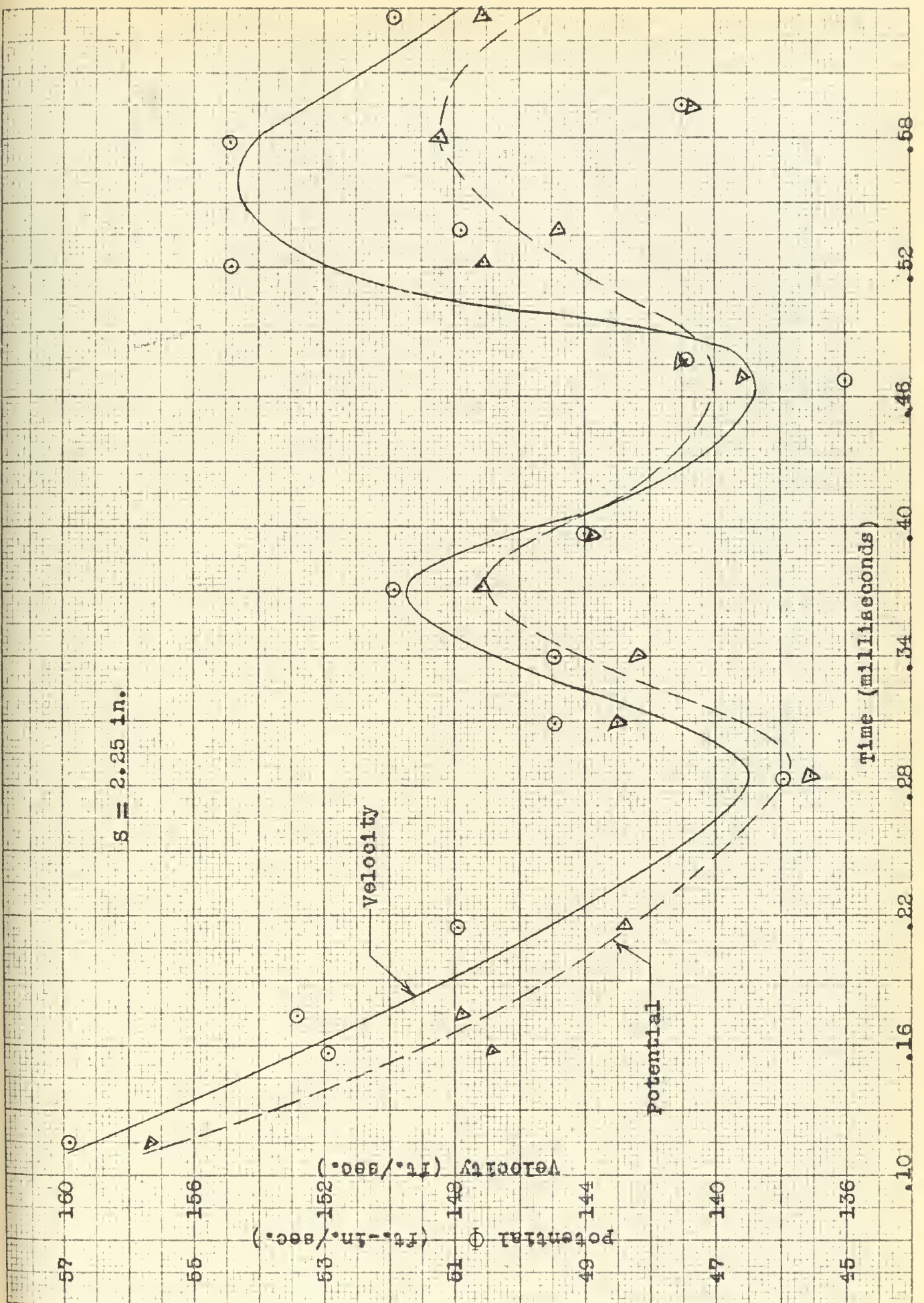


Fig. 52 potential and velocity versus time for $g = 2.25$ inches

$g = 2.50 \text{ in.}$

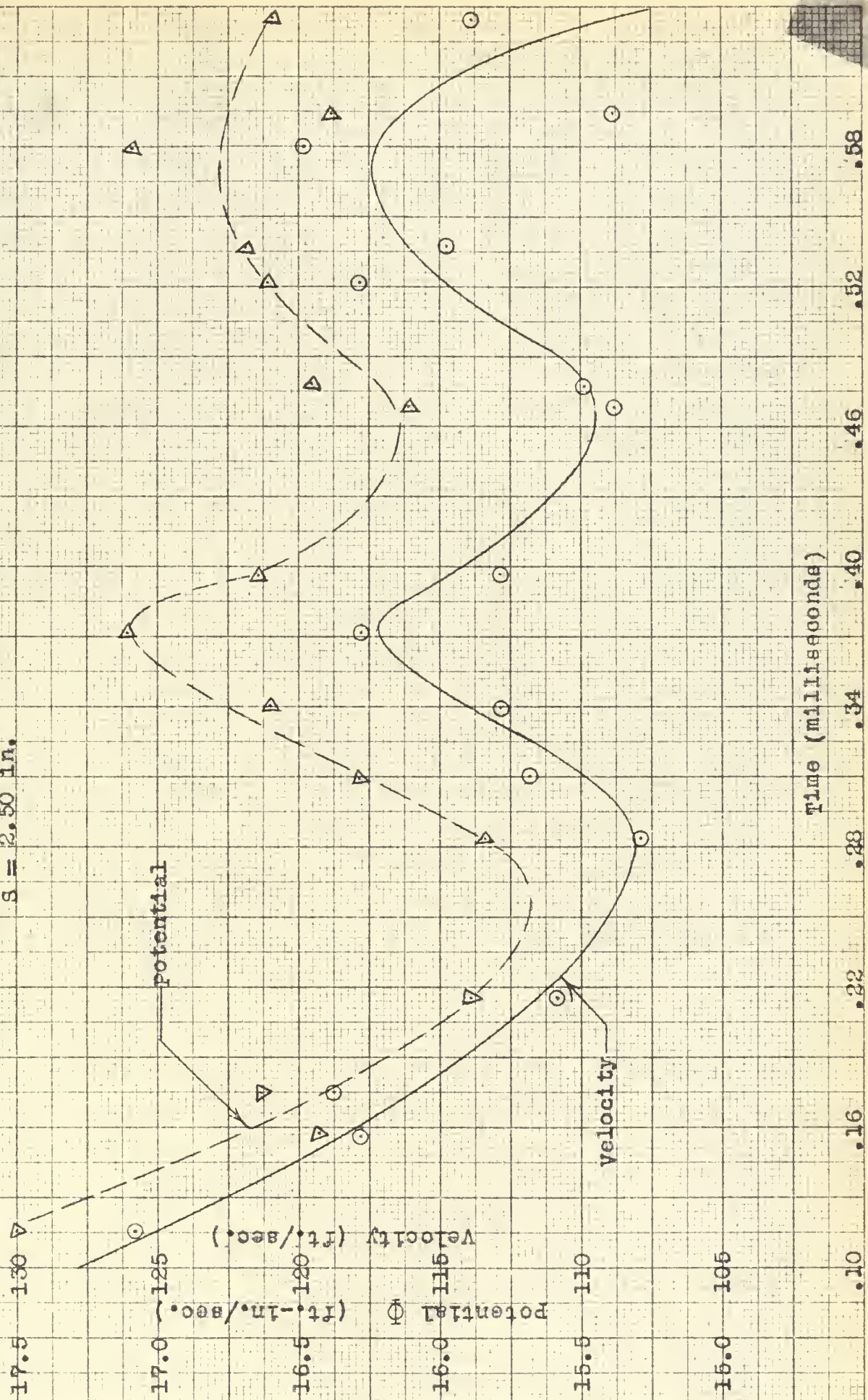


Fig. 53 potential and velocity versus time for $g = 2.50$ inches

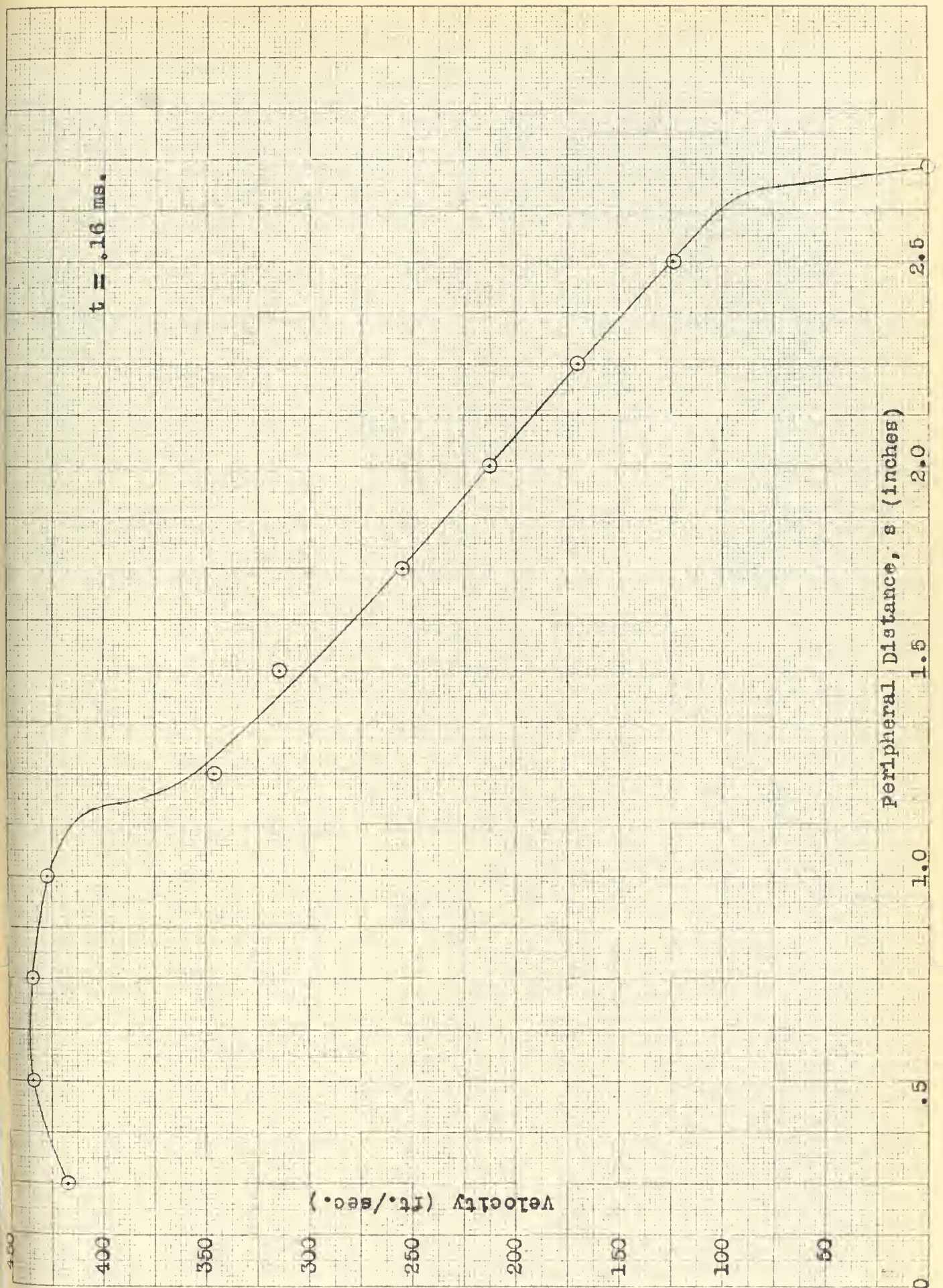


Fig. 54 Velocity versus peripheral distance for $t = .16$ millise

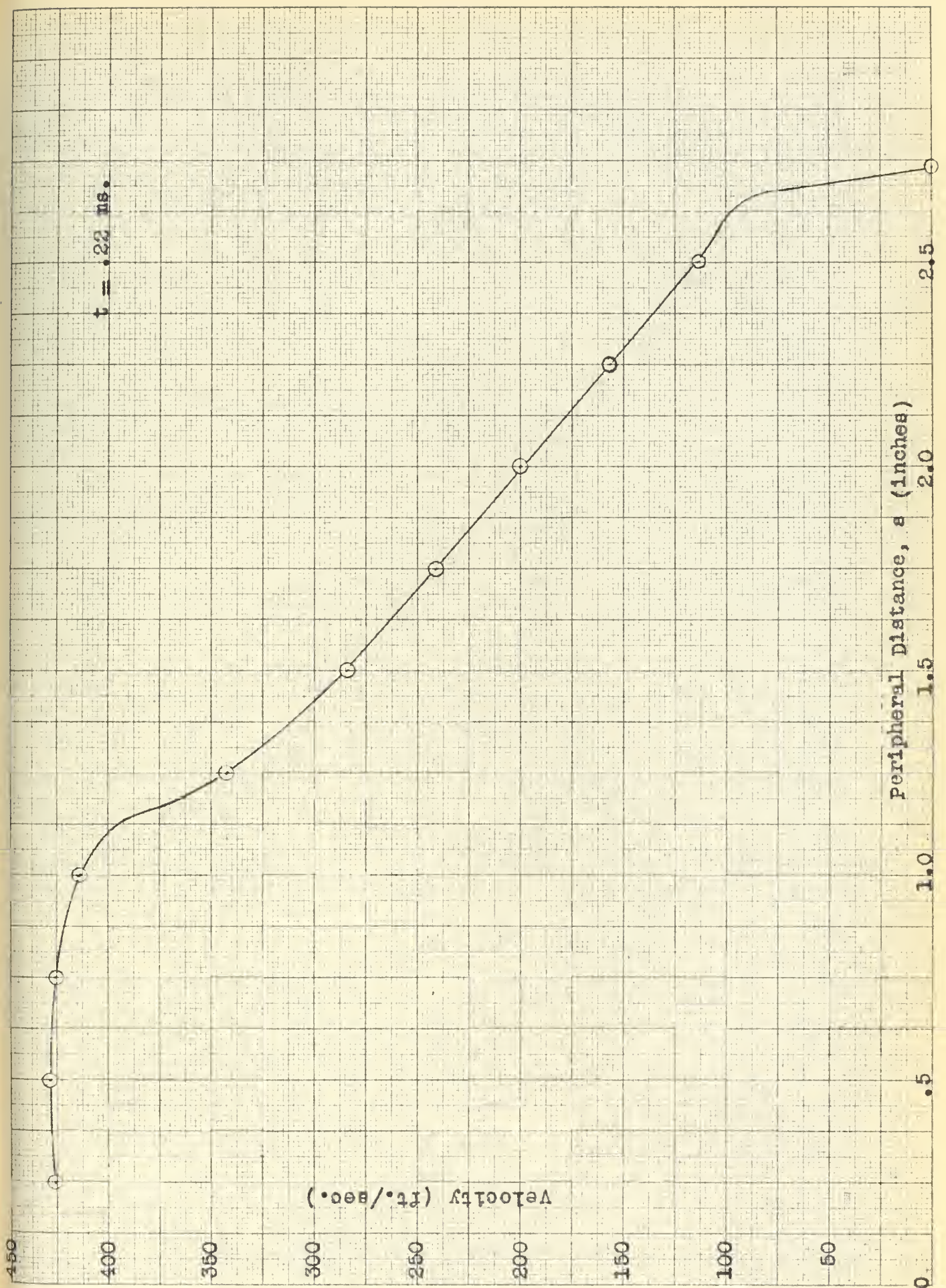


Fig. 55 velocity versus peripheral distance for $t = .22$ millisecc.

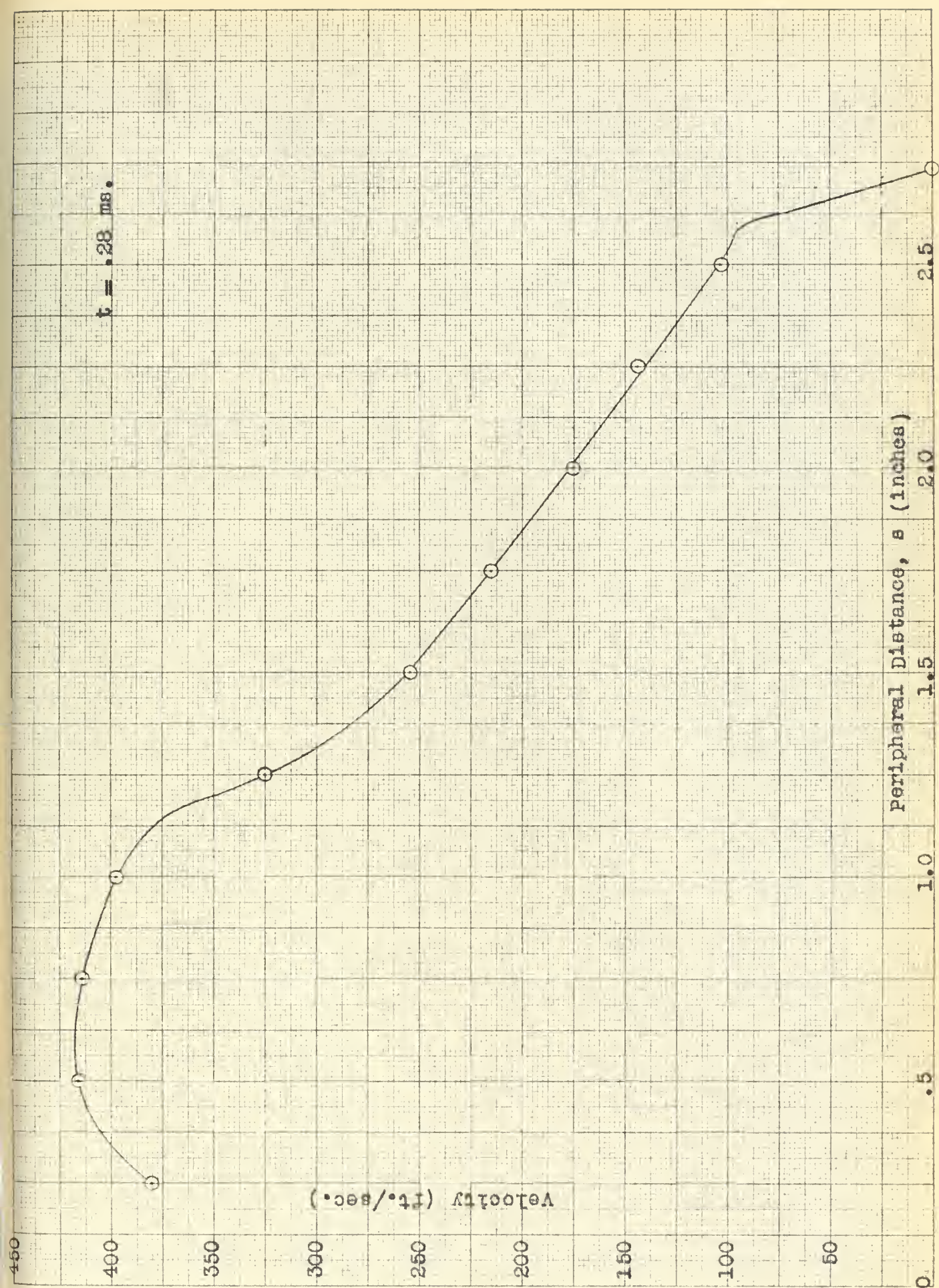


Fig. 56 velocity versus peripheral distance for $t = .28$ millisecc.

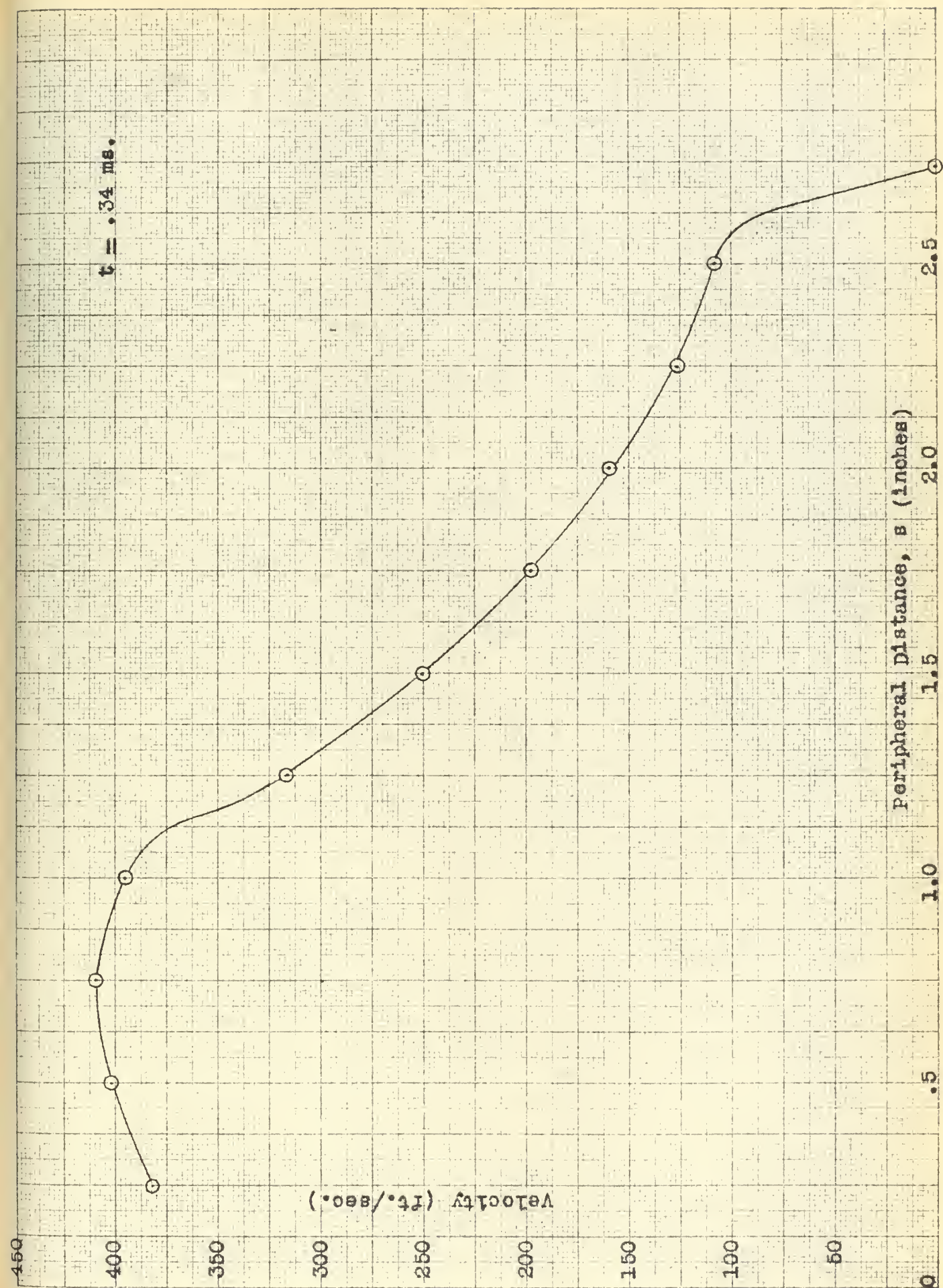


Fig. 57 velocity versus peripheral distance for $t = .34$ millisecc.

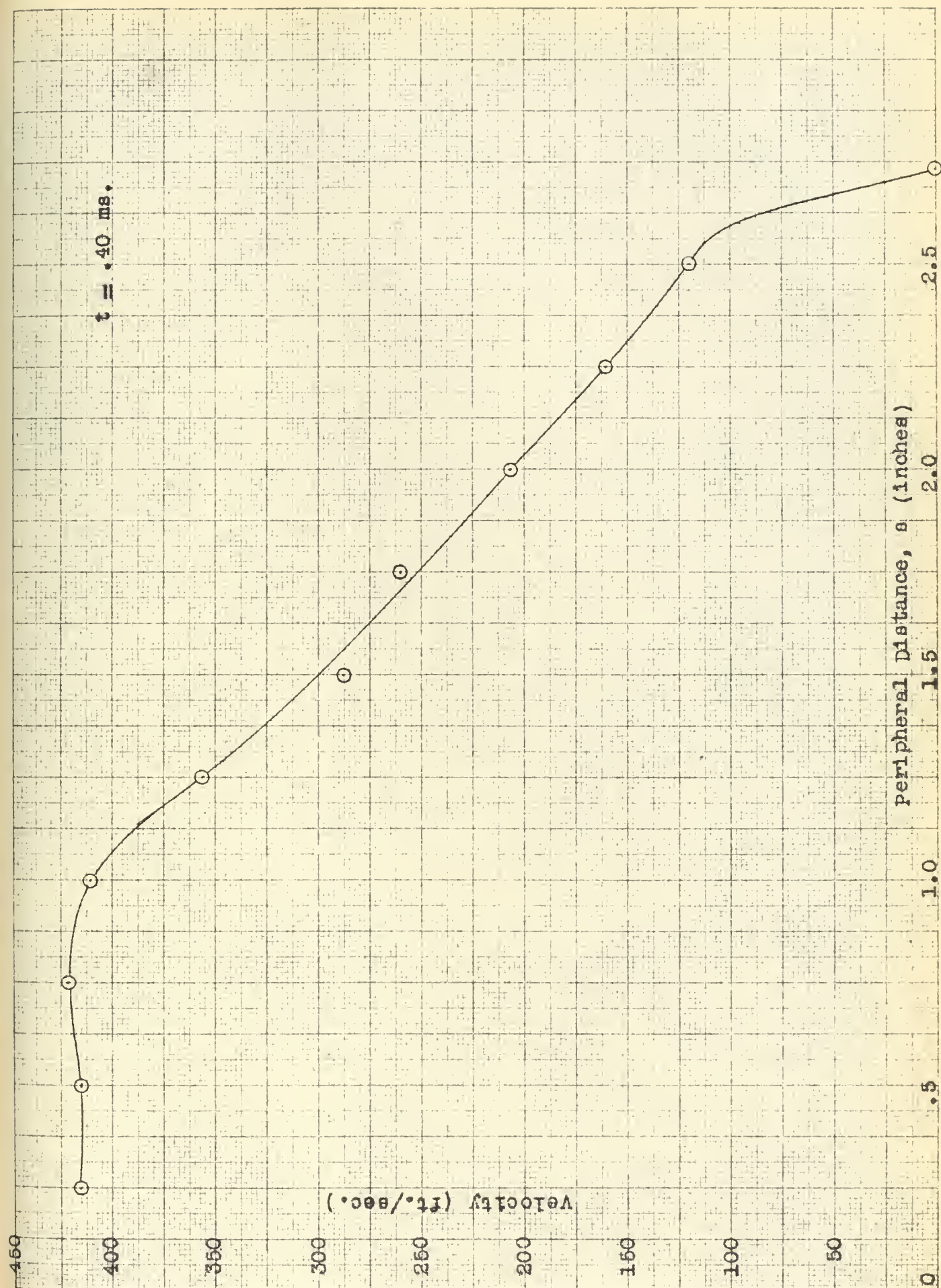


Fig. 58 Velocity versus peripheral distance for $t = .40$ millisecc.

$t = .46 \text{ ms.}$

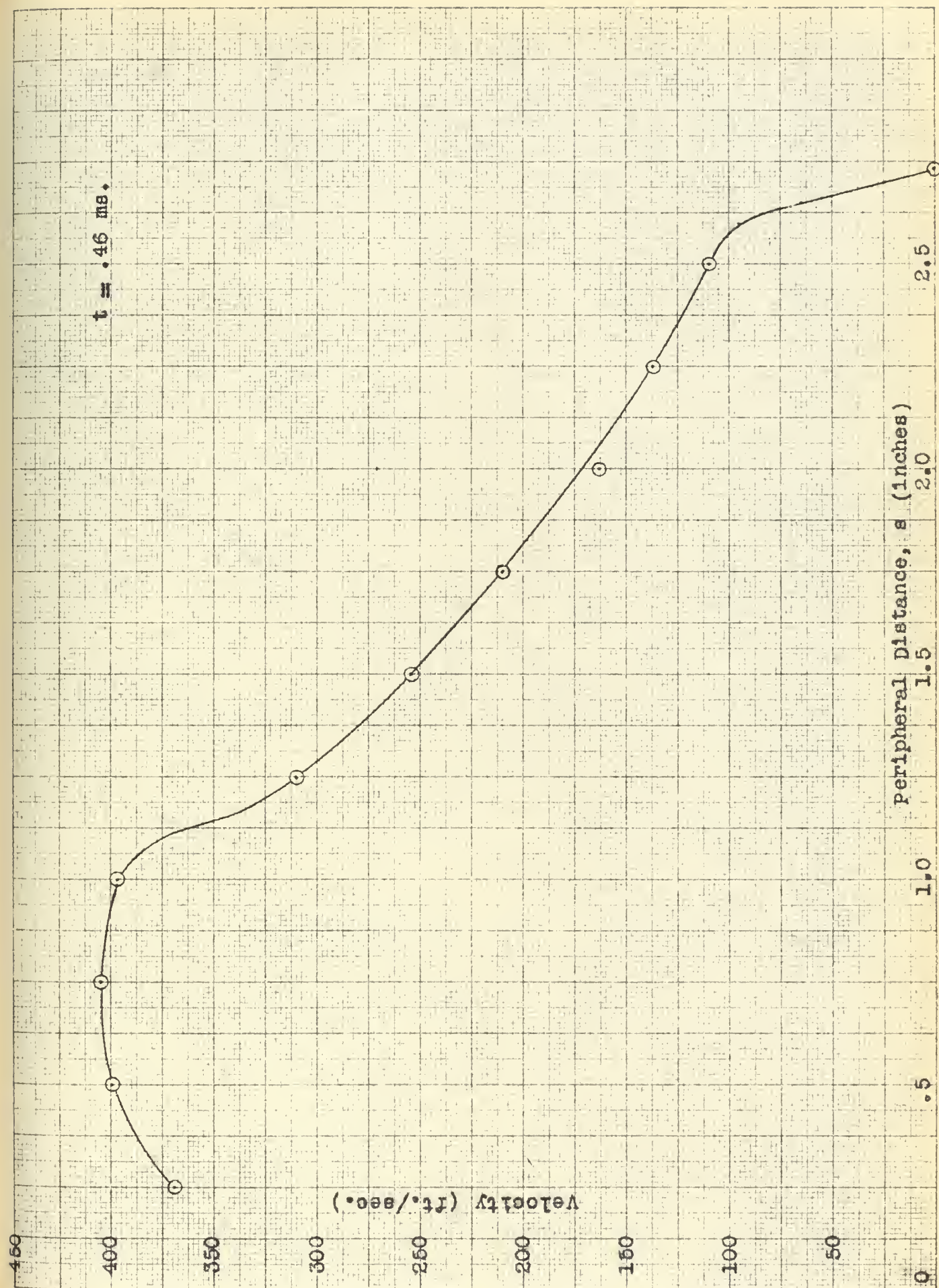


Fig. 59 velocity versus peripheral distance for $t = .46$ milliseo.

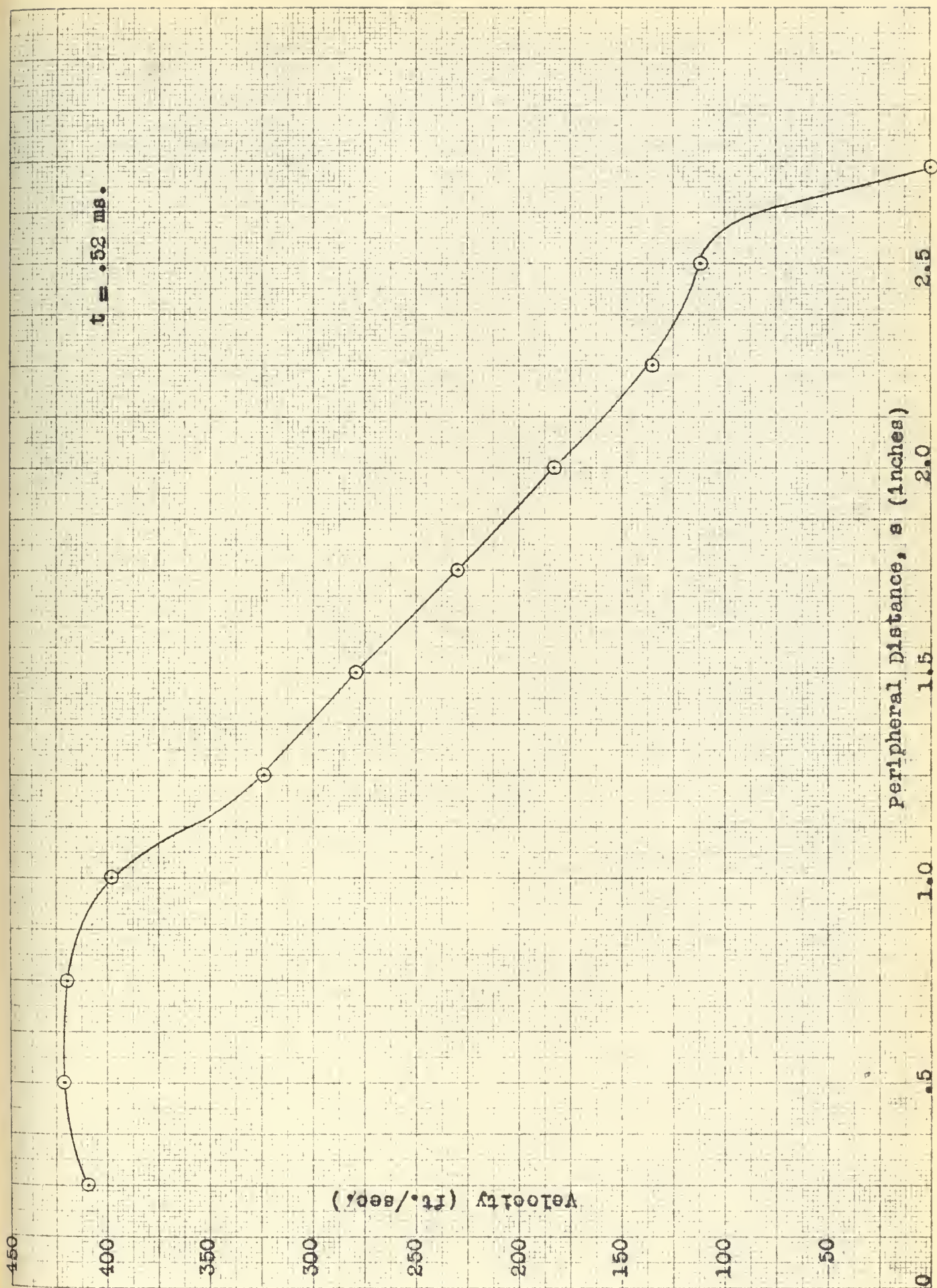


Fig. 60 velocity versus peripheral distance for $t = .52$ millisec.

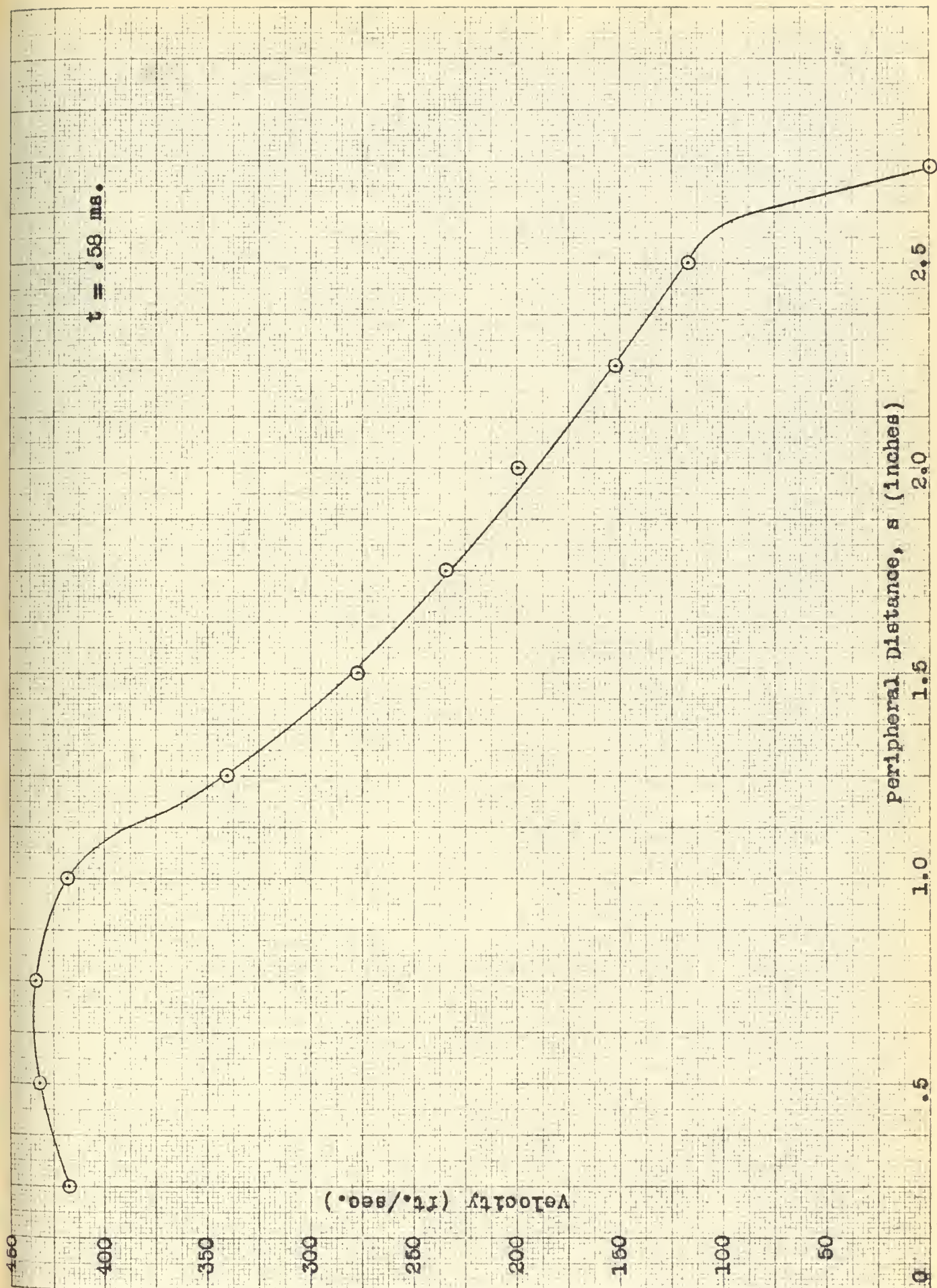


Fig. 61 velocity versus peripheral Distance for $t = .58 \text{ millise.}$

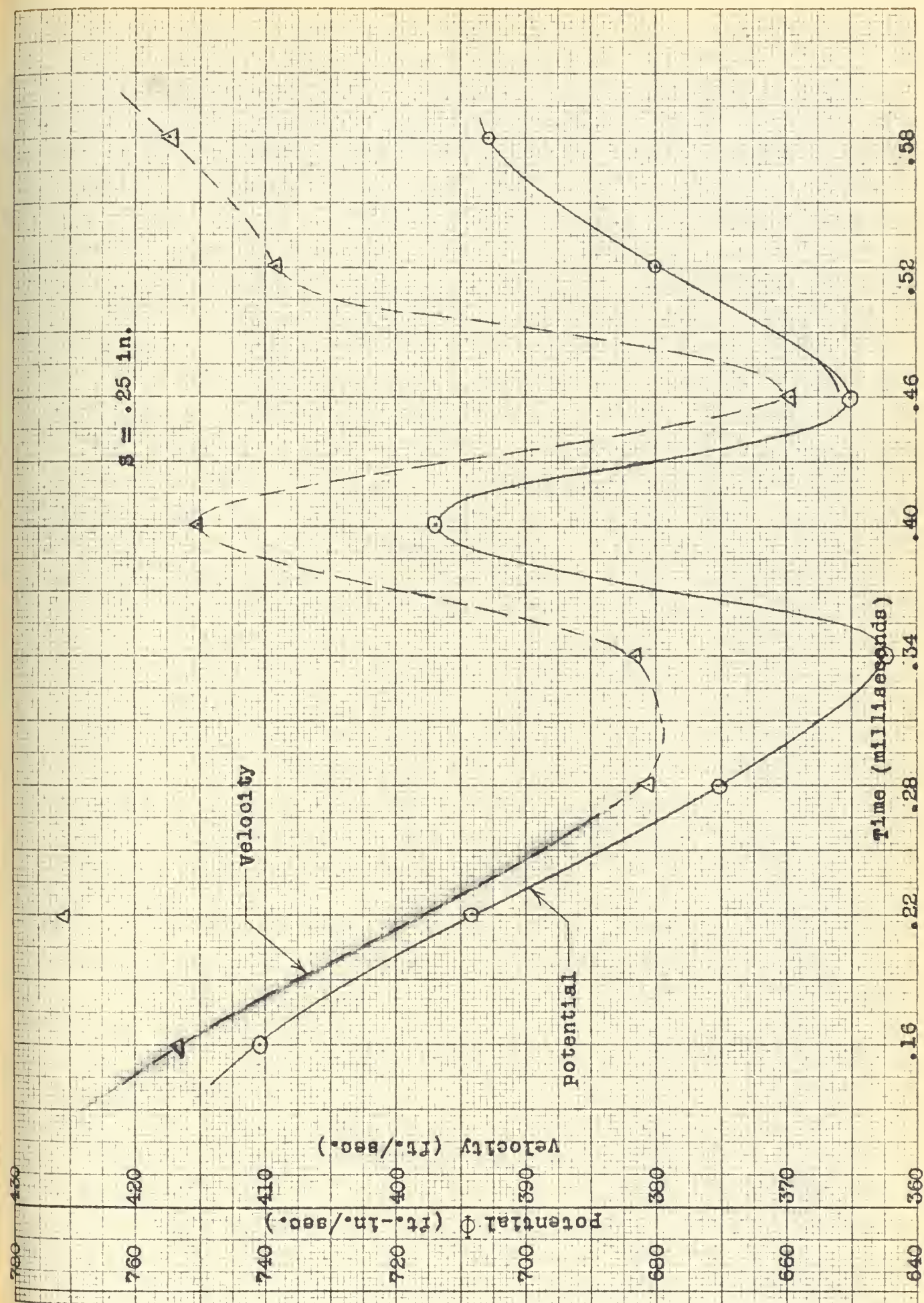


Fig. 62 velocity and potential versus Time for $s = .25$ inches

$s = .50 \text{ in.}$

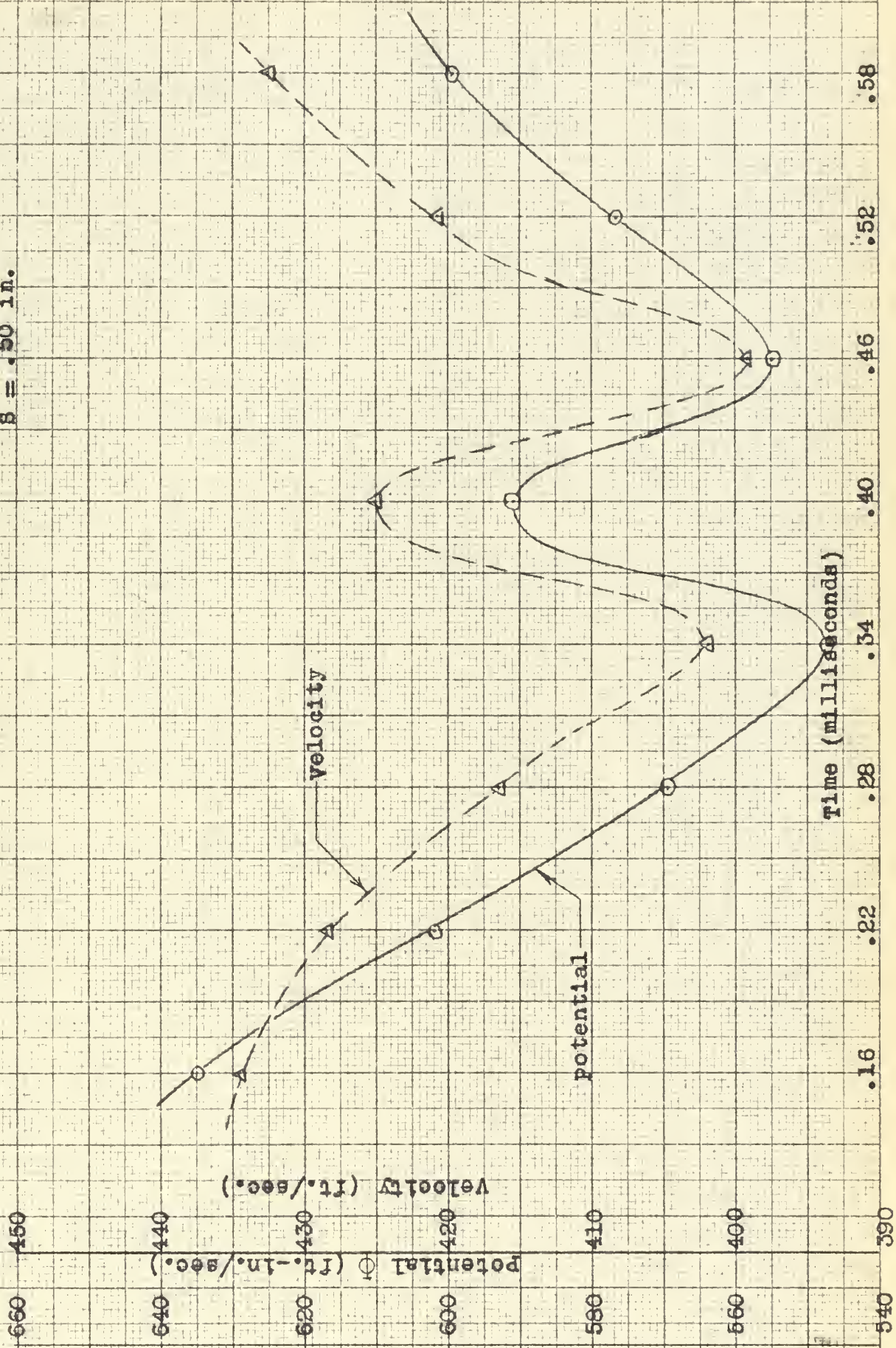


Fig. 63 velocity and potential versus time for $s = .50$ inches

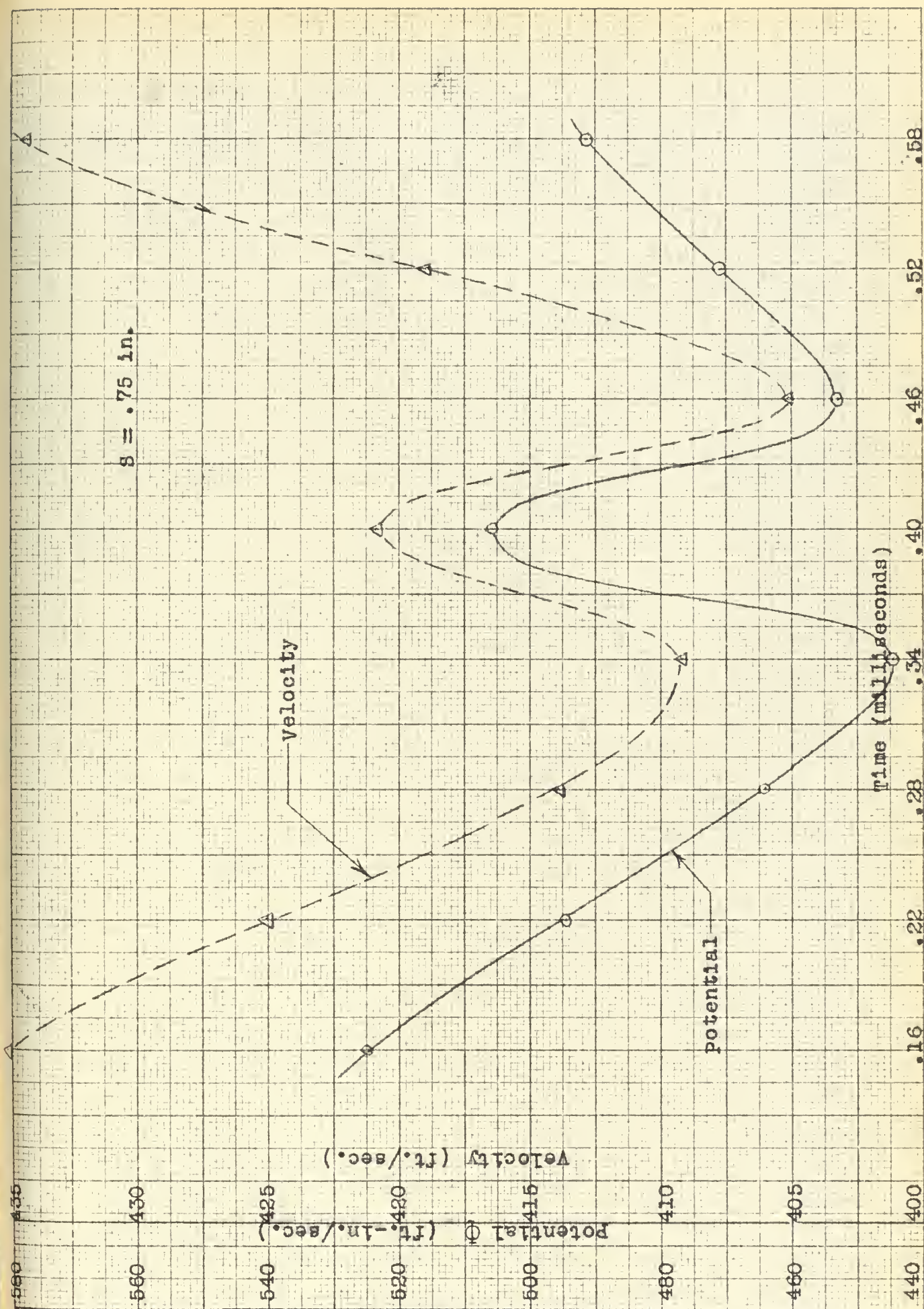


Fig. 64 Velocity and potential versus time for $g = .75$ inches

$s = 1.00$ in.

Potential Φ (ft.-in./sec.)

Velocity (ft./sec.)

velocity

potential

Time (milliseconds)

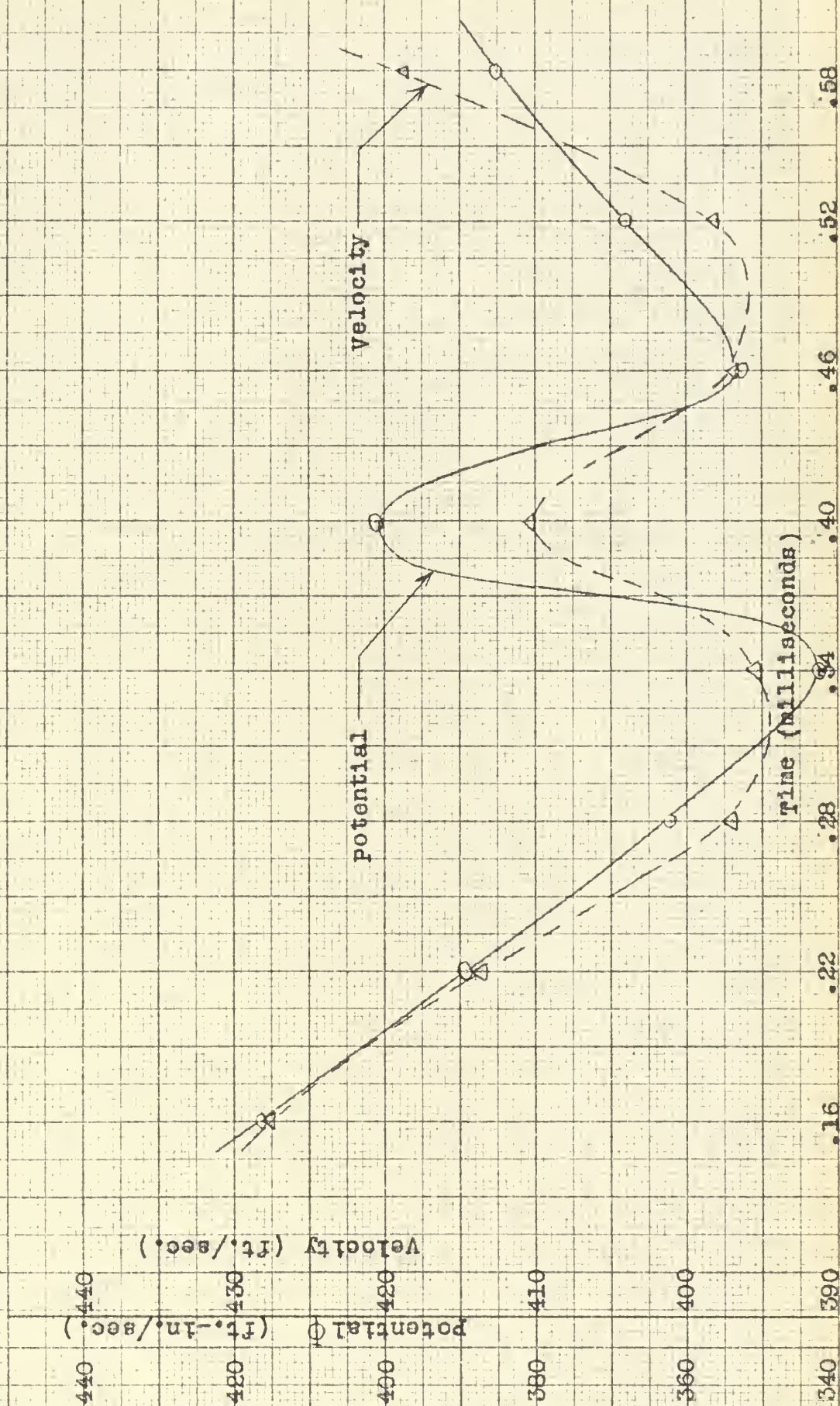


Fig. 65 velocity and potential versus Time for $s = 1.00$ inches

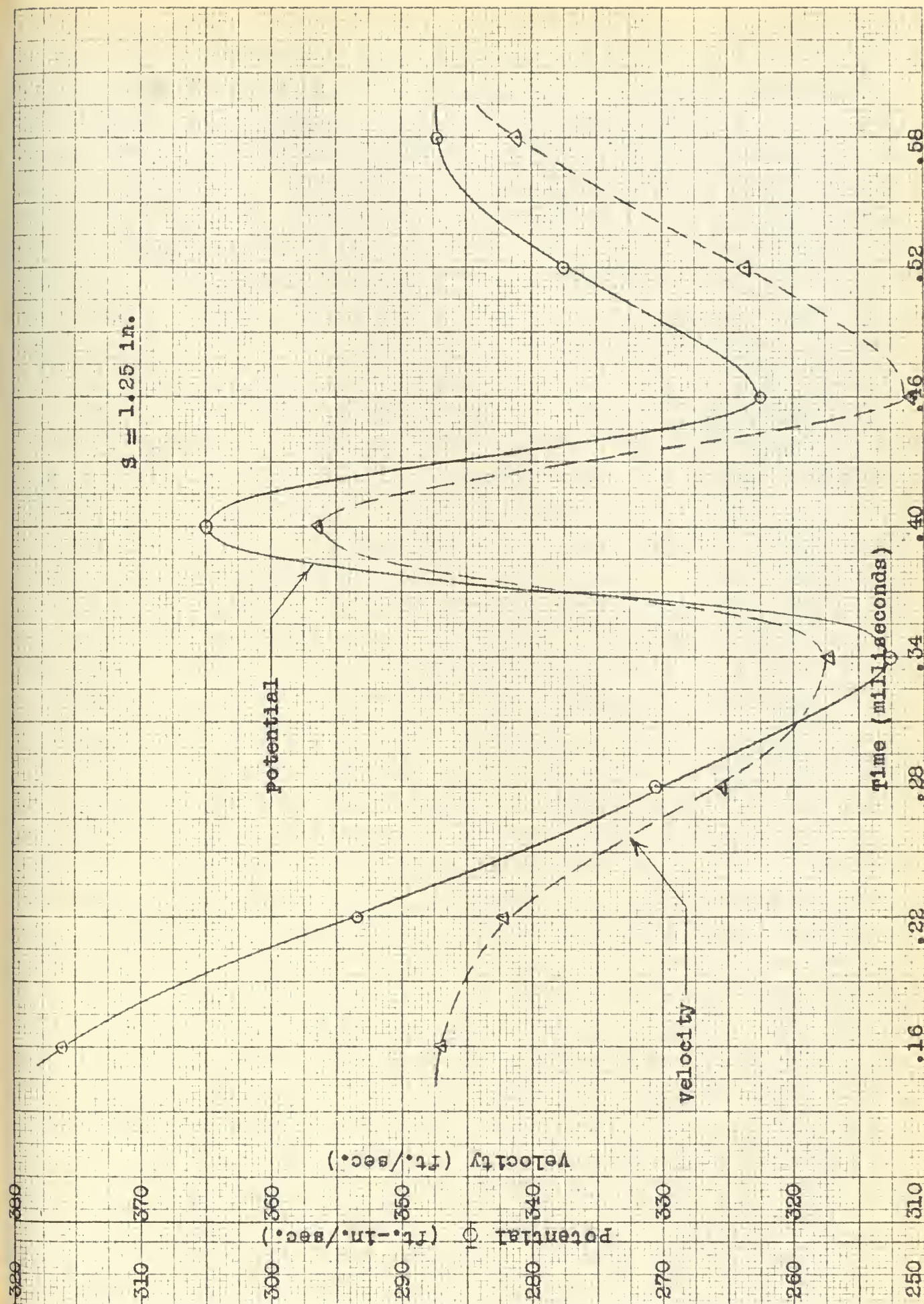


Fig.66 velocity and potential versus Time for $g = 1.25$ inches

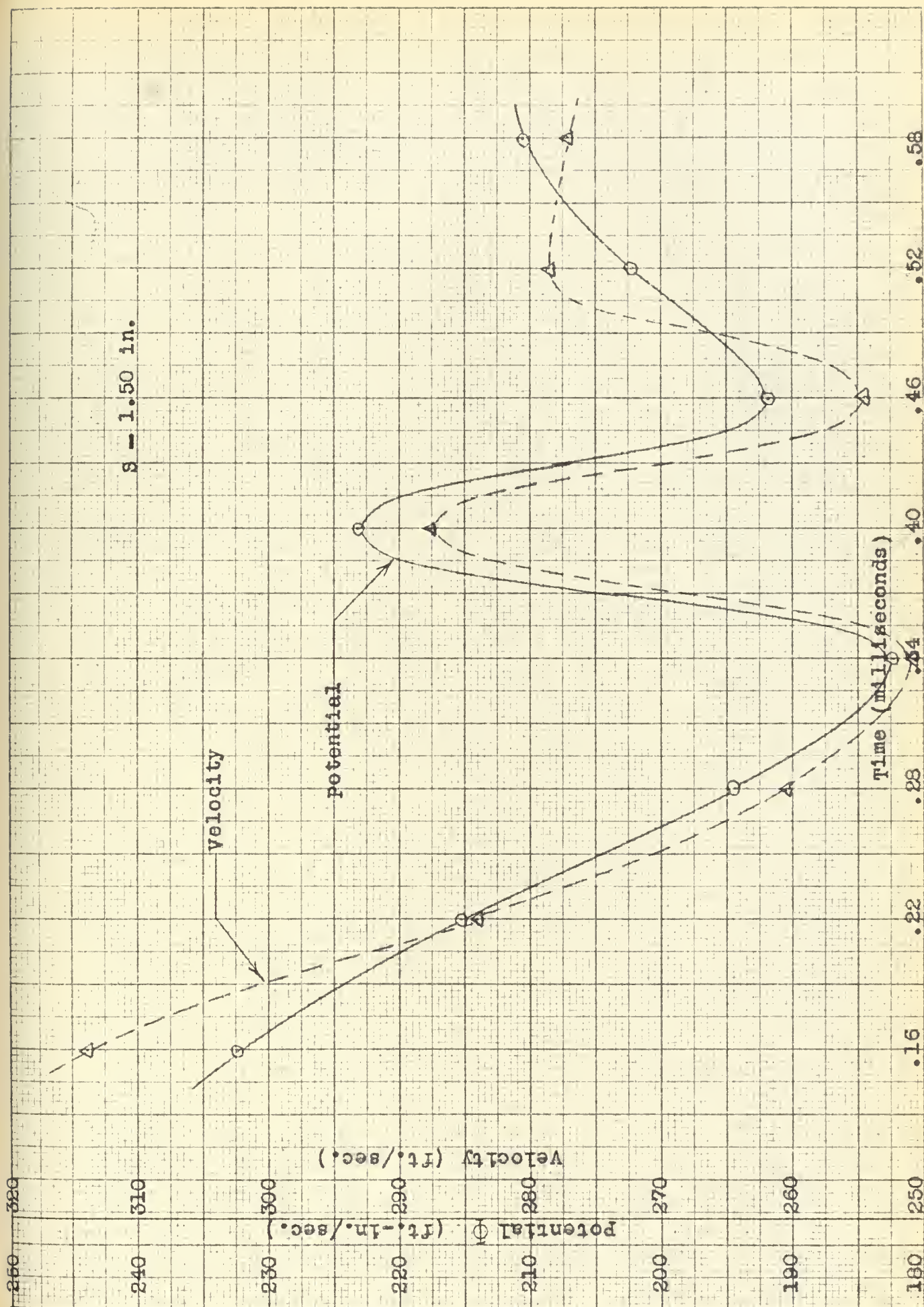


Fig. 67 velocity and potential versus Time for $g = 1.50$ inches

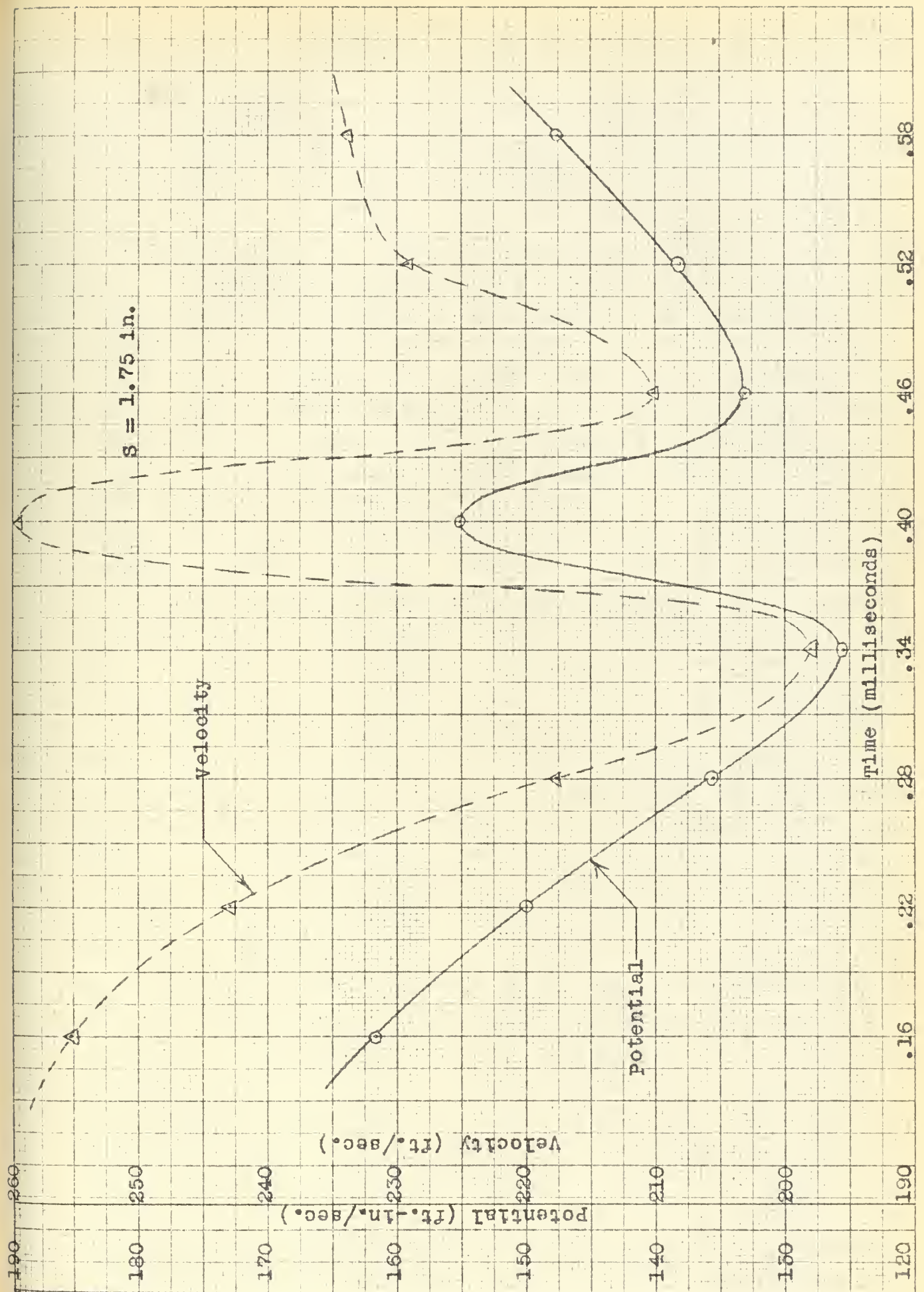


Fig. 68 velocity and potential versus time for $g = 1.75$ inches

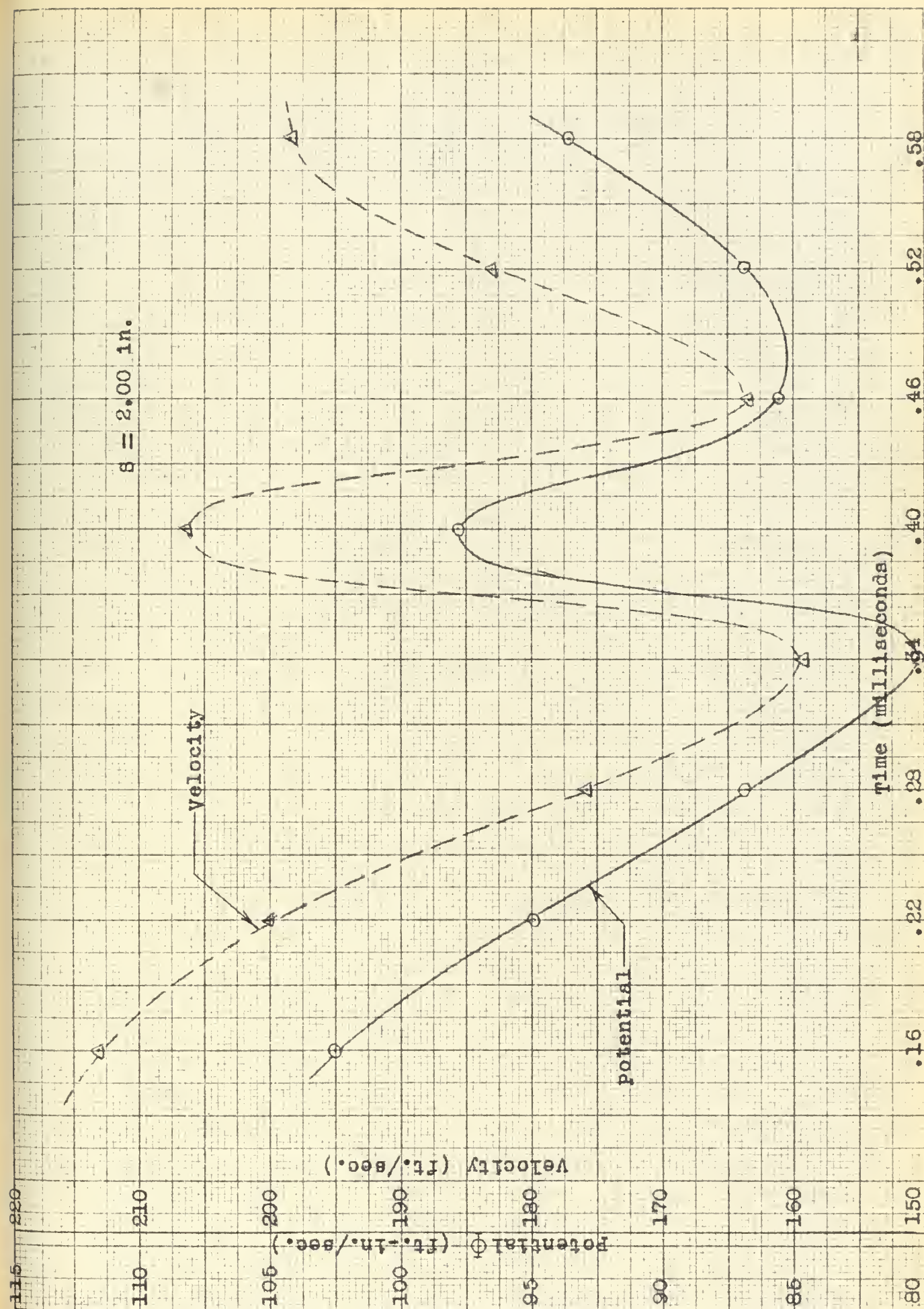


Fig. 69 velocity and potential versus time for $s = 2.00$ inches

$s = 2.25 \text{ in.}$

57 180

55 170

53 160

51 150

49 140

47 130

45 120

Potential Φ (ft.-in./sec.)
Velocity (ft./sec.)

Velocity

Potential

Time (milliseconds)

.58

.52

.46

.40

.34

.28

.22

.16

Fig. 70 velocity and potential versus time for $s = 2.25$ inches

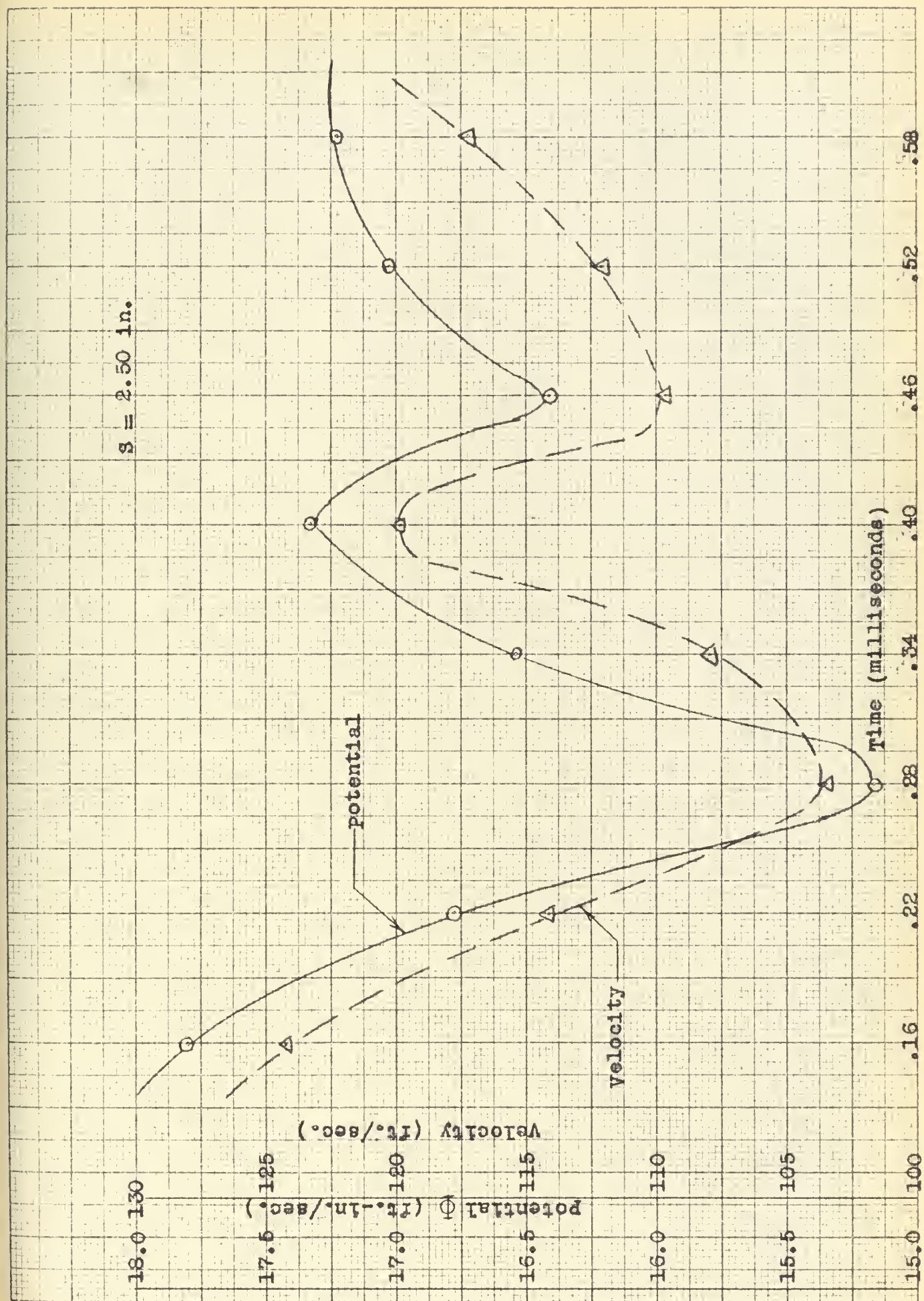


Fig. 71 velocity and potential versus time for $g = 2.50$ inches

$g = 2.50 \text{ in.}$

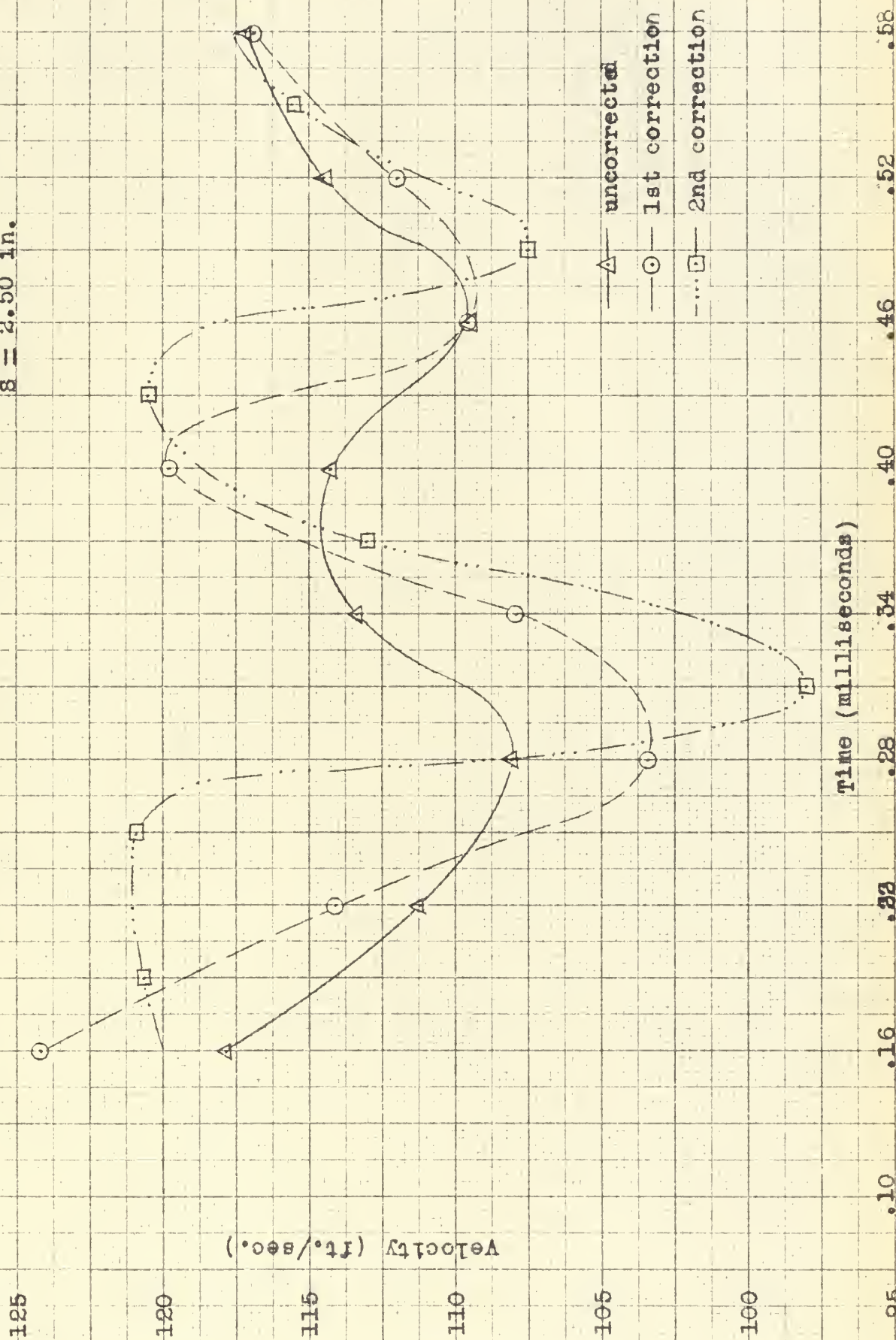


Fig. 72 Corrected velocity versus time for $g = 2.50$ inches

$g = 2.00$ inches

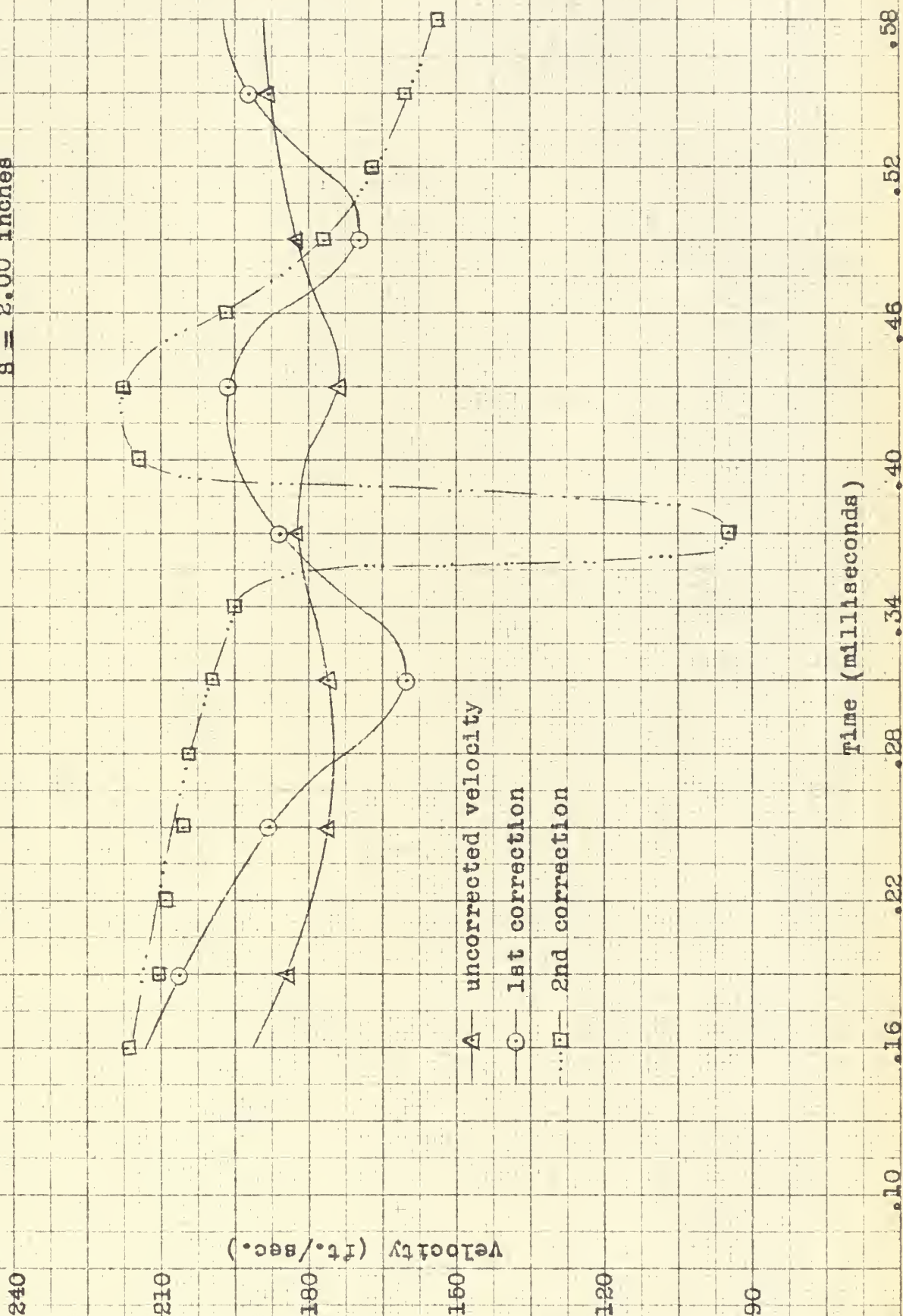


Fig. 73 corrected velocity versus time for $g = 2.00$ inches

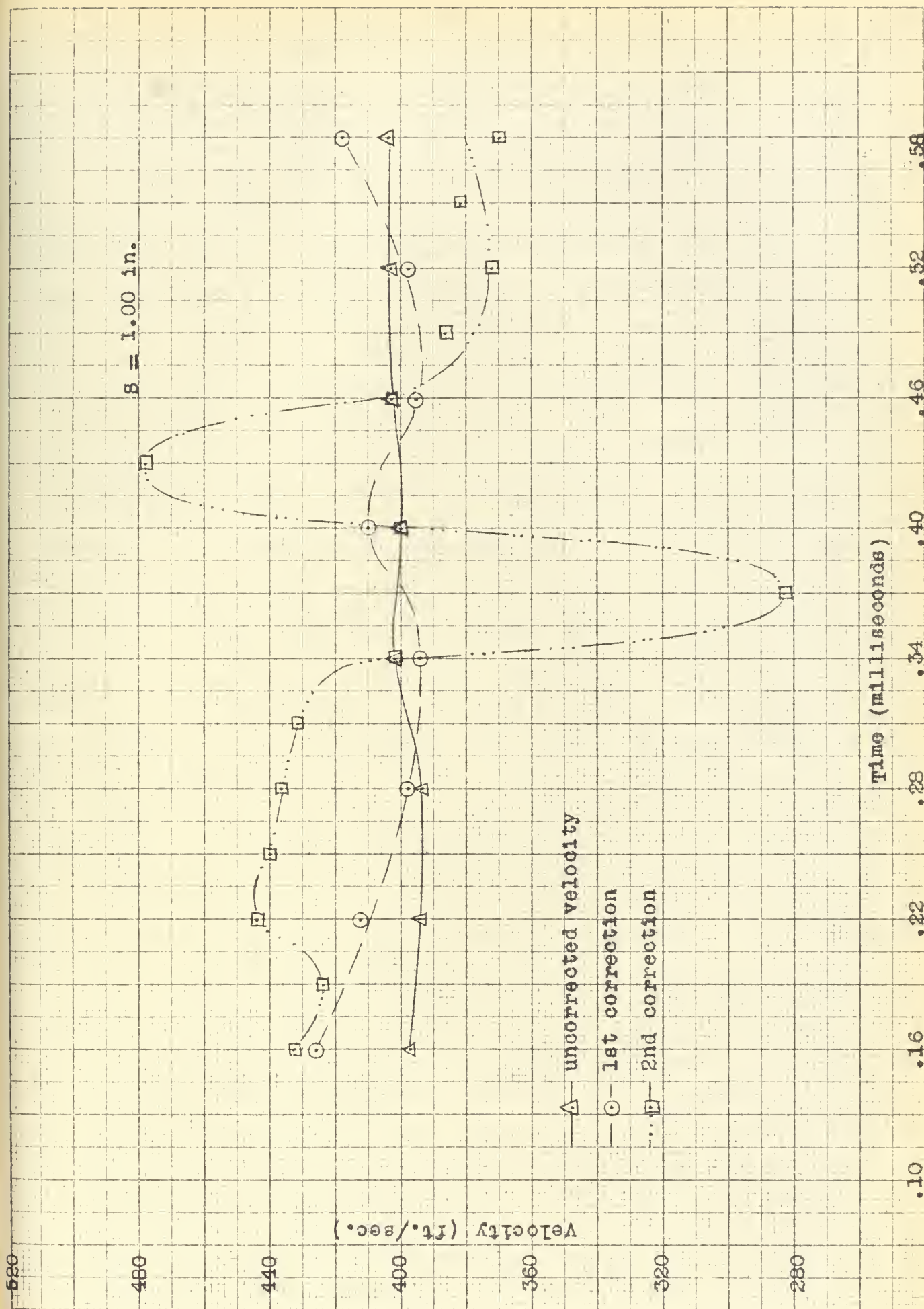


Fig. 74 Corrected velocity versus Time for $s = 1.00$ inches

APPENDIX

For the benefit of those readers who do not have access to Ref. 1 and 2 the following excerpts are included to give a better understanding of the principles of interferometry, the test set-up involved, and the method of data reduction.

INTERFEROMETRY

Fundamentally, the optical method used in the interferometer is based on the fact the speed of light depends on the index of refraction of the medium through which it passes, and the index of refraction of a gas in turn depends on its density. In a high-speed gas flow the density changes are sufficiently large to make these phenomena sizable enough for optical observation. The interferometer measures directly changes in density, and is primarily suited for quantitative determination of the density field.

Fig. 1 shows the essential parts of the Mach-Zehnder interferometer, the type used in this investigation. Referring to Fig. 1, light from the source first passes through a collimating lens which renders the light parallel, and then passes through a monochromatic filter. It then passes through the first "splitting plate" which is a plane half-silvered mirror that passes half the light and reflects half the light. The light which is reflected is changed back to its original direction by the upper mirror and then passes through the test section. The light which passes through the first splitting plate passes through a pair of glass compensating plates which duplicate in thickness and quality the glass side walls of the test section, after being directed to the upper splitting plate by means of the lower mirror. The two beams which divided at the lower splitting plate are recombined at the upper splitting plate and are then

focused by a lens system on a photographic plate. The chief difference between the two beams of light is that the upper beam has passed through the test section. Since the different rays of the upper beam are retarded by different amounts as they pass through portions of the test section of different density, the rays will have various phase differences with the corresponding rays of the lower beam when they are recombined, and thus an interference pattern will be formed at the photographic plate.

The interference pattern is composed of contours of brightness. These contours represent contours of constant index of refraction, and therefore represent contours of constant density in the flow field. Fig. 1, of the report, shows such an "infinite-fringe" interferogram of the flow through the turbine nozzle, the term "infinite-fringe" signifying that the light field is uniform in the absence of flow through the test section. The dark bands in the figure are loci of points where there is complete interference, and represent contours of constant density.

For a more accurate quantitative evaluation, the fringe-displacement method may be used. If the second splitting plate is rotated through a small angle with respect to the first splitting plate, two "coherent" beams of light which were in phase at the first splitter will, through the change in lengths of light paths, be out of phase at the screen. If the splitters are rotated about axes normal to the beam direction, there will be formed on the photographic plate, or screen, successive light and dark fringes, uniformly spaced, with each fringe lying parallel to the axis of rotation.

If the air density in the test section is uniformly increased, this will produce a uniform displacement of all the wave fronts passing through the test section. This displacement in turn will cause the interference bands on the screen to shift in a

direction normal to the bands, although the bands will remain parallel and uniformly spaced. The fringe shift is a measure of the change in density in the test section.

When there is flow in the test section, with corresponding nonuniform density changes, similar fringe shifts will occur, but, as they are no longer uniform, the resultant fringes will be curved.

To analyze the interferometric pictures it is necessary to determine the density associated with each of the fringes, since changes in density are all the interferometer can measure.

The free stream density ρ_{∞} is determined from the values of P_0 , T_{∞} , and q_{∞} which are either determined during the test runs or calculated from the test data.

The density of the remainder of the flow field is determined from the two-dimensional fringe displacement relation:

$$\rho/\rho_{\infty} = 1 + \frac{\gamma}{b} \left(\frac{\lambda_0}{L} \right) \left(\frac{\rho}{n-1} \right) \left(\frac{1}{\rho_{\infty}} \right)$$

Where;

ρ = local density of the air (lb/ft³)

ρ_{∞} = Reference density of the air in the undisturbed fringe field (lb/ft³)

γ = Fringe displacement normal to the undisturbed fringe direction (in.)

b = Fringe spacing (in)

λ_0 = Wave length of light used, in a vacuum (mm)

L = Length of light path in turbine test section (mm)

$\frac{n-1}{\rho}$ = Gladstone-Dale-Constant for air

This is the relation used for the reduction of data from the fringe displacement pictures. The data reduction of this type of interferogram is very tedious, time

consuming, and prone to error, while the use of the infinite fringe interferogram yields constant density contours on the basic interferogram. The only data reduction that is required is the determination of the change in density between any two isopycnic (constant density) contours (which is a constant for the whole field if the properties of the interferometer optics are precise enough) and a calculation of the density in the undisturbed flow region just upstream of the nozzle blade row. Fortunately this density, ρ_∞ , has been found to be nearly constant with time, which is desirable for comparison purposes.

For the series of pictures considered in this report, the density can be determined by the following relation obtained from interferometric theory and utilizing light of a given wave length (4358\AA) with a specified path length of light in the turbine test section:

$$\frac{\Delta \rho}{\rho_\infty} = 0.01027$$

The above relation gives the ratio of the change in density, $\Delta \rho$, referred to the density of the undisturbed upstream field, ρ_∞ between any two isopycnals.

If each dark fringe is numbered in sequence starting with number one at the inlet to the nozzle blade row, the density ratio ρ/ρ_∞ of each isopycnal can then be determined.

It should be noted that since the upstream field is light the density ratio of the first isopycnal would be $(\rho/\rho_\infty)_1 = 1 - \frac{0.01027}{2}$ while the $\Delta \rho/\rho_\infty$ between any two succeeding isopycnals would be equal to 0.01027. This reduction of data is well illustrated in Tables I and II.

TEST SET-UP

The radial flow, single stage impulse turbine used for this study was designed and fabricated by the General Electric Company. A cross sectional and side view of the turbine appear in Figs. 3a and 3b respectively.

The turbine wheel has 208 bucket blades mounted in the periphery. The outside diameter of the wheel at the bucket leading edge is 41.75 in. The span of the bucket blades is 6.00 inches. Four cutouts spaced 90° apart are located in the end plates that contain the buckets to make visible the air flow in these four bucket channels. The bucket cutouts are terminated by one-inch diameter holes downstream of the moving stage to allow an opening for the beam of light used by the electronic flash triggering apparatus. The bucket section is General Electric Type T-1984237 with a 27° bucket entrance angle and a 24° bucket exit angle. With the buckets evenly spaced along the periphery of the turbine wheel the bucket pitch spacing at the O.D. of the wheel is 0.631 in. The pitch spacing at the trailing edge is 0.600 in.

The partial admission air inlet section consists of a wooden bell mouth faired into a steel rectangular flow passage (6.35 in. x 13.98 in.). Provision is made for mounting twelve nozzle partitions with six of the nozzle partitions mounted between optically flat glass plates for viewing purposes. These six steel nozzle partitions are isolated from the glass plates by plastic gasket material to eliminate local stresses in the glass. The nozzle partition is General Electric Type K-6915600. The nozzle sections are located on a basis of 104 equally spaced in 360° with the nozzle trailing edges located on a 41.880 in. diameter giving a nozzle pitch spacing at the trailing edges of 1.295 in. The nozzle exit angle is 13° . The partial admission assembly can

be raised or lowered with respect to the turbine casing giving a variable gap between the nozzle trailing edges and the bucket leading edges.

The air that passes through the turbine is inducted from the laboratory as a stagnation reservoir. The air is taken from a height of about ten feet above the laboratory floor through a calming section which is connected to the turbine partial admission inlet section.

The air flow then passes through the turbine stage and is turned and passes through the turbine outlet in an axial direction.

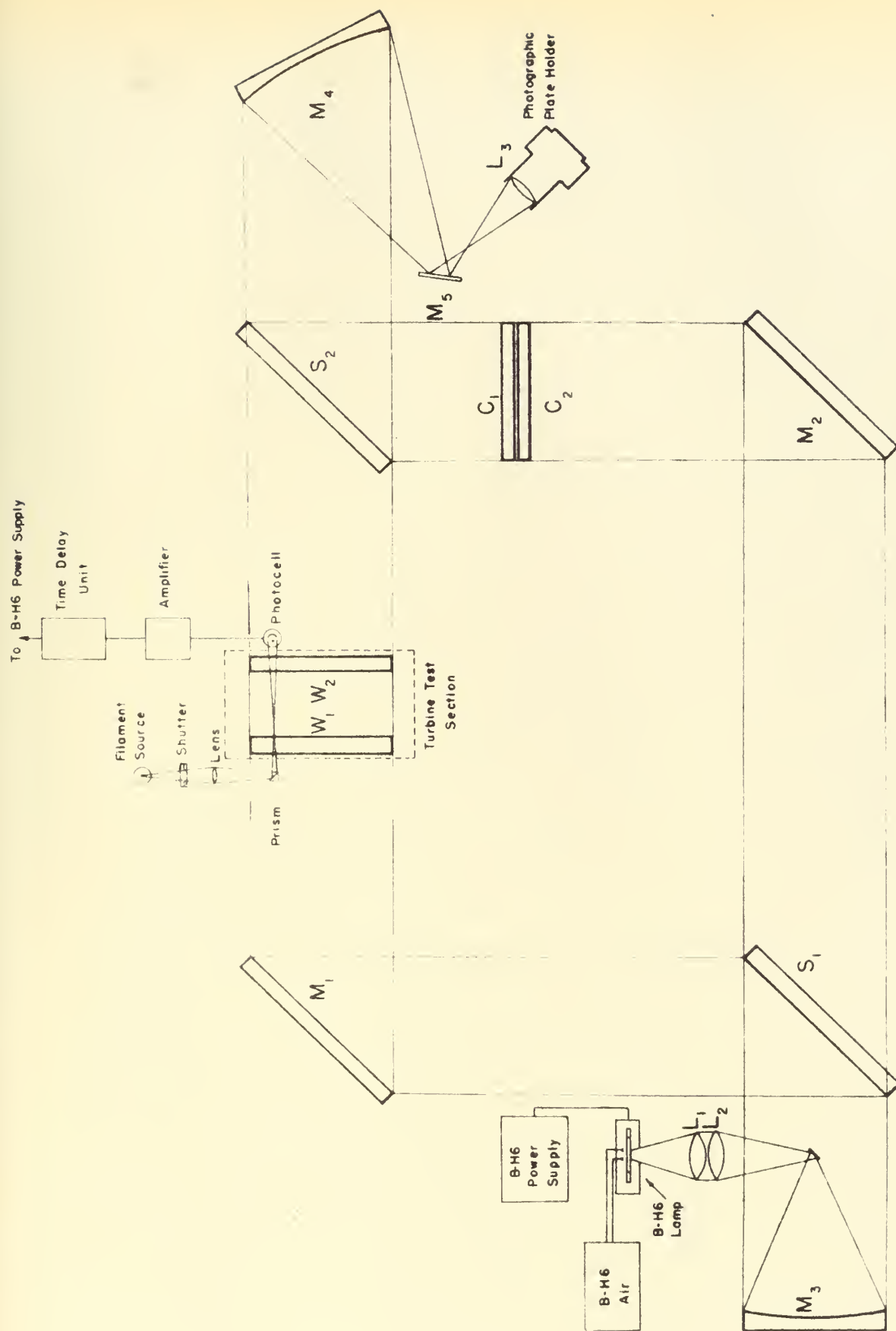
A sketch of the air induction system with the turbine is shown in Fig. 5. In the Figure a blower is shown at the turbine outlet and was used for inducting air into the turbine. The blower has been replaced by an air ejector arrangement which has increased the flow rate through the turbine, with two attendant advantages. First the increased density change through the cascade caused a much greater fringe shift on the interferogram, yielding more accurate quantitative information, and second, placed a sonic throat between the driver and turbine section eliminating any unsteady effects propagated upstream by the air induction system.

The turbine load consists of a 10 H. P., D. C. generator and a bank of 25, 300 watt lamps. The load is adjusted to the desired value by means of a variable rheostat in the generator field and by selecting any desired number of lamps.

ANALYSIS

For general information Figs. 2 and 4 are included. Fig. 2 is a sketch of the vortex shedding phenomenon, showing the general location of the shedding and the path after shedding. UM Figs. 435, 451, 453 show some good examples of this vortex.

Fig. 4 illustrates the numbering of the fringes and the direction of measurement of the peripheral distance. From the numbering can be gained an idea of which fringes correspond, and the location of the fringe of highest density. The right hand blade shows the location of certain peripheral distances mentioned frequently in this report.



Schematic View of Interferometer
And Associated Apparatus

FIGURE I

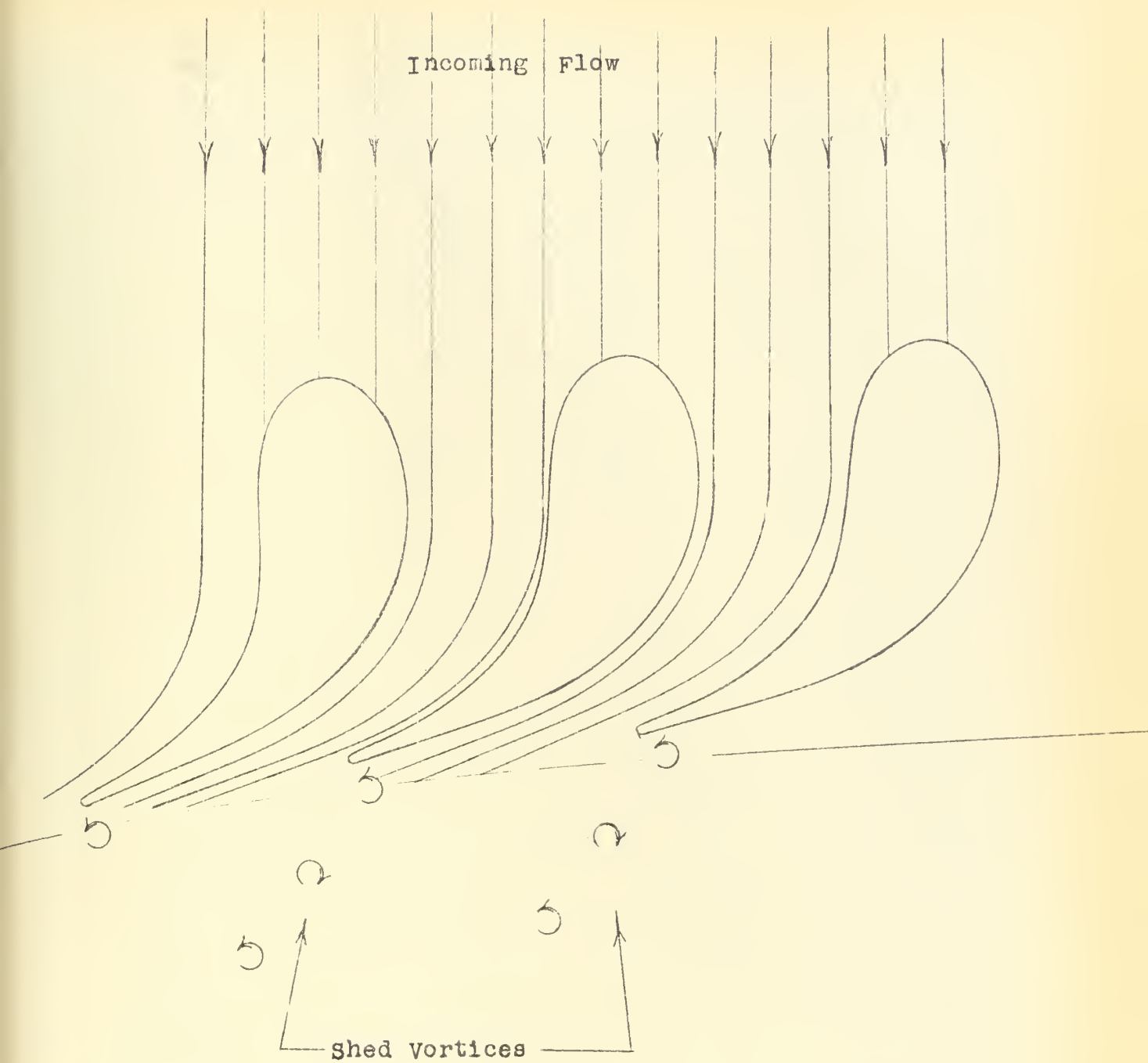
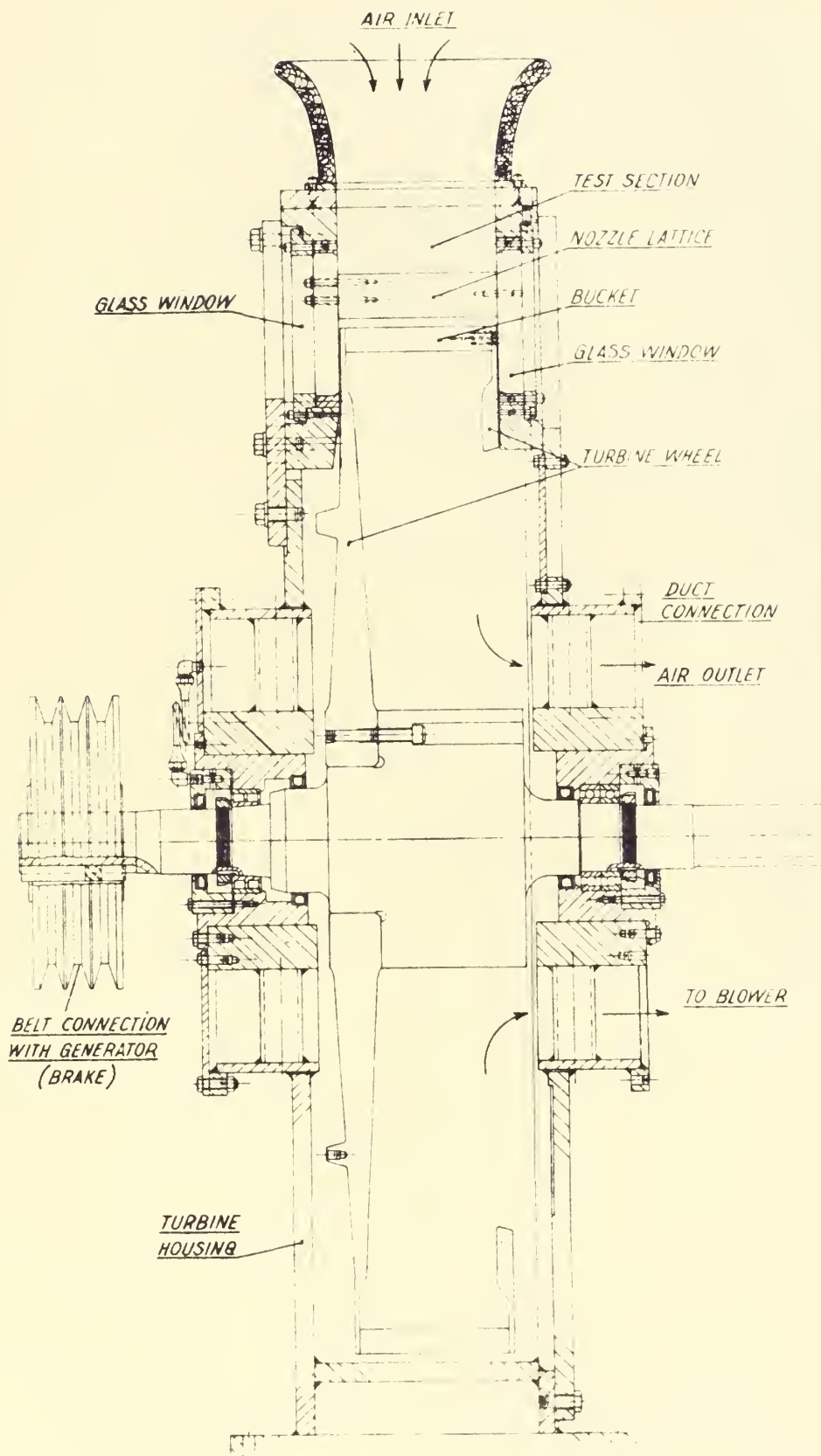
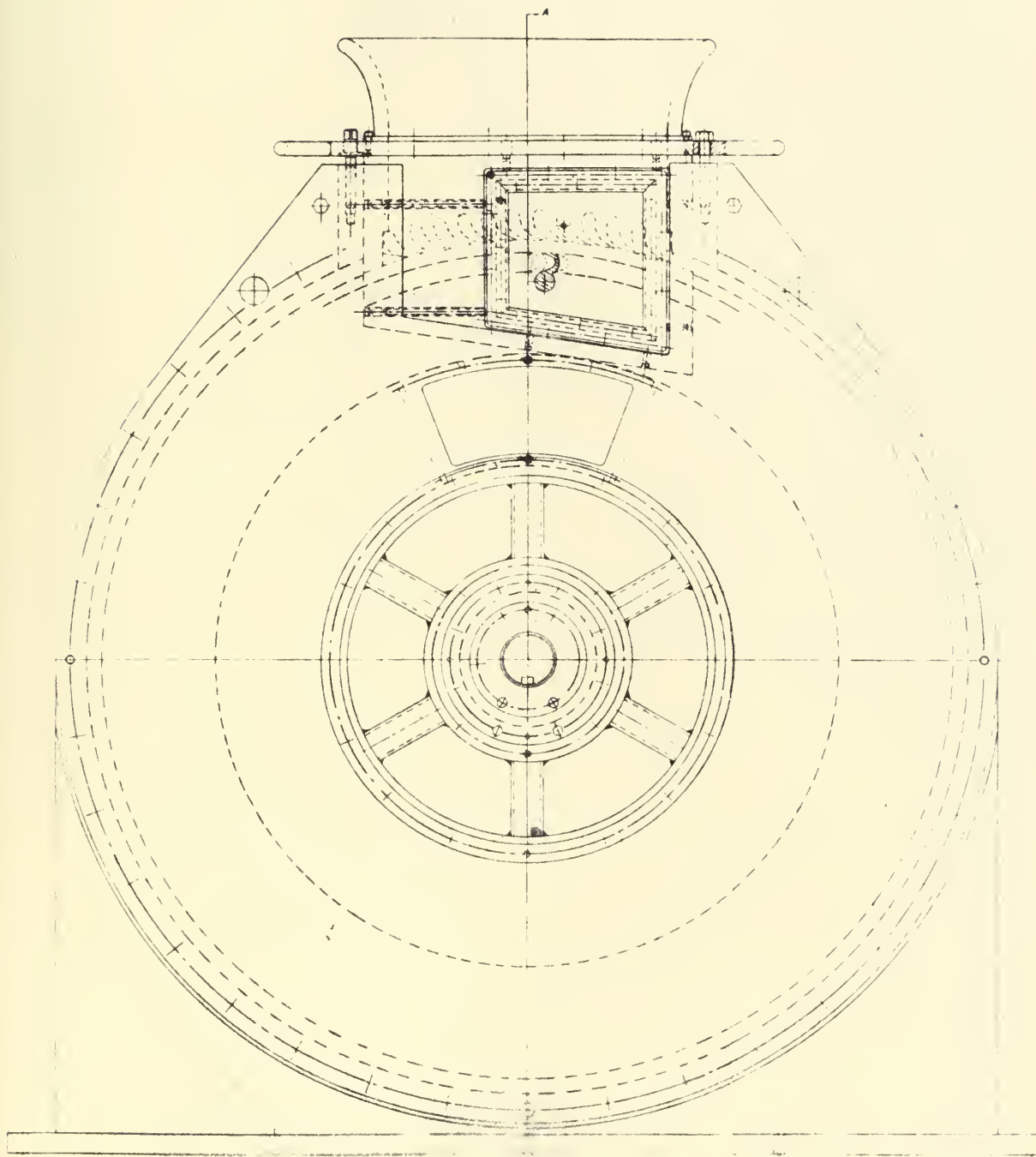


Fig. 2 sketch of Nozzle Blades showing Typical Shed
vortices



CROSS-SECTIONAL VIEW OF TURBINE

FIGURE 3a



SIDE VIEW OF TURBINE

FIGURE 3b

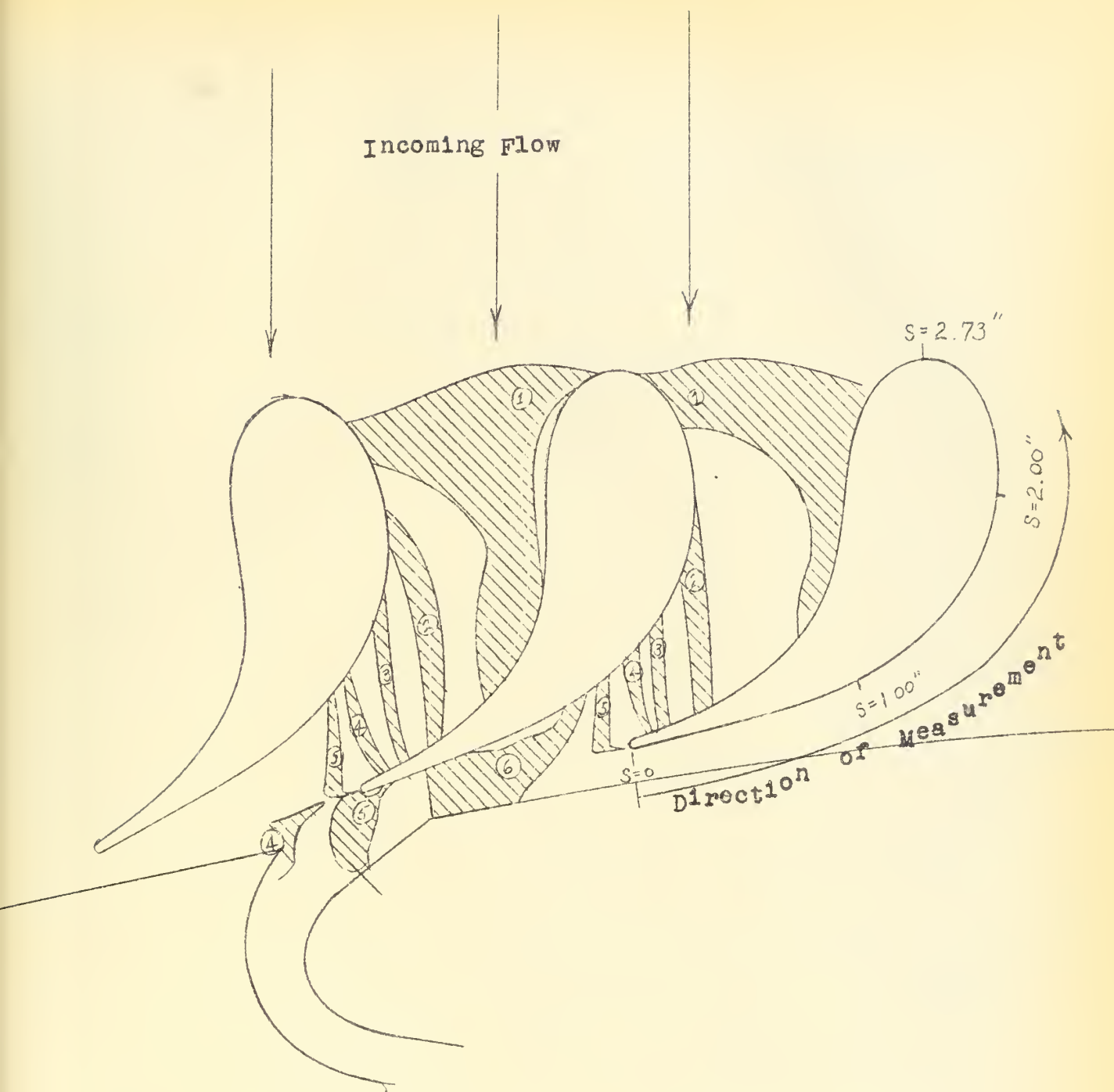
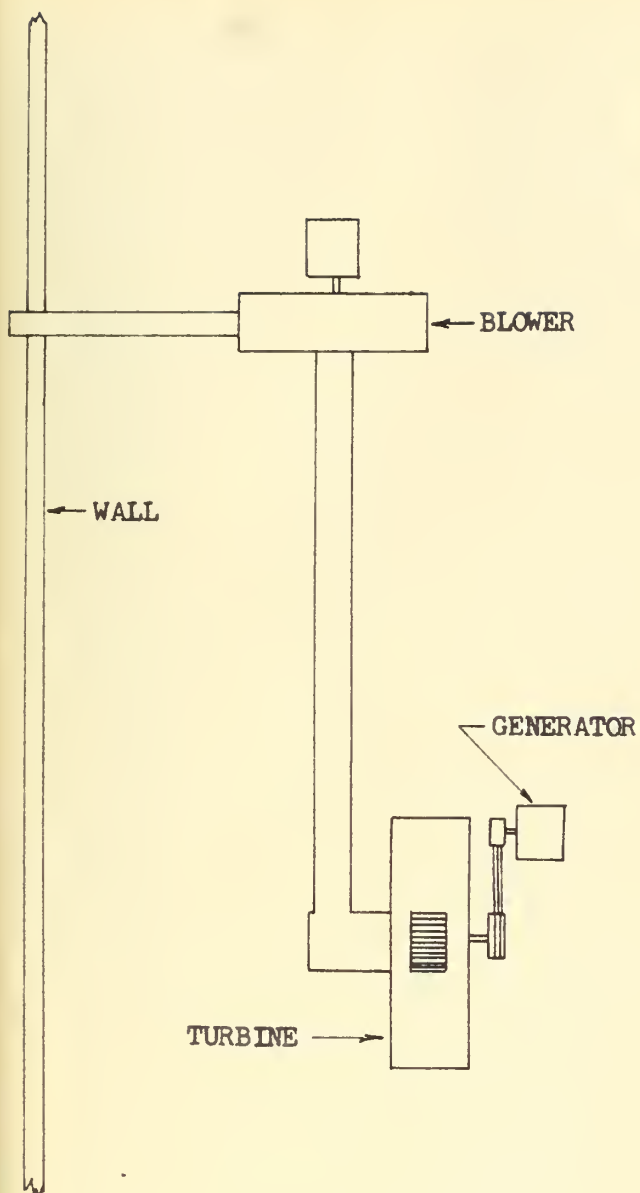
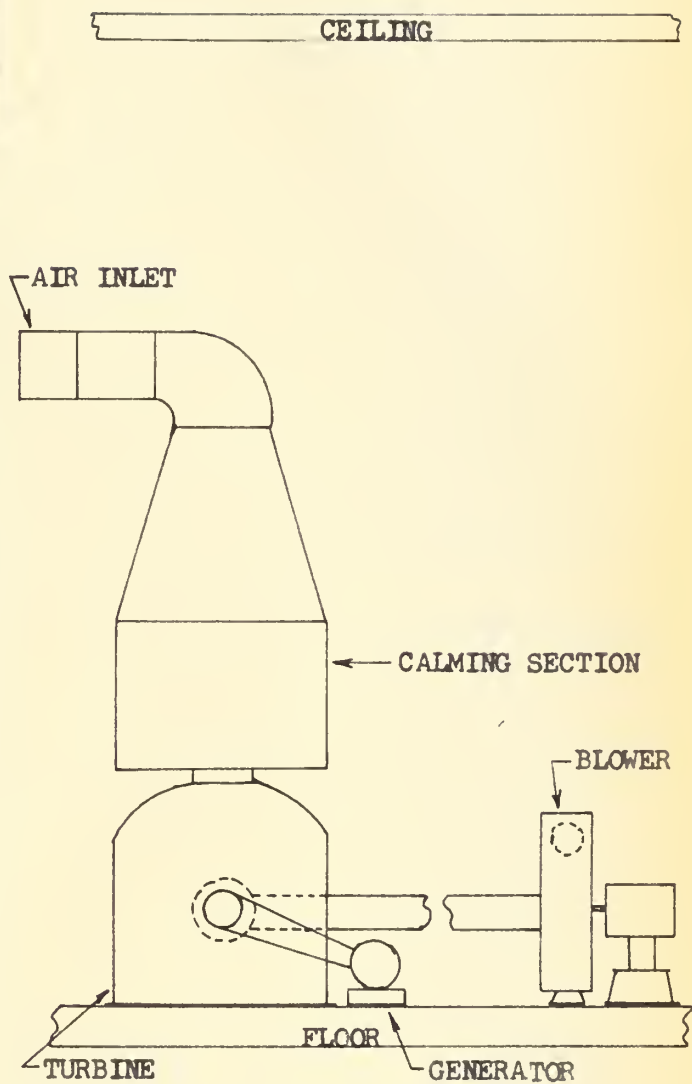


Fig. 4 Fringe Numbering and Measurement of peripheral Distance



PLAN VIEW WITHOUT
AIR INLET SECTION



ELEVATION VIEW WITH
AIR INLET SECTION

SCHEMATIC VIEW OF TURBINE AND AIR INDUCTION SYSTEM

FIGURE 5

thesH194

Interferometric analysis of the time uns



3 2768 002 07619 2

DUDLEY KNOX LIBRARY